

**Characterising dysbiosis in Alzheimer's disease utilising
the APP/PS1 mouse model**

Nicole Finn

**A thesis submitted to the University of Lancaster for the degree of Master of
Science (By Research) in Biomedical Science**

Supervised by Dr. Rachael Rigby

September 2018

Division of Biomedical Life Sciences

Faculty of Health and Medicine

Abstract

The gut brain axis (GBA) is a bi-directional communication system between the gastrointestinal tract (GI) and the brain. Correct functioning of the GBA is essential to human health and its dysfunction has been widely implicated in a variety of diseases including, irritable bowel syndrome (IBS), Parkinson's disease (PD), anxiety, depression, and more recently Alzheimer's disease (AD). Pathological changes associated with GBA dysfunction include: increased permeability of the epithelial gut barrier, localised and systemic inflammation, increased permeability of the blood brain barrier (BBB), insulin resistance and alterations in the production of microbial metabolites.

In our laboratory, we utilised the APP/PS1 transgenic mouse as a model for cerebral amyloidosis in the brain. These mice overproduce β -amyloid ($A\beta$), allowing the study of mechanisms of neuropathology. In this project we used seven and fifteen-month mice as a representation of early and late $A\beta$ plaque deposition. Histological examination of tissue architecture in addition to goblet cell and enteroendocrine cell (EEC) counts were performed. Mucosal and luminal bacterial community profiling was assessed through quantitative real-time PCR (qRT-PCR) and denaturing gel gradient electrophoresis (DGGE).

There was a significant decrease in the phylum Firmicutes and number of EEC's in the colon of seven-month APP/PS1 mice compared to WT littermates. By fifteen-months the dysbiosis had recovered, however there was a decrease in goblet cells in the villi and crypts of the ileum. A three-month age group was introduced which was found to have a significant difference in the mucosal-associated microbiota in the caecum of APP/PS1 mice. The dysbiosis was accompanied by a significant decrease in crypt depth and an increase in EEC numbers in the colon.

The results suggest that dysbiosis in the large intestine occurs in early neuropathology and is normalised by late AD pathology. We propose that dysbiosis induces changes in the tissue architecture and cell population numbers

during the progression of pathology, which exacerbates GBA dysfunction. The potential for this research lies with the possibility of identifying an AD microbiota profile, which could make it possible to identify high-risk individuals by comparing profiles. Altering the microbiota through the use of probiotics or changing certain lifestyle factors such as adopting a Mediterranean diet, may reduce the likelihood of a high-risk person developing or slow down the progression of AD.

Acknowledgements

I would like to firstly express my gratitude to Dr. Rachael Rigby who designed a thoroughly enjoyable project and supported me throughout the year. A huge thank you must be given to Dr. Jayde Whittingham-Dowd for her guidance and for showing me the techniques required. Thanks must also be given to Professor. Christian Hölscher and Dr. Simon Gengler who provided the mice. My gratitude extends to Dr. John Worthington for his advice and suggestions and to Alex Hardgrave and Beth Gallagher for their assistance.

I would also like to thank my incredible family and partner, Theo Dourambeis for their continuous love and support, which without, this project would not have been possible.

Declaration

I declare that this thesis is my own work submitted for the degree of Masters (by research) in Biomedical Science at Lancaster University. This work has not been previously submitted to another University or Institute of Learning for the award of a higher degree.

Contents

Abstract	2
Acknowledgements	4
Declaration	4
Contents	5
List of Figures	9
List of Tables	14
List of Abbreviations	15

1. Literature review

1.1 Organisation of the Gastrointestinal (GI) Tract.....	18
1.2 The Gut Microbiota.....	20
1.3 Balancing the Microbiota through Life	23
1.4 Alzheimer’s disease (AD)	26
1.5 Dysbiosis and AD.....	32
1.6 Possible Origins of Dysbiosis in AD.....	35
1.7 The Gut-Brain Axis is Dysfunctional in AD.....	38
1.8 Components of the GBA in Ageing and AD	
1.8.1 Gut epithelial barrier	41
1.8.2 Blood brain barrier (BBB)	42
1.8.3 Lipopolysaccharides (LPS).....	43
1.8.4 Short Chain Fatty Acids (SCFAs).....	44
1.8.5 Enteroendocrine Cell’s (EEC’s) and Peptides	46
1.8.6 Glucagon-like peptide (GLP-1).....	47
1.8.7 Peptide YY (PYY).....	48
1.8.8 Cholecystokinin (CCK).....	49
1.8.9 Serotonin.....	49
1.8.10 Neuroinflammation.....	50
1.9 Targeting the GBA for Treatment.....	51

2. Project Aims	53
------------------------------	-----------

3. Materials

3.1 Reagents.....	54
3.2 Buffers and solutions.....	55
3.3 Antibodies.....	56
3.4 PCR Primers.....	57

4. Methods

4.1 Animals.....	58
4.2 Tissue Processing.....	59
4.3 Histological Staining	
4.3.1 Periodic Acidic-Schiff (PAS) Alcian Blue (AB) Stain.....	60
4.3.2 Light Microscope.....	60
4.3.4 Fluorescent Immunohistochemistry (IHC).....	61
4.4 Bacterial 16S rDNA Extraction.....	62
4.5 16S rDNA Quantitative Real Time Polymerase Chain Reaction (qRT-PCR).....	62
4.6 Denaturing Gel Gradient Electrophoresis (DGGE)	
4.6.1 PCR and Purification for DGGE.....	63
4.6.2 Reagent Preparation.....	64
4.6.3 Pouring the Gradient Gel.....	64
4.6.4 Gel Visualisation.....	65
4.7 Statistical Analysis.....	66

5. Results.....67

5.1 Seven-month APP/PS1 mice

5.1.1 Assessment of crypt depth and villus height revealed no overt morphological differences, however EEC numbers are decreased in seven-month APP/PS1 mice.....	68
5.1.2 A decrease in the phylum Firmicutes was observed in seven-month APP/PS1 mice.....	79
5.1.3 No difference in bacterial community was seen in seven-month APP/PS1 mice.....	81

5.2 Fifteen-month APP/PS1 mice	
5.2.1 A decrease in goblet cell numbers was observed in the ileum of fifteen-month APP/PS1 mice.....	100
5.2.2 No difference in bacterial community was observed in fifteen-month APP/PS1 mice.....	109
5.3 Three-month APP/PS1 mice	
5.3.1 Crypt depth is decreased in the colon of the APP/PS1 three-month mice.....	129
5.3.2 Microbial diversity is altered in the caecum of three-month APP/PS1 mice.....	138

6. Summary of Results

6.1 Villus height and crypt depth.....	137
6.2 Goblet cell count.....	137
6.3 EEC count.....	148
6.4 Microbial community diversity – qRT-PCR.....	148
6.5 Microbial community diversity – DGGE.....	149
6.6 Average total number of DGGE bands.....	150

7. Discussion

7.1 Dysbiosis in the large intestine occurs in early AD pathology.....	151
7.2 Firmicutes is decreased in colon of fifteen-month mice.....	155
7.3 Dysbiosis is normalised by fifteen-months.....	157
7.4 Sex specific differences.....	159
7.5 Early life microbiota is crucial in the development of disease.....	160
7.6 Utilising the microbiota in the diagnosis and treatment of AD.....	161
7.7 Altering lifestyle behaviours may prevent AD.....	162
7.8 Future work.....	163

8. Conclusion.....	166
9. References.....	168

List of Figures

Figure 1. The cellular organisation of the small and large intestine.....	18
Figure 2. The abundance and predominant microbiota in regions of the GI tract.....	22
Figure 3. Proportions of the main bacterial phyla in the gut throughout life.....	24
Figure 4: The processing of the amyloid precursor protein (APP) via the amyloidogenic and non-amyloidogenic pathway.....	27
Figure 5: The amyloid cascade hypothesis.....	30
Figure 6: Overview of the gut-brain axis.....	39
Figure 7: Histological analysis of the gut in WT and APP/PS1 seven-month mice.....	69
Figure 8: Average number of goblet cells in WT and APP/PS1 seven-month mice.....	71
Figure 9: Representative PAS/AB stained sections in WT and APP/PS1 seven-month mice.....	73
Figure 10: Normal rabbit IgG isotype controls for CgA.....	74
Figure 11: Average number EEC's in WT and APP/PS1 seven-month mice.....	76
Figure 12: Representative flurorescent IHC images of the number of EEC's in seven-month WT and APP/PS1 mice.....	77
Figure 13: Average number of EEC's in male and female WT and APP/PS1 seven-month mice.....	78
Figure 14: Relative percentage change of predominant mucosal-associated phyla in seven-month mice.....	80

Figure 15: Mucosal bacterial community profiling from the ileum of WT and APP/PS1 seven-month mice.....	83
Figure 16: Average total number of bands from a 16S rDNA DGGE of the mucosal bacterial community from the ileum of seven-month WT and APP/PS1 mice.....	84
Figure 17: Luminal bacterial community profiling from the ileum of WT and APP/PS1 seven-month mice	86
Figure 18: Average total number of bands from 16S rDNA DGGE of the luminal bacterial community from the ileum of seven-month WT and APP/PS1 mice.	87
Figure 19: Mucosal bacterial community profiling from the caecum of WT and APP/PS1 seven-month mice.....	89
Figure 20: Average total number of bands from 16S rDNA DGGE of mucosal bacterial community from the caecum of seven-month WT and APP/PS1 mice....	90
Figure 21: Luminal bacterial community profiling from the caecum of WT and APP/PS1 seven-month mice.....	92
Figure 22: Average total number of bands from 16S rDNA DGGE of the luminal bacterial community from the caecum of seven-month WT and APP/PS1 mice	93
Figure 23: Mucosal bacterial community profiling from the distal colon of WT and APP/PS1 seven-month mice.....	95
Figure 24: Average total number of bands from 16S rDNA DGGE profile of mucosal bacterial community from the distal colon of seven-month WT and APP/PS1 mice	96
Figure 25: Luminal bacterial community profiling from the distal colon of WT and APP/PS1 seven-month mice.....	98

Figure 26: Average total number of bands from 16S rDNA DGGE profile of luminal- bacterial community from the distal colon of seven-month WT and APP/PS1 mice.	99
Figure 27: Histological analysis of the gut in fifteen-month mice.....	101
Figure 28: Average number of goblet cells in fifteen-month mice.....	103
Figure 29: Representative PAS/AB stained sections in fifteen-month mice.....	105
Figure 30: Average number of goblet cells in the ileum of male and female fifteen-month mice.	106
Figure 31: Average number of EEC's in fifteen-month mice.....	108
Figure 32: Relative percentage change of predominant mucosal-associated phyla in fifteen-month mice.....	110
Figure 33: Mucosal bacterial community profiling from the ileum of WT and APP/PS1 fifteen-month mice.	112
Figure 34: Average total number of bands from 16S rDNA DGGE profile of mucosal- bacterial community from the ileum of fifteen-month WT and APP/PS1 mice.....	113
Figure 35: Luminal bacterial community profiling from the ileum of WT and APP/PS1 fifteen-month mice.....	115
Figure 36: Average total number of bands from 16S rDNA DGGE profile of luminal- bacterial community from the ileum of fifteen-month WT and APP/PS1 mice	116
Figure 37: Mucosal bacterial community profiling from the caecum of WT and APP/PS1 fifteen-month mice.....	118
Figure 38: Average total number of bands from 16S rDNA DGGE profile of the mucosal bacterial community from the caecum of fifteen-month WT and APP/PS1 mice.....	119

Figure 39: Luminal bacterial community profiling from the caecum of WT and APP/PS1 fifteen-month mice.....	121
Figure 40: Average total number of bands from 16S rDNA DGGE profile of luminal- bacterial community from the caecum of fifteen-month WT and APP/PS1 mice.....	122
Figure 41: Mucosal bacterial community profiling from the distal colon of WT and APP/PS1 fifteen-month mice.....	124
Figure 42: Average total number of bands from 16S rDNA DGGE profile of mucosal- bacterial community from the distal colon of fifteen-month WT and APP/PS1 mice	125
Figure 43: Luminal bacterial community profiling from the distal colon of WT and APP/PS1 fifteen-month mice.....	127
Figure 44: Average total number of bands from 16S rDNA DGGE profile of luminal- bacterial community from the distal colon of fifteen-month WT and APP/PS1 mice.	128
Figure 45: Histological analysis of the gut in WT and APP/PS1 three-month mice.	130
Figure 46: Representative images of WT and APP/PS1 three-month mice.....	131
Figure 47: Average colonic crypt depth in male and female WT and APP/PS1 three-month mice	132
Figure 48: Average number of goblet cells in WT and APP/PS1 three-month mice	133
Figure 49: Average number of EEC's in WT and APP/PS1 three-month mice.....	135
Figure 50: Representative fluorescent IHC images of the number of EEC's in three-month WT and APP/PS1 mice.	136
Figure 51: Average number of EEC's in male and female WT and APP/PS1 three-month mice	137

Figure 52: Relative percentage change of predominant mucosal-associated phyla in three-month mice.....	138
Figure 53: Mucosal bacterial community profiling from the caecum of WT and APP/PS1 three-month mice.....	141
Figure 54: Average total number of bands of 16S rDNA DGGE associated with the mucosal bacterial community from the caecum of three-month WT and APP/PS1 mice.....	142
Figure 55: Luminal bacterial community profiling from the caecum of WT and APP/PS1 three-month mice.....	145
Figure 56: Average total number of bands of 16S rDNA DGGE associated with the luminal bacterial community from the caecum of three-month WT and APP/PS1 mice.....	146

List of Tables

Table 1: Overview of studies investigating dysbiosis at the phylum level in patients and animal models of AD.....	32
Table 2: Summary of the types of EEC's in the GI tract, their primary location and the peptide(s) they secrete.....	46
Table 3: Reagents and manufacturer details.....	54
Table 4: Solutions and their compositions.....	55
Table 5: Antibodies with supplier details and concentrations used.....	56
Table 6: 16S PCR primer sequences.....	57
Table 7: Universal and phylum specific qPCR forward and reverse primers sequences for the 16S gene.....	57
Table 8: Summary of statistical analysis of crypt depth and villus height.....	147
Table 9: Summary of statistical analysis of goblet cell numbers.....	147
Table 10: Summary of statistical analysis of enteroendocrine cell numbers...	148
Table 11: Summary of statistical analysis of qRT-PCR data.....	148
Table 12: Summary of statistical analysis of DGGE profile data.....	149
Table 13: Summary of statistical analysis of the number of bands from DGGE profiles.....	150

List of Abbreviations

5-HT = serotonin
A β = amyloid- β peptide
AB = alcian blue
ACID = amyloid intracellular domain
AD = Alzheimer's disease
ApoE = apolipoprotein
APP = amyloid precursor protein
ANS = autonomic nervous system
BBB = blood brain barrier
BSA = bovine serum albumin
CCK = cholecystokinin
CgA = chromogranin A
CNS = central nervous system
CSF = cerebrospinal fluid
CTF = carboxy-terminal fragment
DGGE = denaturing gel gradient electrophoresis
dH₂O = distilled H₂O
EEC = enteroendocrine cell
ENS = enteric nervous system
ERK = extracellular signal-regulated kinase
GBA = gut brain axis
GF = germ free
GI = gastrointestinal
GIP = gastric inhibitory polypeptide
GLP-1 = glucagon-like peptide 1
GLP-1R = glucagon-like peptide 1 receptor
GLP-2 = glucagon-like peptide 2
GPR = G-protein coupled receptor
HFD = high fat diet
IBD = inflammatory bowel disease
IBS = irritable bowel disease

IFN = interferon
IHC = immunohistochemistry
IR = insulin receptor
IRS = insulin receptor substrate
JAM-A = junction adhesion molecule A
LPS = lipopolysaccharide
LRP-1 = low density lipoprotein receptor-related protein 1
MAMP = microbiota-associated molecular pattern
MAPK = mitogen-activated protein kinase
MAPT = microtubule associated protein tau
MCI = mild cognitive impairment
Min = minute
NF κ B = nuclear factor κ B
NMDS = non-metric multi-dimensional scaling
NSAIDs = non-steroidal anti-inflammatory drugs
PAS = periodic acid-Schiff
PAS/AB = Periodic acid-Schiff / Alcian blue
PBS = phosphate buffered saline
PCR = polymerase chain reaction
PSEN = presenilin
PYY = peptide YY
qRT-PCR = quantitative real time polymerase chain reaction
rRNA = ribosomal RNA
rDNA = ribosomal DNA
RT = room temperature
sAPP = secreted APP
SCFA = short chain fatty acid
SEM = standard error of mean
SPF = specific pathogen free
TEMED = tetramethylethylenediamine
TLR = toll-like receptor
TNF = tumour necrosis factor
TPH = tryptophan hydroxylase

UPGMA = unweighted pair group method with arithmetic mean

WD = western diet

WT = wild type

ZO-1 = zonula occludens-1

1. Literature review

1.1 Organisation of the Gastrointestinal (GI) Tract

The gastrointestinal (GI) tract is an organ system that extends from the mouth to the anus of an organism, including the oesophagus, stomach, small and large intestine (Nguyen et al., 2015). Each region of the GI tract is adapted to optimally perform its function. The small intestine is divided into three regions, namely: the duodenum, jejunum and ileum, which functions to absorb nutrients, water and salt from digested food. Finger like structures known as villi project into the lumen, and the epithelial cells which line the villi also contain tiny protrusions known as microvilli. Together, these structures dramatically increase the surface area allowing for maximum absorption. The small intestine also possesses glandular invaginations into the underlying lamina propria, known as the crypts of Lieberkühn, as shown in figure 1 (Hosoyamada & Sakai, 2005; Humphries & Wright, 2008).

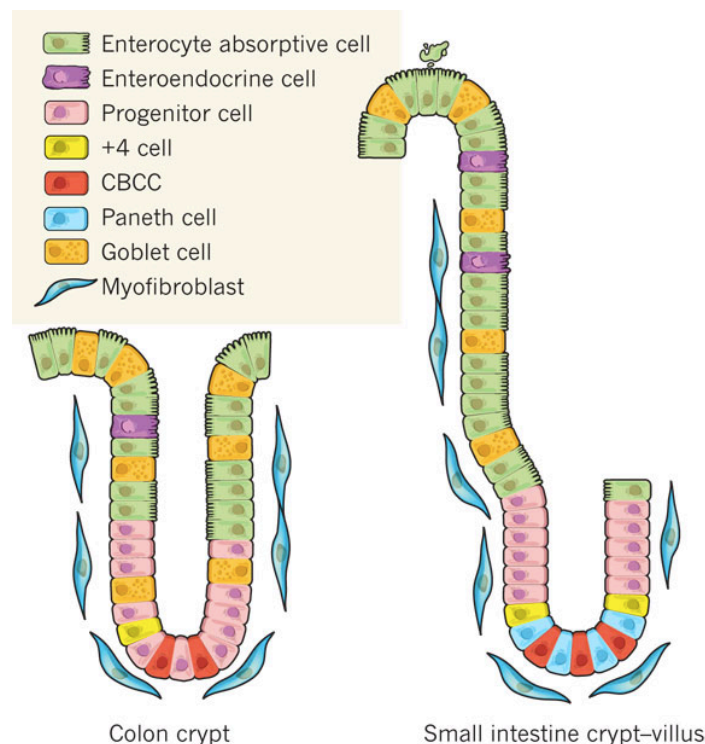


Figure 1: The cellular organisation of the small and large intestine. The small intestine (left) contains villi and crypts whereas the colon (right) contains only crypts. The small and large intestine share several types of cells including: enterocytes, goblet cells, enteroendocrine cells, however Paneth cells are only located in the crypts of the small intestine. Figure taken from Medema and Vermeulen, 2011.

The large intestine, commonly referred to as the colon, only possesses crypts. The colon functions to ferment undigested dietary carbohydrates, reabsorb water from the lumen and store faeces. The caecum, a sac like structure at the proximal end of the large intestine, is also vital in some mammals for fermentation; however in humans its function is near redundant (Gill et al., 2018).

The various cell types of the GI tract are also highly specialised. Enterocytes are present throughout the small and large intestine, and are responsible for the uptake of water and nutrients from the lumen. Goblet cells are mucus-secreting cells which form the mucus layer(s) of the GI tract. They are located in the small and large intestine, however are more abundant towards the colon (Birchenough et al., 2015). Enteroendocrine cells (EEC's) are rare, accounting for 1% of the total epithelial cell count. There are several types of EEC's including: enterochromaffin (EC) cells, L cells D cells and M cells, with their abundance being less diverse in the colon than the small intestine. Examples of hormones secreted by EEC's include: serotonin (5-HT), peptide YY (PYY) and glucagon-like peptide 1 (GLP-1), each of which has specialised functions (Gunawardene, Corfe & Staton, 2011). In contrast, Paneth cells are located in the crypts of the small intestine, although few may be found in the caecum/ appendix, and are involved in secreting anti-microbial peptides (Muniz, Knosp & Yeretssian, 2012).

Located within the wall of the GI tract is the enteric nervous system (ENS), often described as the 'second brain' due to several similarities, such as structure and function, shared with the brain (Abot, Cani & Knaug, 2018). The ENS is organised into two major ganglionated plexuses composed neurons and enteric glia, the former of which allows the ENS to operate independently of the CNS and in conjunction with the vagus nerve. The submucosal plexus is located between the muscle layers and the mucosa, and functions to control glandular secretion and gut motility. The second ganglionated plexus, the myenteric plexus, is located between the muscle layers and also regulates gut motility (Breit et al., 2018; Furness, 2012). The ENS also has an important role in immune and endocrine

function by modulating intestinal immune homeostasis and responding to peptide hormones secreted by EEC's (Abot, Cani & Knaug, 2018).

1.2 The Gut Microbiota

Within the GI tract resides a community of organisms including bacteria, archaea, viruses and unicellular eukaryotes, collectively known as the gut microbiota (D'Argenio & Salvatore, 2015). Characterising the gut microbiota has become increasingly accessible over the years due to the introduction of molecular techniques, enabling sequencing of the 16S ribosomal RNA (rRNA) gene (Mayer, Savidge & Schulman, 2014; Odamaki et al., 2016).

Estimates suggest the gut contains in the region of one to one hundred trillion microbes, consisting of up to 1000 different bacteria species (Amon & Sanderson, 2017). The most abundant bacteria phyla are Firmicutes and Bacteroidetes, with Proteobacteria, Actinobacteria, Fusobacteria and Verrucomicrobia present in a lower abundance (Eckurg et al., 2005). However, it is also important to note that abundance is also dependent on the location within the GI tract, as shown in figure 2.

The gut microbiota can either reside within the lumen or be associated with the mucosal layer in the small or large intestine. An oxygen gradient is present between the lumen and the mucosal layer resulting in anaerobic microbes tending to reside in the lumen and anaerobes in the mucosal layer, with microbes exhibiting a spectrum of aerotolerance between the two regions (Tang et al., 2015).

The mucosal layer in the small intestine comprised of MUC2, is discontinuous and not attached to epithelial cells. The mucosa of the colon is also composed of MUC2 however in contrast, the mucosa consists of two layers; the inner most is continuously secreted by the goblet cells, resulting in a dense layer that is attached to the epithelial cells and is mostly devoid of microbiota. The outer layer, which harbours the vast majority of the mucosal microbiota, is flexible and unattached to the epithelium (Johansson, Sjövall & Hansson, 2013). The mucosal-associated microbiota have an important role in the functioning of the immune system. This transpires through direct contact with the epithelial cells or indirectly through the use of microbiota-associated molecular patterns (MAMPs) on the surface of bacteria or metabolites produced by the microbiota (Van den Abbeele et al., 2011).

In contrast, the microbiota residing in the lumen primarily function in the fermentation of undigested dietary compounds to produce energy substrates utilised by the host, in addition to synthesising vitamin K and B12 and amino acid metabolism (LeBlanc et al., 2013; Lin et al., 2017; Morrison & Preston, 2016). It has been suggested that the mucosal-associated microbiota is maintained by the microbes residing within the lumen, the immune system and the correct functioning of the epithelial barrier (Tang et al., 2015).

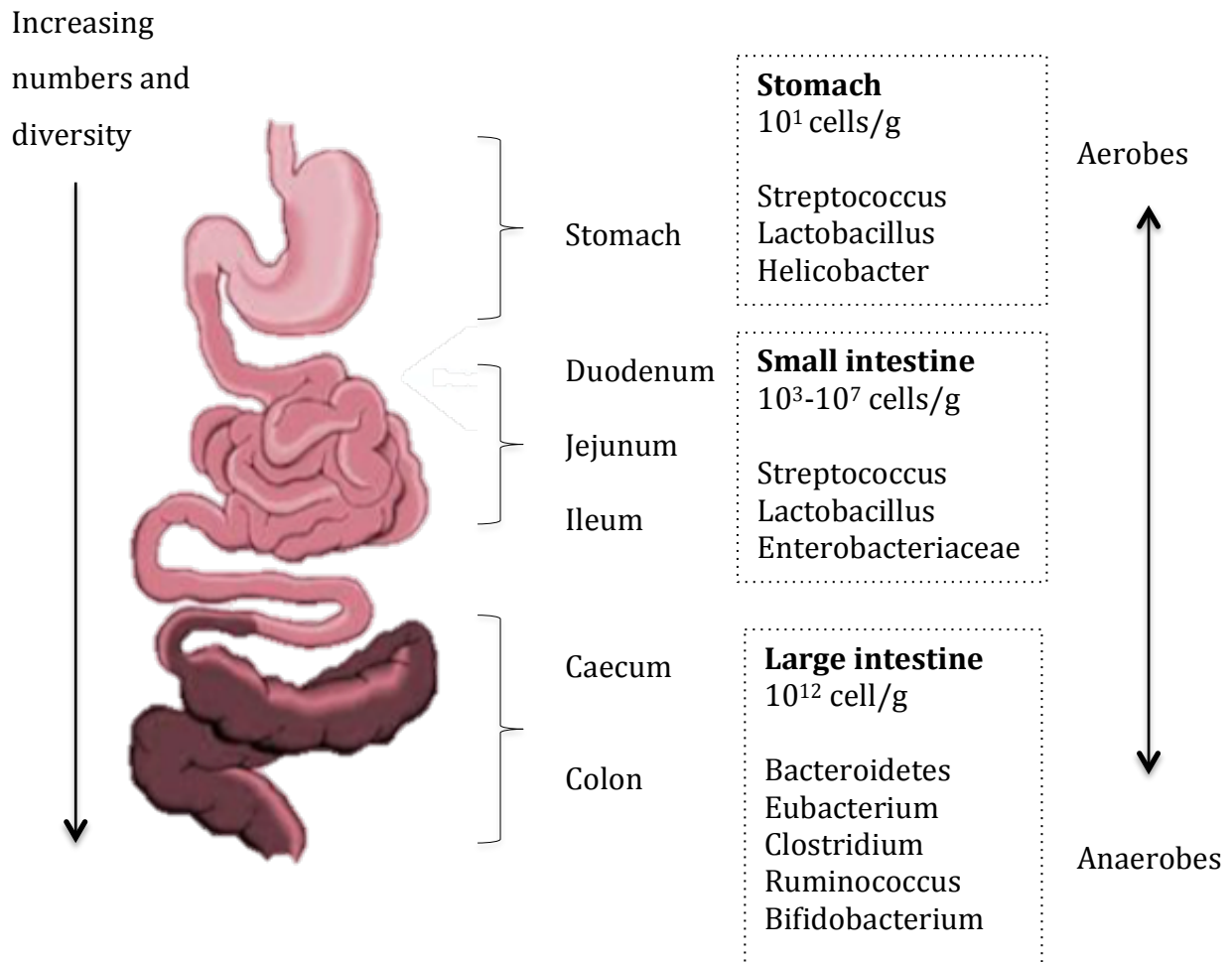


Figure 2: The abundance and predominant microbiota in regions of the GI tract. The stomach contains the fewest number of microbes which are mostly aerobes. In contrast, the colon has the greatest number of microbes, which are characterised by anaerobes. Adapted from Sekirov et al. (2010), Simrén et al. (2012) and Tsabouri et al. (2014).

1.3 Balancing the Microbiota through Life

The importance of the gut microbiota, although not a novel concept, is one that has been previously overlooked in the study of health and disease. However, a major breakthrough in microbiome research came with the initiation of the Human Microbiome Project in 2008. The aim was to sequence the 16S rRNA gene from three hundred healthy individuals across fifteen body sites to gain a greater understanding of the role the microbiota plays in health and disease (Cho & Blaser, 2012; WWW, NIH Human Microbiome Project).

The gut microbiota does not remain constant through life, as shown in figure 3. Experiments previously utilising culture-based techniques led to the conclusion that the amniotic fluid and placenta are sterile. However, molecular techniques have revealed that both areas may harbour a microbiota; therefore development of the microbiota could actually start *in utero* (Collado et al., 2016; Perez-Muñoz et al., 2017). Correlations between the microbiota from the amniotic fluid, placenta and infant meconium have been identified and are characterised by low diversity, low richness and the dominance of the phylum Proteobacteria (Ardisson et al., 2014; Collado et al., 2016).

There is a high degree of variability in the microbiota of neonates, which is largely dependent on environmental factors. Neonates delivered via caesarean have a microbiota across several body sites, including the gut, that resembles the maternal skin, whereas the microbiota of vaginally delivered neonates resembles that of the maternal vagina (Dominguez-Bello et al., 2010). Furthermore, the gut microbiota of breast-fed infants is dominated by the genera *Bifidobacterium* and *Bacteroides*, as their growth is stimulated by the presence of undigested human milk oligosaccharides in the colon (Marcobal & Sonnenburg, 2012; Wang et al., 2015). In contrast, formula-fed infants have more *Streptococcus* and *Enterococcus* than breast-fed infants (Timmerman et al., 2017). In addition, several studies have also highlighted that infant microbiota is influenced by antibiotic use and feeding patterns (Yang et al., 2016).

At three years of age, the gut microbiota stabilises and remains relatively constant through adulthood with Firmicutes and Bacteroidetes being the dominant phyla and Proteobacteria, Actinobacteria, Fusobacteria and Verrucomicrobia present in lower abundance (Eckurg et al., 2005).

A decrease in the Firmicutes to Bacteroidetes ratio is often associated with an elderly gut microbiota. Claesson et al. (2011) observed Bacteroidetes accounted for 57% and Firmicutes 40% of the total gut microbiota, however large inter-individual variations were also reported with Bacteroidetes ranging between 3-92% and Firmicutes 7-94%.

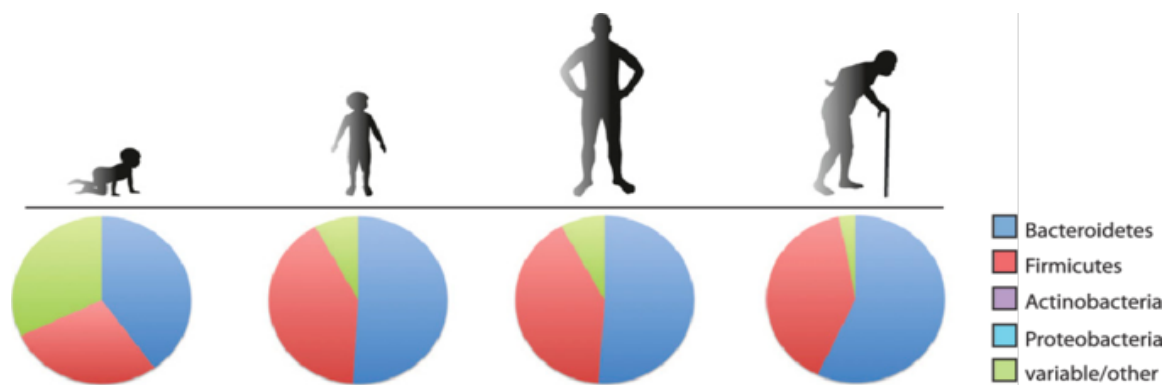


Figure 3: The proportions of the main bacterial phyla in the gut throughout life. The infant microbiota is characterised by high variability which is a result of its environment. At three years of age the gut microbiota stabilises and remains constant until old age where an increase in Bacteroidetes and decrease in Firmicutes is observed (Claesson et al, 2011). Adapted from Kostic, Howitt & Garrett (2013).

Interestingly, centenarians have a gut microbiota profile that is distinct from normal elderly populations, characterised by decreased diversity (Biagi et al., 2010). This may suggest that the secret to longevity may be in the gut microbiota. However, discrepancies in microbiota profiles often exist in studies of centenarians due to small sample size, isolated geographical locations and a lack of longitudinal studies, making it difficult to draw consistent and meaningful conclusions.

In addition to age, the gut microbiota is also shaped by genetic and environmental factors. For example, infants possess a gut microbiota with low diversity that could be due to the lack of variety in the diet and the high level of fermentation of undigested oligosaccharides from milk. In contrast, children and adults who eat solid food have a more varied diet which is reflected by the greater diversity in their microbiota (Tamburini et al., 2016). Regardless of the individual's age and requirements, imbalances in the normal gut microbiota communities, termed dysbiosis, is usually associated with a negative impact on health and is associated with several diseases including Parkinson's disease (PD), inflammatory bowel disease (IBD), type 2 diabetes, allergies and more recently Alzheimer's disease (AD) (Nguyen et al., 2015).

1.4 Alzheimer's Disease

Alzheimer's disease (AD) is a progressive, neurodegenerative disorder, first identified in 1907 by the Bavarian psychiatrist, Alois Alzheimer (Tanzi & Bertram, 2005). AD is the most common form of dementia, accounting for around 50-70% of cases, and is becoming an increasing problem due to the greatest risk factor being age and the presence of an expanding ageing population. In 2015, 46.8 million people worldwide were estimated to be living with dementia which is expected to reach 131.5 million by 2050. This places not only a strain on society, but also a financial burden on governments and health care systems with the worldwide cost of AD estimated as \$818 billion in 2016, which was predicted to increase to a trillion dollars in 2018 (Winblad et al., 2016; WWW World Alzheimer report, 2016).

The pathology of AD is characterised by the formation of extracellular senile plaques and intracellular neurofibrillary tangles (NFT) in the brain (Cai, Hussain & Yan, 2014). This results in symptoms including: progressive memory loss, issues with orientation and balance, alterations in behaviour, decline in motor functions, loss of speech and eventually death (McKhann et al., 2011).

Senile plaques are composed of β -amyloid ($A\beta$), which is formed through a two-step cleavage of the amyloid precursor protein (APP) located on chromosome 21 (Wiseman et al., 2015). Despite APP being highly expressed in neurons, the normal physiological function of APP is not fully understood but is thought to have roles in modulating the growth of axons and dendritic processes, maintaining synapses and detecting and transducing information involving damage to neurons (van der Kant & Goldstein, 2015). APP can be processed by either the non-amyloidogenic pathway or the amyloidogenic pathway, the latter of which is dominant in AD. The mechanisms of both pathways are described in figure 4.

The resulting $A\beta$ monomers undergo a nucleation phase where they misfold and aggregate to form soluble oligomers. The oligomers then enter the elongation

stage where the addition of further monomers produces protofibrils and eventually an A β fibril, leading to subsequent deposition of senile plaques in the brain (Kumar & Walter, 2011).

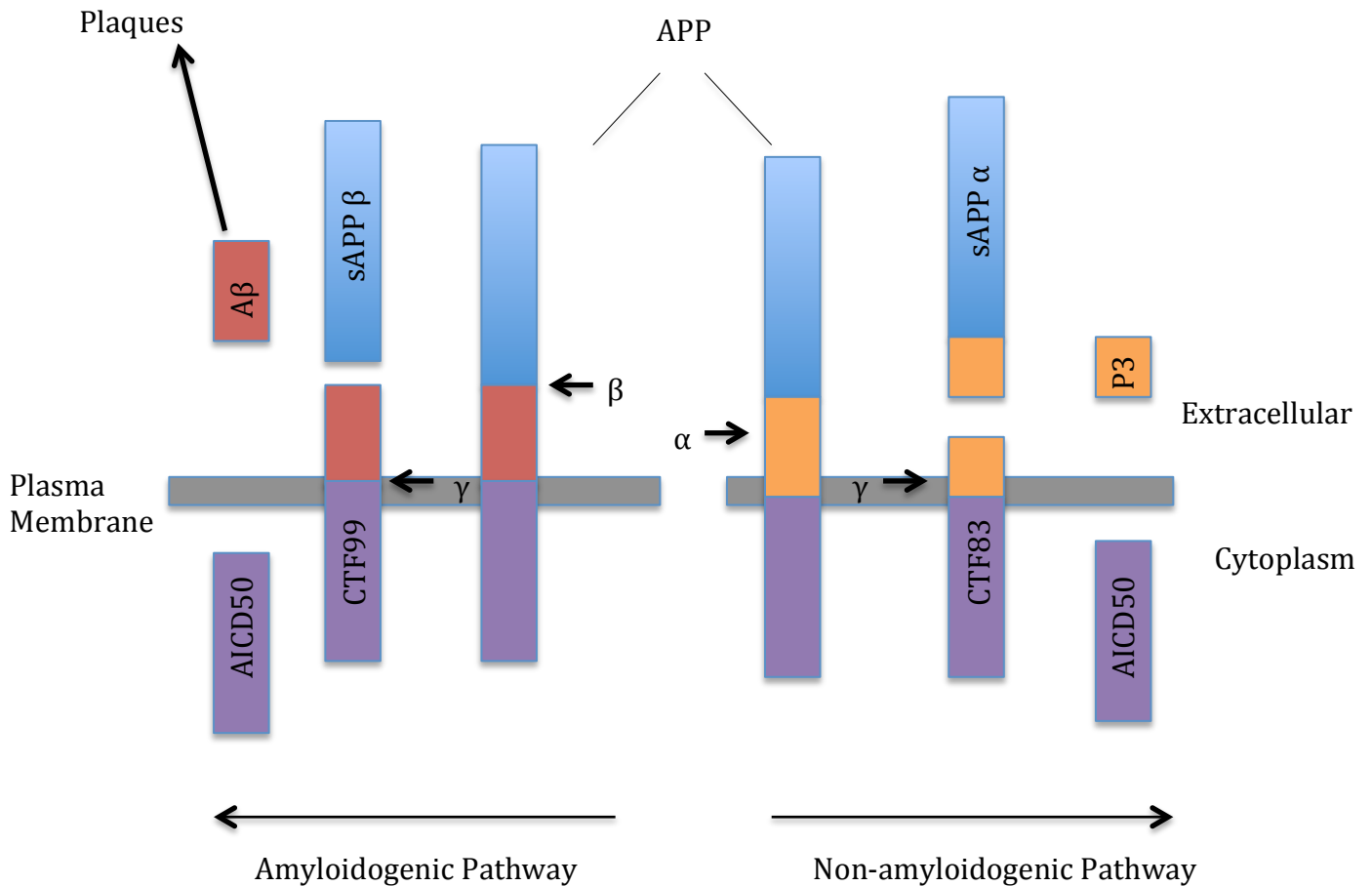


Figure 4: The processing of the amyloid precursor protein (APP) via the amyloidogenic and non-amyloidogenic pathway. APP in the non-amyloidogenic pathway is cleaved firstly by α -secretase to produce CTF83 and sAPP α . CTF83 is then cleaved by γ -secretase to produce an AICD50 and a non-pathological extracellular p3 fragment. In the amyloidogenic pathway APP is cleaved by β -secretase to produce sAPP β and CTF99, the latter of which is then cleaved by γ -secretase to produce AICD50 and pathological A β . γ -secretase does not cleave at a precise amino acid, therefore it is able to generate a variety of A β species varying in length. Approximately 80-90% of the A β generated is 40 amino acids long (A β -40), followed by A β -42 which makes up 5-10% of the population. However, the addition of two hydrophobic amino acids, isoleucine and alanine, at the C-terminal end makes A β -42 more prone to aggregate and therefore more pathological (Bonfilli et al., 2017; Murphy & LeVine 2010; Saito et al., 2011) AICD50 = amyloid intracellular domain 50; APP = amyloid precursor protein; ; CTF83 = carboxyterminal fragment 83; CTF99 = carboxyterminal fragment 99; sAPP α = secreted APP α ; sAPP β = secreted sAPP β . Diagram adapted from Chow et al., (2010).

The second major pathology associated with AD is the intracellular NFT, composed of the microtubule associated protein, tau. In humans, six isoforms exist, each one generated through alternative splicing of the mRNA from the microtubule associated protein tau (*MAPT*) gene. As the name suggests, tau is a microtubule associated protein and interacts with tubulin in neurons to promote their assembly into microtubules. Therefore, tau has a crucial role in axonal transport in neurons, a function controlled by its degree of phosphorylation. In AD, altered kinase and phosphatase activity results in tau becoming hyperphosphorylated and unable to bind to tubulin, causing it to polymerise into paired helical filaments mixed with straight filaments forming NFT. A loss of microtubule associated transport in neurons results in cell death (Bonfilli et al., 2017; Medina, Hernández & Avila, 2016).

The amyloid cascade hypothesis, shown in figure 5, has been at the forefront of our understanding of AD for the last 25 years, and has been the primary focus of drug targets (Hardy & Higgins, 1992). The central point of the hypothesis is that the presence of A β is responsible for the downstream effects of AD that eventually results in cognitive decline. More recently, accumulating evidence such as the presence of A β in the brain of healthy non-cognitively impaired individuals, and that A β load does not always correlate with disease severity, has suggested that an update or reconsideration of the amyloid cascade hypothesis may be required (Chételat et al., 2013). In addition, attention has turned to the theory that oligomers could be the most toxic species. Rats injected with oligomers into the left lateral ventricle show a greater degree of neurodegeneration and memory impairment than those injected with fibrils (He et al., 2012). Furthermore, reducing A β oligomers in aged mice using the D-enantiomeric peptide, RD₂ has shown to improve cognition, learning and reduce anxiety behaviour (Schemmert et al., 2018).

Despite the discussions surrounding the amyloid cascade, much of the core ideas still remain relevant (Hardy & Higgins, 1992). The first assumption of the hypothesis is that the origin of AD is either familial or sporadic. Familial AD is responsible for approximately 5% of cases and typically occurs before the age of

65. Mutations in the amyloid precursor protein (*APP*), presenilin 1 (*PSEN1*) or presenilin 2 (*PSEN2*) genes are inherited in an autosomal dominant fashion (Heneka, Golenbock & Latz, 2015; Hill et al., 2014). Early recognition of the genetics of familial AD was demonstrated by individuals with Down syndrome having a propensity to develop AD at a young age due to Trisomy 21, the same chromosome *APP* is located on (Olson and Shaw, 1969). In contrast, sporadic AD accounts for roughly 95% of cases and typically occurs after the age of 65 (Hill et al., 2014). Sporadic AD can be considered more complex due to a combination of environmental risk factors such as: age, stress, infection and inflammation, diabetes, education level, pesticides and herbicides, in addition to presence of the apolipoprotein E (ApoE) ϵ 4 allele (Cai, Hussain & Yan, 2014; Corder et al., 1993; Heneka, Golenbock & Latz, 2015, Westfall et al., 2017).

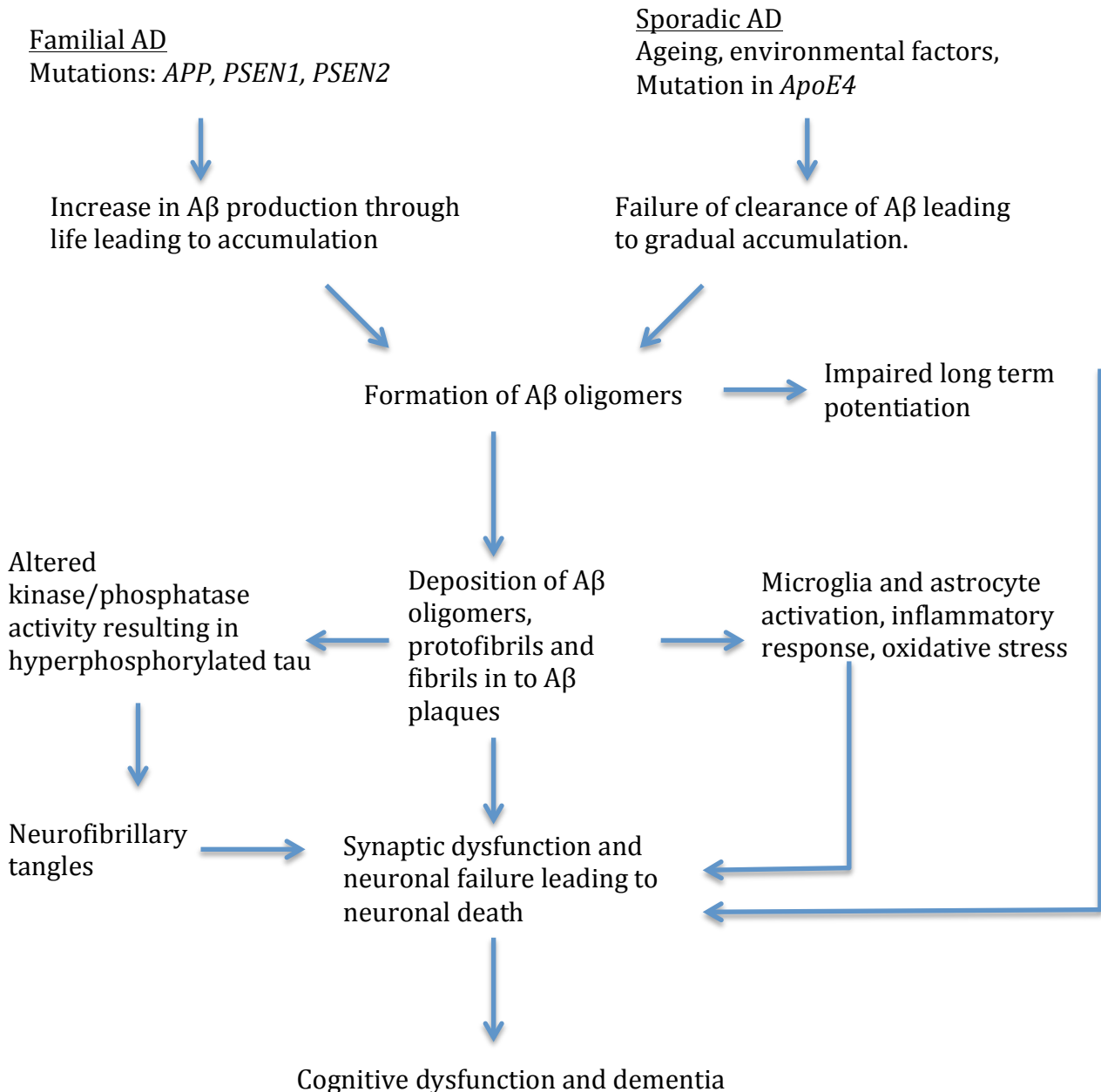


Figure 5: The amyloid cascade hypothesis. The amyloid cascade hypothesis assumes that the accumulation of A β is central to the downstream pathways which ultimately leads to AD. A β accumulation can be initiated by mutations in the *APP*, *PSEN1* or *PSEN2* genes in familial AD leading to an increase in A β over an individual's life. Alternatively, accumulation could arise from sporadic AD where environmental factors or presence of ApoE4 result in an imbalance between the production and clearance mechanisms resulting in A β accumulation. The build-up of A β aggregates in to toxic oligomers, protofibrils and fibrils are deposited as extracellular A β plaques. This leads to microglial and astrocyte activation inducing an inflammatory response and oxidative stress, which ultimately results in synaptic failure and neuronal death. In addition altered kinase and phosphatase activity results in the hyperphosphorylation of tau and deposition of neurofibrillary tangles, which results in neuronal failure and death. The build-up of neuronal death results in progressive cognitive dysfunction and ultimately AD. (Hardy & Higgins, 1992). A β = β -amyloid; AD = Alzheimer's disease, APP = amyloid precursor protein; PSEN1 = presenilin 1; PSEN2 = presenilin 2. Figure adapted from Blennow et al., (2010).

Although sporadic AD has been primarily thought of as a genetic disease with some external environmental factors contributing to pathogenesis, observations of gut dysbiosis have led to the investigation of the internal environment as a potential risk factor. This has led to research groups looking at the possibility that the gut-brain axis may be responsible for or contribute to AD.

1.5 Dysbiosis and AD

As previously discussed, the gut microbiota naturally changes through life, however dysbiosis can also occur and is often associated with disease (Nguyen et al., 2015). As shown in table 1 a limited number of studies have characterised dysbiotic changes in both human and animal models of AD.

<u>Organism and model</u>	<u>Age</u>	<u>Phylum level</u>	<u>Author</u>
AD patients	Elderly	↓ Firmicutes, Actinobacteria ↑ Bacteroidetes	Vogt et al., 2017
AD patients	Elderly	↓ Bacteroidetes ↑ Firmicutes	Provasi et al., 2017
Mice (APP/PS1)	1 month	No significant differences	Harach et al., 2017
	3 month	No significant differences	
	8 month	↓ Firmicutes, Verrucomicrobiota, Actinobacteria, Proteobacteria ↑ Bacteroidetes, Tenericutes	
Mice (5xFAD)	6 week	No significant differences.	Brandscheid et al., 2017
	9 week	↓ Bacteroidetes ↑ Firmicutes	
	18 week	No significant differences	

Table 1. Overview of studies investigating dysbiosis at the phylum level in patients and animal models of AD.

Vogt et al. (2017) studied microbial associated changes in faecal samples of elderly AD patients and found a decrease in microbial richness and diversity when compared to age-matched controls. In particular, a decrease in Firmicutes was due to reductions of several families including *Ruminococcaceae* and *Peptostreptococcaceae*, however some families were also increased. In contrast, the decrease observed in Actinobacteria was solely due to a decrease in the family *Bifidobacteriaceae*. Furthermore, the increase in Bacteroidetes was due to the families: *Bacteroidaceae* and *Rikenellaceae*.

In contrast, Provasi et al., (2017) reported an increase in the phylum Firmicutes and a decrease in Bacteroidetes in elderly AD patients. However, an issue with human AD studies is the potential for environmental factors such as medication and diet to impact dysbiosis, which may account for the differences observed in the studies.

A handful of studies in the literature have investigated dysbiosis in an AD mouse model, particularly the APP/PS1 mouse model. Harach et al. (2017) studied dysbiosis in faecal samples in one, three and a half and eight month APP/PS1 mice. The abundance of Firmicutes was lower in one and three and a half month APP/PS1 mice, however it didn't reach statistical significance until eight months, due to a large decrease observed in the genus *Allobaculum*. Reductions in Verrucomicrobia (with a significant decrease in the genus *Akkermansia*), Proteobacteria and Actinobacteria and an increase in Bacteroidetes (largely in the families Rikenellaceae and S24-7) and Tenericutes were also observed at eight months.

Zhang et al. (2017) investigated dysbiosis in one, three, five to six and eight to twelve month APP/PS1 mice. They found the greatest richness was at five to six months and the greatest decrease in diversity at eight to twelve months. The microbiota profiles of the one and three month APP/PS1 mice was more closely related to the WT counterparts than the aged APP/PS1 to their WT counterparts.

Shen, Liu & Ji (2017) utilised three, six and eight month APP/PS1 and found that diversity was greatest at three month APP/PS1 mice and decreased in an age dependent manner which was not observed in the WT mice. Dysbiosis at the phylum level was not investigated, however significant increases in the families Helicobacteraceae and Desulfovibrionaceae which are both members of the Proteobacteria phylum, was observed in the APP/PS1 mice.

The 5xFAD mouse model of AD, which displays an earlier and more aggressive AD phenotype than the APP/PS1 model has also be studied (Oakley et al. 2006). Brandscheid et al., (2017) examined the gut microbiota at six, nine and eighteen weeks of age and reported no dysbiosis at six or eighteen weeks, however an increase in the phylum Firmicutes and a decrease in Bacteroidetes were observed at nine weeks

These studies highlight that there may be an association between dysbiosis and AD, however there are conflicting results at the phylum level. This could be due different experimental techniques such as DNA extraction, or environmental factors not normalised in the sample collection. Furthermore, reproducibility across different facilities could be an issue, as factors such as the cage, type of bedding and chow have been shown to have a significant effect on the microbiota within the same facility (Ericsson et al., 2018).

1.6 Possible Origins of Dysbiosis in AD

Several lifestyle and environmental factors are thought to cause dysbiosis including: diet, antibiotic use, non-antibiotic medication and travel (Bastard et al., 2017; David et al., 2014; Fröhlich et al., 2016; He et al., 2018). It is also apparent that dysbiosis often coincides with diseases such as AD, PD, autism, type 2 diabetes, irritable bowel syndrome (IBS) and autoimmune diseases (Carding et al., 2015). Whilst several of these diseases have a genetic component, it is now becoming clear that the genetics only predisposes an individual to the disease, and that it is environmental and lifestyle factors that drive changes in the microbiota which is involved in the initiation of disease.

The western diet (WD), characterised by high caloric intake and high amounts of saturated fats and sugars is thought to be associated with an increased risk of developing AD. Consumption of a WD has been reported to decrease levels of the beneficial bacteria of the genera *Bifidobacterium*, *Akkermansia* and *Lactobacillus* (He et al., 2018; Zhang et al., 2010). In addition, the low nutrient value is thought to promote the growth of the phylum Bacteroidetes in the colon due to a decrease in production of SCFA (Cremer, Arnoldini & Hwa, 2017).

Diet induced obesity through consumption of a WD in the E4FAD mouse model, which is genetically predisposed to developing AD due to the presence of the transgenes 5xFAD and human ApoE4, was shown to increase AD pathology such as A β plaque deposition and glial activation compared to E3FAD mice which possess the lower risk ApoE3 allele (Moser & Pike, 2017). The impact of dysbiosis induced by a WD can also be seen in human population-based longitudinal studies. For example, the prevalence of AD in Japan has increased from 1% in 1985 to 7% in 2008, which is thought to be due to a switch to WD over time (Grant, 2014).

Antibiotic use has been associated with a decrease in microbiota diversity (Rogers & Aronoff, 2016). Dethlefsen & Relman (2011) studied the gut microbiota during and after two antibiotic courses of ciprofloxacin. During each

course a decrease in diversity and change in composition of the microbiota was reported by day three to four, although the microbiota began to return to its normal state one week after the course ended. However crucially, the microbiota did not fully return back to its initial state, therefore with each antibiotic course the microbiota deviates slightly further away from its normal state leading to, in some cases, dysbiosis. Furthermore, antibiotic induced dysbiosis has also been shown to have a long-term effect. Jakobsson et al. (2010) followed faecal microbiota profiles in individuals for four years post treatment with clarithromycin and metronidazole. A significant decrease in diversity was seen within one week of treatment, which had not fully recovered four years later.

Whilst there is currently no literature on the use of antibiotics and risk of AD, antibiotic use in childhood has been shown to increase the risk of developing IBD and asthma, which are often associated with dysbiosis (Hviid, Svanström & Frisch, 2011; Risnes et al., 2011). Furthermore, antibiotic use in adults is associated with increased risk of depression, which is also associated with dysbiosis (Jiang et al., 2015; Lurie et al., 2015). The variety of diseases associated with dysbiosis and whose risk is increased by the use of antibiotics may suggest that the risk of AD would also be increased with antibiotic use. However, further studies would be required to confirm this.

In addition to antibiotics, non-antibiotic drugs have also been shown to induce dysbiosis. A large *in vitro* screening of one-thousand non-antibiotic drugs against forty bacterial strains revealed that 24% of drugs whose targets were human cells also impacted the growth of at least one bacterial strain (Maier et al., 2018). There are several examples in the literature of a variety of drugs causing dysbiosis, for example, metformin used to treat type 2 diabetes is associated altered short chain fatty acid (SCFA) production and an increase in *Escherichia coli*. Furthermore, long term use is also thought to increase the risk of developing AD in individuals with type 2 diabetes (Kuan et al., 2017; Zhernakova et al., 2016). In addition, antidepressants have been shown to increase the abundance of the family Enterobacteriaceae (Rogers & Aronoff, 2016). Whilst antidepressants are believed to increase the risk of developing AD, the proposed

mechanism suggested thus far is the drugs anticholinergic properties. However, future studies are required to assess the extent that dysbiosis contributes to the risk of developing AD (Richardson et al., 2018).

Hospital stay, particularly those in an intensive care unit can also cause dysbiosis. Faecal microbiota samples on patients upon their admission and departure of an intensive care unit showed a lower abundance of the phyla Firmicutes and Bacteroidetes, but an increase in Proteobacteria when leaving, showing that the dysbiosis was acquired in hospital. Overall diversity was reduced, with particular reductions in anti-inflammatory bacteria such as the genus *Faecalibacterium* (Lankelma et al., 2017). A decrease in microbiota diversity observed in a murine model of AD, in addition to long term cognitive impairment reported after stays in intensive care units, could suggest that dysbiosis acquired within hospitals may increase the risk of some individuals developing AD, although further studies would be required to confirm this (Pandharipande et al., 2013; Shen, Liu & Ji, 2017; Zhang et al., 2017).

1.7 The Gut-Brain Axis is Dysfunctional in AD

The gut brain axis (GBA) is a bi-directional communication system between the gut and the brain. It is mediated by neuronal factors, endocrine pathways and immunological signalling as shown in figure 6, which are crucial to regulating its functions. The neural branch of the GBA consists of the parasympathetic and sympathetic branches of the autonomic nervous system (ANS) in addition to the ENS. The vagus nerve is a cranial nerve that is part of the parasympathetic arm of the ANS, and is the main afferent pathway from the GI tract to the brain (Rabot et al., 2016; Sherwin et al., 2016). The celiac branch of the vagus nerve innervates the muscular and mucosal layers in the lamina propria and muscularis externa in the gut and controls gut motility, glandular secretions and satiety (Breit et al., 2018). The endocrine pathway includes microbial metabolites and endocrine hormones and the immunological signalling includes cytokines and chemokines (Holzer & Farzi, 2014; Westfall et al., 2017). However, the precise mechanisms of many of the components have not been fully elucidated.

The GBA has numerous functions including: influencing behaviour and mood, regulating neurotransmission, neurogenesis and neuroinflammation in the brain, modulating glucose homeostasis, permeability of the gut barrier and influencing intestinal transit (Sherwin et al., 2016). Dysfunction of the GBA has been associated with several diseases such as: IBS, anxiety and depression, type 2 diabetes, PD and more recently AD (Clapp et al., 2017; Grasset et al., 2017; Kennedy et al., 2014; Perez-Pardo et al., 2017; Pistollato et al., 2016).

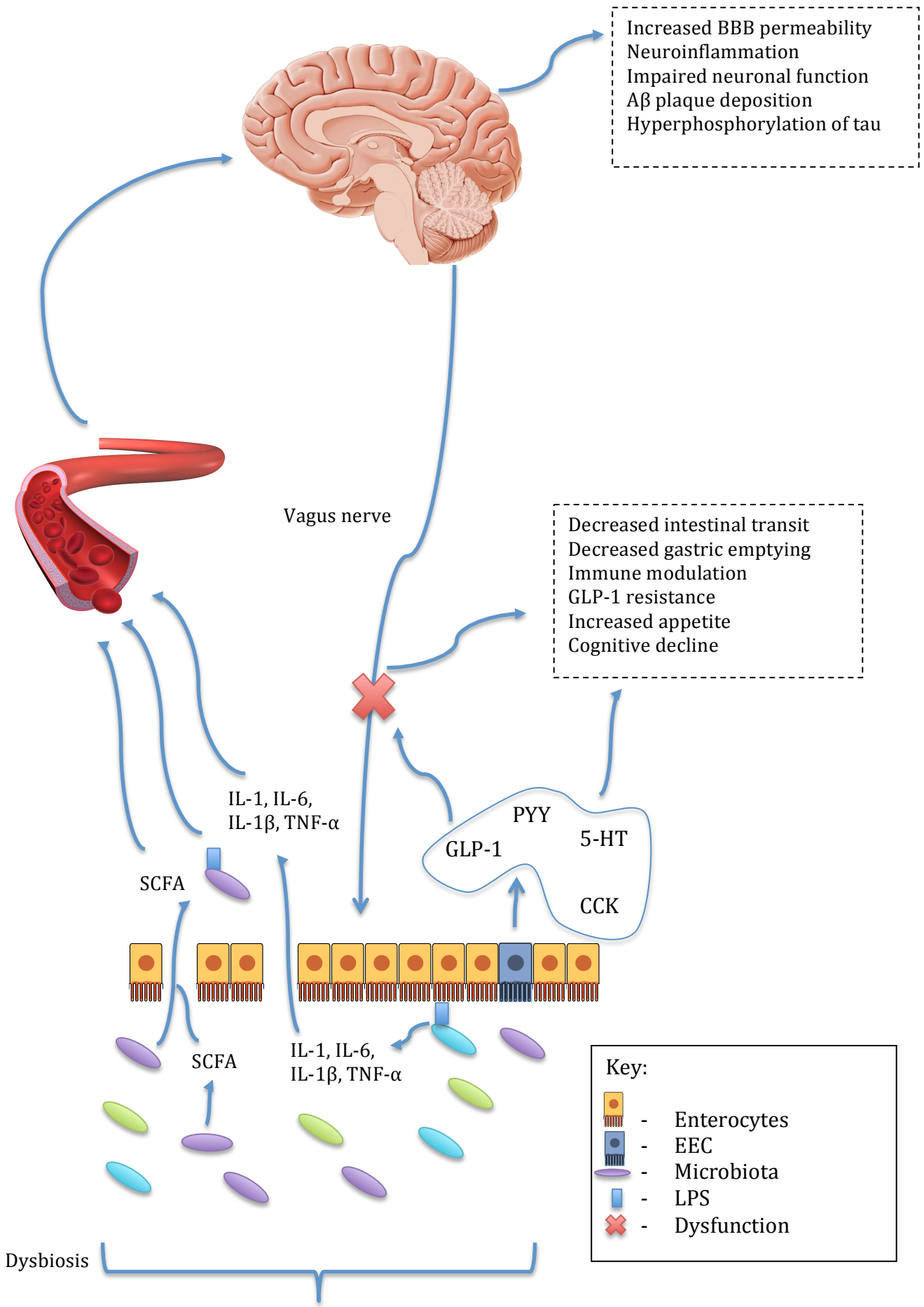


Figure 6: Overview of the gut-brain axis dysfunction in AD. The GBA is a bidirectional communication system linking the gut and its microbiota with the brain. Dysbiosis is observed in the gut in AD, which influences the production of microbial metabolites such as SCFAs. LPS present on the cell surface of Gram-negative bacteria bind to TLR4 on epithelial cells resulting in the release of pro-inflammatory cytokines. Increased permeability of the epithelial gut barrier permits the translocation of SCFA, cytokines and microbiota across the lumen and in to the systemic circulation. They are then able to enter the brain due to an increase in permeability of the BBB, causing neuroinflammation, impaired neuronal function, A β plaque deposition and hyperphosphorylation of tau. The peptide hormone, GLP-1 secreted by EEC's is unable to stimulate the vagus nerve resulting in loss of glucose homeostasis, GLP-1 resistance and insulin resistance which exacerbates AD pathology. High levels of GLP-1 and PYY in AD also result in decreased intestinal transit which promotes dysbiosis. Increased levels of CCK increase appetite, and low levels of 5-HT disrupt the immune system and promote cognitive decline in the brain (Goodall et al., 2018; Grasset et al., 2017; Nazem et al., 2018). 5-HT = serotonin; A β = β -amyloid; AD = Alzheimer's disease; BBB; blood brain barrier; CCK = cholecystokinin; GBA = gut-brain axis; GLP-1 = glucagon like peptide 1; LPS = lipopolysachharide; PYY = peptide YY; SCFA = short chain fatty acid; TLR4 = toll like receptor 4.

Owing to difficulties in studying the GBA in living humans such as the lack of control over factors such as diet, weight and geography means the majority of studies are carried out using animal models. However, the conserved nature of the system between species means animal models still provide a useful tool for GBA studies (Mayer, Savidge & Shulman, 2014). However, differences between the human and murine gut microbiota do exist, for example; the genera *Prevotella*, *Faecalibacterium* and *Ruminococcus* are found to be in greater abundance in humans, whereas *Lactobacillus*, *Alistipes* and *Turicibacter* are more abundant in mice (Nguyen et al., 2015). This creates barriers to the translational relevance of these studies and care must be taken when making conclusions.

Many studies on GBA function utilise animal models with a manipulated microbiota, for example germ free (GF), specific pathogen free (SPF) and gnotobiotic animals (Cryan & Dinan, 2012). Whilst GF animals are useful in colonisation studies, they possess underdeveloped GI tracts and differences in intestinal and central nervous system (CNS) physiology, which can influence the results (Bauer, Hamr & Duca, 2016). Therefore, altering the microbiota through the use of pre/probiotics and antibiotics is also a valuable tool in GBA studies.

Other techniques commonly used as methods to alter the gut microbiota include infection with a known bacteria and colonising animals with the faecal microbiota from another animal (Cryan & Dinan, 2012).

1.8 Components of the GBA in Ageing and AD

1.8.1 Gut epithelial barrier

Ageing in non-human primates has been associated with alterations in the expression of tight junction proteins: zonula occludens-1 (ZO-1), occludin and junction adhesion molecule A (JAM-A) resulting in an increase in epithelial barrier permeability (Tran & Greenwood-Van Meerveld, 2013). Man et al., (2015) also found an increase in epithelial permeability in the human ageing gut, however they report that a localised increase in of the pro-inflammatory cytokine, interleukin (IL) 6 increased the expression of claudin-2, with no changes in ZO-1 or occludin. Interestingly, Tran & Greenwood-Van Meerveld (2013) also found an increase in pro-inflammatory cytokine IL-6, however these discrepancies may be accounted for by differences in the organism investigated and the study of the large versus the small intestine.

Increased gut barrier permeability is commonly reported in AD, and can be demonstrated by bacteria and metabolites that are mostly confined to the GI tract being detected in the systemic circulation. Lipopolysaccharide (LPS), an endotoxin normally preventing from entering the systemic circulation by the gut epithelial barrier, has been reported to be three times higher in the plasma of AD patients compared to controls (Zhang et al., 2009). The increase in epithelial barrier permeability allows for the translocation of bacteria and their metabolites from the lumen of the gut in to the systemic circulation.

1.8.2 Blood Brain Barrier (BBB)

The blood brain barrier (BBB) separates the blood in the microvessels from the CNS parenchyma and prevents large molecules and microbes from entering the brain (Kelly et al., 2015). The BBB consists of endothelial cells, sealed by tight junctions, which line the microvessels. Astrocytes, pericytes, neurons and an extracellular matrix reinforce the barrier and together make up the neurovascular unit (Michel & Prat, 2016).

The permeability of the BBB is influenced by the gut microbiota as Braniste et al. (2014) demonstrated increased permeability in GF mice compared to SPF mice. This was caused by a decrease in the expression of the tight junction proteins occludin and claudin-5, which could be restored by transferring the SPF microbiota to the GF mice.

Similar to the gut epithelial barrier, changes in the BBB permeability has been demonstrated as a natural feature of ageing in humans and mice. A decrease in expression of the tight junction protein ZO-1 was observed in mice, but has not been confirmed in humans. However, the accumulation of serum proteins within the aged human brain suggests BBB disruption, although age associated changes in the BBB of humans still remains poorly characterised (Goodall et al., 2018).

Despite natural changes in BBB permeability associated with ageing, a further increased permeability has been demonstrated in patients with mild cognitive impairment (MCI) compared to healthy age matched controls. Increased serum proteins were found in the cerebrospinal fluid (CSF), in addition to high levels of soluble platelet-derived growth factor β , a biomarker for pericyte injury (Montagne et al., 2015). Furthermore, a transgenic mouse model expressing human APP, which overproduce A β demonstrated a decreased expression of claudin-1 and claudin-5, and an increase expression of matrix metalloproteinase (MMP) 2 and MMP-9 leading to increased BBB permeability. The expression of ZO-1 and occludin was not affected (Hartz et al, 2011).

1.8.3 Lipopolysaccharides (LPS)

LPS, a component of the outer cell wall present in most Gram-negative bacteria, has important functions in maintaining structural integrity of the outer membrane and forming a protective barrier (Steimle, Autenrieth & Frick, 2016).

LPS is able to initiate inflammation both locally and systemically in the body. Localised inflammation in the GI tract is induced by LPS binding to toll like receptor (TLR) 4 on epithelial cells and neurons of the ENS, stimulating the release of pro-inflammatory cytokines including: IL-1, IL-6, IL-1 β and tumour necrosis factor (TNF) α (Nazem et al, 2015). The pro-inflammatory cytokines in the gut are able to communicate with the brain through stimulation of the vagus nerve (Hakansson & Molin, 2011; Nazem et al., 2015).

Systemic inflammation is initiated by the microbiota and LPS translocating across the leaky gut barrier and entering the systemic circulation where LPS can further induce the release of pro-inflammatory cytokines through TLR4. LPS is also able to induce increased permeability of the gut barrier by increasing TLR4 expression and the expression and localisation of CD14 to enterocytes, enhancing its translocation across the epithelial barrier (Guo et al., 2013). Furthermore, cytokines produced locally in the gut are also able to enter the systemic circulation via the same mechanism (Hakansson & Molin, 2011; Nazem et al., 2015).

LPS is also able to enter the brain due to increased BBB permeability, and bind to TLR4 on microglial cells and astrocytes activating them and inducing the release of pro-inflammatory cytokines. In addition, LPS also associates with the neuronal nuclei in the parenchyma, the neocortex and temporal lobe, particularly the hippocampus in AD patients (Zhao et al., 2017; Zhao, Cong & Lukiw, 2017). Furthermore, inflammation initiated by peripheral administration of LPS has been shown to impair A β efflux out of the brain which may contribute to A β accumulation. This may be due to LPS reducing expression of low density lipoprotein receptor-related protein 1 (LRP-1), a receptor involved in A β efflux,

which was demonstrated *in vitro*, however the same results were not reproduced in an *in vivo* mouse model (Erickson et al., 2012).

A crucial factor in inflammation observed in AD may be the microbial communities involved in the dysbiosis, as different types of LPS can induce varying degrees of inflammation. For example: the LPS associated with the commensal species *Bacteroides fragilis* is able to cause a potent microglial activation (Lukiw, 2016). This suggests that the extent of the localised and systemic inflammation could depend on the nature of the dysbiosis.

1.8.4 Short Chain Fatty Acids (SCFA)

The gut microbiota are able to ferment undigested complex carbohydrates, where host endogenous enzymes are absent, resulting in the production of SCFA which the host can utilise as an energy source (Morrison & Preston, 2016). SCFA have several beneficial effects to the host. Butyrate is metabolised and used as the primary energy source of colonic enterocytes, whereas propionate and acetate travel to the liver via the systemic circulation and are involved in gluconeogenesis and lipid biosynthesis (den Besten et al., 2013).

A prominent feature of AD is inflammation, both localised in the gut and in the brain. SCFA have anti-inflammatory effects by regulating cytokine production by immune cells. *In vitro* stimulation of Caco-2 and T84 cells with TNF α and incubation with SCFA reduced the TNF α signalling pathways including nuclear factor κ B (NF κ B), mitogen-activated protein kinase (MAPK) and extracellular signal-regulated kinase (ERK)1/2 resulting in suppression of production of inflammatory cytokines including IL-8 and IL-6 (Hung & Suzuki, 2018). However, dysbiosis in the APP/PS1 mouse model is associated with a decrease in SCFA production with low amounts being detected in both the faeces and brain,

compared to wild type (WT) controls, which could promote pro-inflammatory effects in the gut and brain in AD (Zhang et al., 2017).

There is also evidence to suggest SCFA may also have a role on epithelial gut and BBB integrity. The SCFA butyrate is associated with maintaining barrier function in the colon by influencing the expression of tight junction proteins (Yan & Ajuwon, 2017). Furthermore, SCFA is also able to increase BBB integrity. Mono-colonising GF mice with the butyrate producer *Clostridium tyrobutyricum* or with the acetate and propionate producers *Bacteroidetes thetaiotaomicron* decreased BBB permeability (Braniste et al., 2014).

A reduced SCFA may also have a direct impact on A β pathology, as homeostatic levels of SCFA have neuroprotective roles. Ho et al. (2018) demonstrated *in vitro* that valeric acid, butyric acid and propionic acid reduced A β 40 peptide aggregation, with valeric acid also inhibiting A β 42. Furthermore, valeric acid and butyric acid have the additional benefit of inhibiting A β 40 and A β 42 fibril formation.

1.8.5 Enteroendocrine Cell's (EEC's) and Peptides

EEC's are rare cells, accounting for <1% of the total epithelial population. There are several different types of EECs, each characterised by their location and the peptides they secrete, as shown in table (Gunawardene, Corfe & Staton, 2011).

<u>EEC</u>	<u>Primary Location</u>	<u>Secretory product</u>
EC	Throughout GI tract	5-HT
A (x-like) cells (rat), PD/1 (humans)	Stomach	Ghrelin
ECL cells		Histamine
P cells		Leptin
G cells		Gastrin
D cells	Stomach and small intestine, rare in colon	Somatostatin
I cells	Proximal small intestine	CCK, 5-HT
K cells		GIP, 5-HT
S cells		Secretin
M cells	Small intestine	Motilin
L cells	Distal small intestine and large intestine	GLP-1, GLP-2, PYY, glicentin, ocyntomodulin, 5-HT
N cells	Small and large intestine	Neurotensin

Table 2: Summary of the types of EEC in the GI tract, their primary location and the peptide(s) they secrete. (Furness et al., 2013; Gunawardene, Corfe & Staton, 2011; Latorre et al., 2016). 5-HT = serotonin; CCK = cholecystokinin; EC = enterochromaffin; ECL = enterochromaffin-like cells; GIP = gastric inhibitory polypeptide; GLP-1 = glucagon-like peptide 1; GLP-2 = glucagon-like peptide 2; PYY = peptide YY.

1.8.6 Glucagon-like peptide 1 (GLP-1)

GLP-1 is a hormone secreted from the basolateral side of L cells in response to food and nutrient intake. GLP-1 has different functions depending where it is secreted. When secreted in the small intestine, GLP-1 modulates glucose homeostasis, whereas in the colon, a large part of its function involves controlling intestinal transit (Greiner & Bäckhed, 2016; Wichmann et al., 2013).

GLP-1 secretion is stimulated by SCFA binding to G-protein coupled receptor (GPR) 41 or GPR43 on L-cells, although a recent study proposed that SCFA stimulation of GLP-1 secretion in the colon occurred independently of GPR43 and GPR41 receptors, and suggested it was the metabolism of the SCFA by colonocytes that induced GLP-1 secretion (Christiansen et al., 2018; Psichas et al., 2015). Secreted GLP-1 binds to its receptor, GLP-1R on ENS neurons and the vagus nerve, which stimulates the secretion of insulin from β -cells and inhibits glucagon secretion by α -cells in the islets of Langerhans and induces glucose uptake in to muscle and adipose tissues (Nadkarni, Chepurny & Holz, 2014).

Grasset et al., (2017) found dysbiosis in the ileum induced by a high fat diet (HFD) resulted in GLP-1 resistance. Dysbiosis was associated with a reduction in the expression of GLP-1R and neuronal nitric oxide synthase causing a reduction the synthesis of nitric oxide. This prevented activation of the paracrine ENS signalling pathway and the vagus nerve, resulting in reduced insulin secretion. Interestingly, the type of dysbiosis is thought to influence GLP-1 resistance as mice fed a HFD and no carbohydrates exhibited greater insulin resistance than mice fed a HFD and high carbohydrates.

Furthermore, insulin resistance is commonly associated with AD, and is thought to arise from A β oligomers removing insulin receptors (IR) from the cell membrane of neurons and also inducing an increase of TNF- α . Subsequent activation of the stress kinase JNK results in the phosphorylation of insulin receptor substrate (IRS), preventing activation of IR (Bedse et al., 2015).

Insulin signalling is crucial in synaptic plasticity, learning and memory; therefore its dysfunction contributes to the decline of neuronal function and cognitive dysfunction in AD (Kleinridders et al., 2014). In addition, dysfunctional signalling is also shown to be linked to hyperphosphorylation of tau, however one study suggested it has no impact on the aggregation of tau, although this could be due to the absence of a tau mutation in the hTau model used, as previous studies have demonstrated increased aggregation in P301L transgenic pR5 model which overexpresses tau (Gratuze et al., 2017; Ke et al., 2009).

1.8.7 Peptide YY

Peptide YY (PYY) is a hormone secreted by L cells from the basolateral side in response to food and nutrient intake. PYY has roles in modulating gastric emptying, gastrointestinal mobility, secretion of gastric acid and regulating food intake via interaction with its receptors on the vagus nerve (Cooper, 2014).

A limited number of studies have identified alterations in PYY in the AD. One study identified lower levels of PYY in the brain in AD, which was positively correlated with the severity of AD (Lee et al., 2014). By contrast, no alteration in CSF concentration has been identified (Wikkelsö et al., 1991).

Similarly to GLP-1, SCFA are known to influence the secretion of PYY. Incubation of an *in vitro* intestinal cell line with SCFA showed butyrate and propionate were able to increase the expression and secretion of PYY in the caecum and proximal small intestine (Larraufie et al., 2018).

1.8.8 Cholecystokinin (CCK)

Cholecystokinin (CCK) is secreted from the basolateral side of I cells in the small intestine in response to food and nutrient intake. It is the major satiety hormone and is responsible for release of digestive enzymes from the pancreas, increasing intestinal motility and inhibiting gastric emptying, and has also been shown to have neuroprotective roles during neurogenesis (Steinert et al., 2016; Reisi et al., 2015).

Plasma CCK levels are higher in healthy elderly adults compared to younger adults, however post-mortem analysis shows that CCK levels are reduced in AD (MacIntosh et al., 1999; Mazurek & Beal, 1991). In addition, AD patients and murine models have an increase in appetite, which is not altered by exogenous administration of CCK in 3xTgAD mice, suggesting impaired signalling of CCK in AD (Adebakin et al., 2017; Kai et al., 2015).

1.8.9 Serotonin (5-HT)

Around 90% of the total 5-HT in the body is synthesised from its precursor, the dietary amino acid tryptophan, in the GI tract. EC cells secrete 5-HT apically and basolaterally using the rate limiting enzyme tryptophan hydroxylase 1 (TPH1). Other EEC populations such as: I, K and L cells and also neurons of the ENS make minor contributions, the latter of which utilises the TPH2 isoform (Furness et al., 2013). Additionally, tryptophan can enter the systemic circulation and be converted to 5-HT by serotonergic neurons of the CNS using TPH2 (Jenkins et al., 2016).

5-HT is a neurotransmitter that has several functions in humans including: regulating mood, controlling the circadian rhythm, cognitive function and memory, in addition to recruitment of immune cells, intestinal mobility and secretion in the GI tract (O'Mahony et al., 2015).

The gut microbiota are able to influence levels of 5-HT in the colon, as GF mice display lower levels of 5-HT than SPF mice and GF mice colonised with the faecal microbiota of SPF mice (Hata et al., 2017; Yano et al., 2015). SCFA produced by the microbiota are able to raise 5-HT production by causing increased expression of TPH1 in EC cells, which drives an increase in 5-HT biosynthesis (Yano et al., 2015). SCFA's have been shown *in vitro* to influence 5-HT synthesis by increasing the expression of TPH1 (Reigstad et al., 2015). Therefore, a dysbiosis-associated decrease in SCFA observed in AD is likely decrease 5-HT synthesis (Zhang et al., 2017). In addition, EC cells of the small intestine are enriched in GLP-1R, therefore when GLP-1 is bound 5-HT secretion is stimulated (Lund et al., 2018).

1.8.10 Neuroinflammation

Microglia are the most abundant immune cell in the brain and are activated by pathogens, dying host cells and A β . Known as the macrophages of the brain, microglia remove foreign material and potential threats via phagocytosis and degradation. They also secrete pro-inflammatory cytokines such as IL-1, IL-6, interferon (IFN) γ and TNF- α , which stimulates an immune response in the brain further contributing to A β removal (Tse, 2017).

In the brain, A β activates microglia via TLRs resulting in the secretion of the pro-inflammatory cytokines, chemokines, reactive oxygen species and complement proteins. In addition, microbiota that have entered the brain via the leaky gut barrier and BBB activate microglia by the SCFA propionate (Erny et al., 2015). The chronic activation of microglia, caused by increasing levels of A β leads to the chronic release of pro-inflammatory cytokines resulting in a positive feedback loop which maintains microglia in an activated state. Chronically activated microglia lose the ability to clear A β plaques, which in turn enhances A β accumulation and furthers AD progression (Cai, Hussain & Yan, 2014; Sherwin et al., 2016; Tse, 2017).

1.9 Targeting the GBA to prevent disease

Although a vast amount of time and money has been dedicated to researching new drugs and therapeutic targets in AD, there is currently no cure. The drugs currently available on the market include cholinesterase inhibitors such as donepezil, rivastigmine and galatamine. In addition, the *N*-methyl-D-aspartate antagonist, memantine, is commonly used to treat severe AD, and can also be used in combination with cholinesterase inhibitors (Geldenhuys & Darvesh, 2015). However, these drugs only provide symptomatic release, which eventually cease to work as neuronal loss increases as the disease progresses (Heppner, Ransohoff & Becher, 2015; Zheng, Zhou & Wang, 2016). The lack of a cure and limited therapeutic options to an AD patient highlights the need to focus on the prevention of AD.

The potential for probiotic therapeutics in AD could be vast, as altering the gut microbiota is able to influence cognitive functions. Tillisch et al., (2013) provided healthy females with fermented milk products containing *Bifidobacterium animalis subsp Lactis*, *Streptococcus thermophiles*, *Lactobacillus bulgaricus* and *Lactococcus lactis subsp. Lactis* and reported reduced brain activity in the sensory regions in response to a task.

The use of probiotics has been shown to have beneficial effects in AD and several other diseases. Bonfilli et al., (2017) demonstrated the effective use of the probiotic SLAB51 in improving cognitive performance in 3xTg-AD mice compared to their untreated age matched littermates. Probiotic administration was associated with a decrease in the size of the lateral ventricles, a reduction in pro-inflammatory cytokines, dysbiosis and most importantly significantly reduced levels of A β 42 in twelve-week-old mice.

However, complications in utilising probiotics as a treatment have been demonstrated by the failure to translate the results from a murine model to humans. The probiotic *Lactobacillus rhamnosus* has been shown to reduce stress related behaviour and corticosterone release in mice, however when used in

healthy human adult males it failed to be no more successful than the placebo (Kelly et al., 2017). Despite studies in animals showing potential for the therapeutic use of probiotics, we are still a long way from routine clinical use in humans.

Further work in this field is required to elucidate the exact mechanisms of the GBA, in particular, how dysbiosis can influence its dysfunction and contribute to AD. Understanding how dysbiosis impacts the GBA will make it easier to develop probiotic cocktails which could decrease the risk of an individual developing AD.

2. Project Aims

In this thesis we are observing changes in the gut microbiota and alterations in the morphology and cell populations of the small and large intestine, in early and late AD pathology using the APP/PS1 murine model.

The aims of this project are:

- To investigate alterations in the morphology of the gut in APP/PS1 mice by assessing villus height and/or crypt depth.
- To identify changes in goblet cell numbers using PAS/AB stain and EEC numbers using fluorescent IHC in the APP/PS1 mouse gut.
- To determine whether dysbiosis is present at the phylum level by assessing changes in the two major phyla: Firmicutes and Bacteroidetes in the mucosal associated and luminal associated microbiota of the small and large intestine using qRT-PCR.
- To investigate differences in beta diversity at the lower taxonomic levels and assess changes in beta diversity using DGGE.

3. Materials

3.1 Reagents

<u>Reagent</u>	<u>Manufacturer</u>	<u>Catalogue number</u>
3-aminopropyltriethoxysilane (APES)	Sigma Aldrich	A3648
Ammonium persulphate (APS)	Sigma Aldrich	A3678
Bovine serum albumin (BSA)	Sigma Aldrich	A9647
DAPI	New England Biolabs	4083S
DNeasy® Powerclean® Pro Cleanup Kit	Qiagen	12997-50
Donkey serum	Sigma-Aldrich	D9663
MinElute™ PCR Purification Kit	Qiagen	28004
N, N, N',N'-Tetramethylethylenediamine (TEMED)	Sigma Aldrich	T7024
PAP Pen	Sigma Aldrich	Z377821
QIAamp Fast DNA Stool Kit	Qiagen	51604
RedTaq® ReadyMix™ PCR Reaction Mix	Sigma Aldrich	R2523
Spinkote Lubricant	Beckman Coulter	306812
SYBR® Gold Nucleic Acid Gel Stain (10,000x)	Thermo Fisher Scientific	S11494
SYBR® Green JumpStart™ Taq Readymix™	Sigma Aldrich	S4438
Triton X-100	Sigma Aldrich	T8787
Vectashield® Mounting Medium	Vector Laboratories	H-1000

Table 3: Reagents and manufacturer details.

3.2 Buffers and Solutions

<u>Solution</u>	<u>Composition</u>
0% denaturant	5 ml acrylamide, 14.6 ml of dH ₂ O and 0.4 ml 50x TAE.
100% denaturant	8.4 g urea, 5ml acrylamide, 8 ml formamide, 0.4 ml 50x TAE and stirred with a magnetic flea at 50°C until the urea dissolves.
10x Phosphate buffered saline (PBS)	80 g NaCl, 2.4 g K ₂ HPO ₄ , 14.4 g NaH ₂ PO ₄ , 2 g KCl, 800 ml dH ₂ O, pH 7.4, make up to 1 L with dH ₂ O.
50x Tris acetic acid (TAE) buffer	242 g Tris base dissolved in 750 ml dH ₂ O. 57.1 ml glacial acetic acid, 100 ml of 0.5 M EDTA (pH 8.0), make up to 1 L.
100 mM Sodium citrate buffer, 0.5% Tween 20	29.4 g sodium citrate tribasic dihydrate, 5 ml Tween 20, 1L of dH ₂ O and pH to 6.0.
10x gel loading dye	0.25 g bromophenol blue, 0.25 g xylene cyanol, 1.5 g Ficoll 400 in 10 ml dH ₂ O. 4 ml of which is added to 6 ml of glycerol.
Methacarnoy's Solution (500 ml)	300 ml methanol, 150 ml chloroform, 50 ml acetic acid (added last).

Table 4. Solutions and their compositions.

3.3 Antibodies

<u>Antibody</u>	<u>Manufacturer</u>	<u>Catalogue number</u>	<u>Concentration</u>	<u>Working dilution</u>
Alexa Fluor® 488 donkey anti-rabbit IgG (H+L)	Invitrogen	A-21206	2 mg/ml	1:500
Anti-chromogranin A	Abcam	ab15160	0.355 mg/ml	1:200
Normal rabbit IgG	Santa Cruz	Sc-2027	200 µg/0.5 ml	1:500

Table 5: Antibodies with supplier details and concentrations used.

3.4 PCR Primers

16S rRNA	341F_GC	5' <u>CGCCCGCCGCGCGCGGGCGGGGCGGGGCGGGG</u> <u>CSCGGGGGGCCTACGGGSGGCSGCSG</u> -3'
	518R	5'-ATTACCGCGGCTGCTGG -3'

Table 6: 16S PCR primer sequences. Underlined sequence donates a GC rich clamp positioned at the 5' end of the forward primer.

Universal	906F	F: 5'-AAACTCAAAGGAATTGACGG-3'
	1062R	R: 5'-CTCACRRCACGAGCTGAC-3'
Firmicutes	928F	F: 5'-TGAAACTYAAAGGAATTGACG-3'
	1040R	R: 5'-ACCATGCACCACCTGTC-3'
Bacteroidetes	798cfbF	F: 5'-CRAACAGGATTAGATACCCT-3'
	cfb967R	R: 5'-GGTAAGGTTCTCGCGTAT-3'

Table 7: Universal and phyla specific qRT-PCR forward and reverse primer sequences for the 16S gene.

4. Methods

4.1 Animals

APP/PS1 and WT mice on a C57BL/6 genetic background were bred and housed in standard animal house conditions at Lancaster University using a 12-hour light/dark cycle. Mice were housed in single sex, mixed genotype groups of 1-5 mice per cage. The cages were individually ventilated and food and water were provided *ad-libitum*. All procedures using animals were conducted in accordance with the laws of the Animals Scientific Procedures Act, 1986 and were approved by the Home Office, London, UK.

The APP/PS1 mouse model is a double transgenic model of cerebral amyloidosis commonly used in AD research. The mice express the Swedish mutation in the *APP* gene and the L166P mutation in the *presenilin-1* gene (*PS1*), which are under the control of the Thy-1 promoter. The mice overexpress APP and exhibit A β plaque deposition and neuronal loss in an age dependent manner. However tau pathology is absent (Radde et al., 2006; Sasaguri et al., 2017).

Mice were euthanized by exposure to an increasing concentration of CO₂, and death was confirmed by cervical dislocation. Individuals conducting experiments were kept blinded from the genotypes until all experiments and analysis were completed.

For histological analysis, 5 mm sections from the ileum and distal colon (three, seven and fifteen-month mice), in addition to the caecal tip (seven and fifteen-month mice only) were removed and cleaned of excess adipose tissue. The tissues were transferred into cassettes and fixed in methacarnoy's solution for a minimum of 4 hours, washed in methanol for 1 hour and stored in 100% ethanol until processed.

For microbial analysis, the remaining ileum, caecum and distal colon was removed from the seven and fifteen-month mice, cleared of excess adipose

tissue, snap frozen in liquid nitrogen and stored at -80°C. The caecum from three-month mice was also removed, snap frozen and stored at -80°C.

4.2 Tissue Processing

Prior to tissue sectioning, frosted microscope slides (Deltalab) were washed in acetone for 5 min then immersed in 2% APES in acetone for 1 min. The slides were washed twice in distilled H₂O (dH₂O) and left to air-dry overnight.

The tissues in the cassettes were rehydrated by passing through an increasing ethanol gradient of 70%, 90%, 100% and 100% for 20 min each. The samples were placed in the clearing agent xylene three times for 20 min each.

The cassettes were incubated in two hot paraffin wax baths for 30 min each. Tissues were embedded in paraffin wax using a shallow mould, with the tissue orientated so the lumen was perpendicular to the base of the mould.

The tissues were sectioned at a thickness of 5 µm using a microtome (Leica) and transferred to APES coated microscope slides. The slides were left to air-dry overnight.

4.3 Histological Staining

4.3.1 Periodic acid-Schiff (PAS) Alcian Blue (AB) Stain

Paraffin embedded tissue sections were deparaffinised in two 10 min washes in xylene and rehydrated with two 100% ethanol washes for 2 min, followed by two brief washes with dH₂O. The sections were stained with 1% Alcian blue (AB) solution (Merck) for 5 min, followed by two quick washes with dH₂O and one wash for 2 min. The sections were stained with 1% Periodic acid solution (Merck) for 5 min in darkness, followed by two quick washes with dH₂O, and one wash for 2 min. The sections were stained with Schiff reagent (Merck) for 15 min, and washed quickly twice with dH₂O, and once for 2 min. The sections were then washed in cold running water for 5 min prior to staining with Harris' haematoxylin (Thermo Scientific) for 1 min and then washed in warm running water for 5 min. The samples were dehydrated with two washes in 100% ethanol for 2 min, and twice in xylene for 2 min. DPX mountant (Sigma) and coverslips were applied to the sections and left to air dry.

4.3.2 Light Microscope

The morphology of the guts was assessed by capturing images using the IMS software at 10x magnification on a Motic BA210E Upright microscope. A scale bar from the IMS software was used to calibrate the measurements on ImageJ (version 1.50i). For each sample ten villi and/or twenty crypts were randomly selected and measured using ImageJ. The number of goblet cells present in each of the ten villi and/or twenty crypts was also counted.

4.3.3. Fluorescent Immunohistochemistry (IHC)

Fluorescent immunohistochemistry (IHC) was carried out using an antibody raised against chromogranin A (CgA) to assess EEC numbers. Sections were deparaffinised by two washes in xylene for 10 min and rehydrated in decreasing ethanol gradients of: two washes in 100% ethanol, one wash in 90% and 70% ethanol, each for 2 min. The sections were washed three times in 1x PBS buffer for 2 min.

Antigen retrieval was carried out to remove covalent crosslinks formed during the fixation process that may have blocked antibody binding sites. The sections were immersed in sodium citrate buffer (10 mM sodium citrate, 0.05% Tween 20, pH 6.0) and heated at full power in a microwave oven for 10 min. When cool, the sections were washed in 1x PBS for 1 min. A PAP pen was used to create a hydrophobic barrier around each tissue section

The cells were permeabilised by incubating with 0.25% Triton X-100 in 1x PBS for 10 min. A blocking step was carried out to block any non-specific antigens by incubating for 30 min with 10% donkey serum in 1x PBS containing 3% BSA. The sections were incubated for 18 hours at 4°C with anti-CgA primary antibody (Abcam) diluted 1:200 in 1x PBS containing 3% BSA. An isotype control normal rabbit IgG (Santa Cruz) diluted 1:500 in 1x PBS containing 3% BSA was also included.

The sections were washed three times in 1x PBS for 2 min. All subsequent steps were carried out in the dark at room temperature (RT). The secondary 488 donkey anti-rabbit IgG (H+L) antibody (Invitrogen), diluted 1:500 in 1x PBS, was incubated on the sections for 1 hour. The sections were washed three times in 1x PBS for 2 min each. DAPI (New England Biolabs), diluted 1:1000 in 1x PBS, was incubated on the sections for 5 min. The slides were mounted with Vectashield (Vector Laboratories) and a coverslip, and fixed in place. The sections were stored in the dark at RT until required and viewed using the Zeiss Axio Scope A1 microscope.

4.4 Bacterial 16S rDNA Extraction

The tissues were defrosted on ice. Each tissue was dissected down the middle to expose the luminal contents. DNA extraction was carried out firstly on the luminal contents and then the mucosal layer using the QIAamp Fast DNA Stool Kit (Qiagen) according to manufacturers specifications. The following steps were adjusted for optimisation: the first heating step was increased to 95°C for 30 min. The volume of proteinase K was increased to 30 µl. The volume of supernatant removed, and the volume of Buffer AL and ethanol added was increased to 400 µl. The volume of Buffer ATE added to the membrane was decreased to 100 µl and the incubation period was increased to 5 min.

4.5 16S rDNA Quantitative Real-Time Polymerase Chain Reaction (qRT-PCR)

The abundance of the two main microbial phyla, Firmicutes and Bacteroidetes, was analysed using universal and phylum specific primers (table 7). Each sample was analysed in triplicate in a 96 well plate, with 100 ng DNA in 12ul added to each well. 12.5 µl of master mix, containing 12 µl SYBR® Green JumpStart™ Taq Readymix™ (Sigma) and 0.25 µl forward primer and reverse primer (table 7) was added to each well. A no sample control (water) was also used for each set of primers to ensure there was no contamination. The 96 well plate was sealed using a sealing film (Bio-rad) and briefly centrifuged at 100 x g. The PCR parameters were as follows, 1 cycle at 95°C for 5 min, 39 cycles at 95°C for 20 sec, 61.5°C for 20 sec, 72°C for 30 sec and 1 cycle at 72°C for 5 min. The relative abundance of each phylum was assessed using the $2^{-\Delta\Delta^{-CT}}$ method as described by Linak & Schmittgen (2001).

4.6 Denaturing Gradient Gel Electrophoresis (DGGE)

Denaturing gradient gel electrophoresis (DGGE) is a technique used to identify single base changes in a section of DNA, the theory of which was first described by Fischer and Lerman (1983). A highly conserved 200 base pair sequence adjacent to the hypervariable V3 region of the 16S rRNA gene was amplified in the mucosal and luminal samples using universal 16S rRNA primers (table 6) (Muyzer, De Waal & Uitterlinden, 1993).

4.6.1 PCR and Purification of 16S rDNA for DGGE

The DNA extracted from the mucosal and luminal contents were diluted 1:10 in nuclease free H₂O, from which 100ng of DNA in 9.5 µl nuclease free water was prepared for each sample. A master mix was prepared containing for each sample; 12.5 µl Taq polymerase, 1 µl BSA, 1 µl of the forward and reverse universal 16S rRNA primers (table 6). 15.5 µl of the master mix was added to each PCR reaction. The PCR parameters were as follows: 1 cycle at 95°C for 5 min, 29 cycles of 95°C for 30 sec, 57°C for 30 sec, 72°C for 30 sec, and 1 cycle at 72°C for 5 min.

The PCR products were purified using MinElute PCR Purification Kit (Qiagen) and DNeasy® Powerclean® Pro Cleanup Kit (Qiagen) according to manufacturer's specifications. The following adjustments were made for optimisation: the volume of Buffer EB used in the MinElute Kit was decreased to 20 µl. In the DNeasy® Powerclean® Pro Cleanup Kit (Qiagen) the volume of EB solution was increased to 20 µl and the incubation period was increased to 5 min. The DNA concentration was quantified using NanoDrop™ 2000c Spectrophotometer (Thermo Fisher) and stored at -80°C until required.

4.6.2 Reagent Preparation

A 16 cm and 10 cm glass plate were cleaned with acetone. Spacers were coated with Spinkote Lubricant (Beckman Coulter) and placed at the edges of the 16 cm glass plate with the 10 cm glass plate placed on top with the edges flush. The sandwich clamps were attached and tightened to each side of the plates, and the set was mounted into the casting stand with the sponges and the cam levers engaged.

A high-grade solution (70%) was prepared containing 11.2 ml of 100% denaturant and 4.8 ml of 0% denaturant, and a low-grade solution (30%) was prepared with 4.8 ml 100% denaturant and 11.2 ml 0% denaturant (table 4). The solutions were stored at -20°C for 20 min to slow down polymerisation.

10% ammonium persulphate (Sigma) was prepared in 1 ml dH₂O.

4.6.3 Pouring the Gradient Gel

Immediately prior to pouring, 150 µl of 10% ammonium persulphate and 8.5 µl of tetramethylethylenediamine (TEMED) (Sigma) were added to both 70% and 30% solutions to initiate the polymerisation process.

The gel was cast using a gradient pourer to ensure an increasing gradient gel was produced. Upon placement of the well comb, 8.5 µl of TEMED was added to each side of the comb to speed up polymerisation and the gel was left to set for 30 min.

The DGGE tank (Biorad) was filled with 1x TAE running buffer and preheated to 60°C. Upon comb removal wells were flushed with 1x TAE to remove any remaining TEMED. The gel was placed in the tank and allowed to warm to 60 °C.

Samples composed of 150 ng of purified DNA, 12 µl dH₂O and 4 µl 10x loading dye (table 4) were loaded into the wells of the gel and the DGGE ran for 16 hours at 60°C and 63 V.

4.6.4 Gel Visualisation

Following electrophoresis the gel was washed with dH₂O and incubated with 1x SYBR® Gold Nucleic Acid Gel Stain in 20 mL dH₂O in darkness for 30 min, then washed thoroughly with dH₂O.

The gel was visualised using the Chemidoc XRS+ system (Biorad) using Image lab software. The exposure time was optimised for each gel. Band detection and band matching of the gel in addition to the production of an unweighted pair group method with arithmetic mean (UPGMA) phylogenetic tree was completed using PyElph 1.4 software. The generation of a non-metric multi-dimensional scaling (NMDS) plot using RStudio (version 1.1.453) was carried out as a means to visualise the relationship of rank orders using a distance matrix with a reduced number of dimensions. A stress value in the NMDS plot of <0.2 was deemed a good quality fit of data. Statistical analysis was also carried out using RStudio.

4.7 Statistical Analysis

The results were presented as the average \pm standard error of mean (SEM). The morphological analysis of the ileum, caecum and distal colon was statistically tested using an unpaired two-tailed t-test in excel. The qRT-PCR data was presented as relative percentage change, and statistically tested using an unpaired two-tailed t-test. Statistical analysis of microbial community profiling from DGGE's was completed using RStudio. A value of $p \leq 0.05$ was deemed to be statistically significant (* $p \leq 0.05$, ** $p \leq 0.01$, *** $p \leq 0.001$).

5. Results

Seven and fifteen-month old APP/PS1 mice were used as models to study early and late A β pathology in AD. Mice were chosen at seven-months as A β plaque deposition is well established, appearing in the neocortex at six weeks and the hippocampus between two to five months (Radde et al., 2006). Cognitive impairment in spatial learning and memory becomes apparent at seven-months and is therefore representative of the time point at which symptom recognition in AD patients is most likely to occur (Petersen, 2009). Fifteen-month mice were chosen as a model for late A β pathology as the pathological phenotype increases in an age-dependent manner (Radde et al., 2006; Serneels et al., 2009 Shen, Liu & Ji, 2017).

To assess morphological changes in the gut, paraffin embedded sections from the ileum, caecum and distal colon from seven and fifteen-month mice were stained with PAS/AB. Measurements of villus height and/or crypt depth were completed using ImageJ. Changes in goblet cell numbers were determined by PAS/AB stained sections and EEC numbers using fluorescent IHC with a rabbit polyclonal CgA primary antibody.

5.1 Seven-month APP/PS1 mice

5.1.1 Assessment of crypt depth and villus height revealed no overt morphological differences, however EEC numbers are decreased in seven-month APP/PS1 mice

As indicated in figure 7A, there was no significant difference in villus height in the ileum of seven-month APP/PS1 mice, with the villi tending to be 10.5% longer in the APP/PS1 mice compared to WT littermates ($p = 0.29$). Similarly, there was no difference in crypt depth in the gut of APP/PS1 mice compared to WT littermates as shown in figure 7B. The crypts within the ileum tended to be 4.1% shorter which was not statistically significant ($p = 0.71$). Likewise, there was no difference in the crypt depth of the large intestine between APP/PS1 and WT mice, with a 14.4% and 13.4% increase observed in the caecum and distal colon ($p = 0.94$ and $p = 0.37$ respectively).

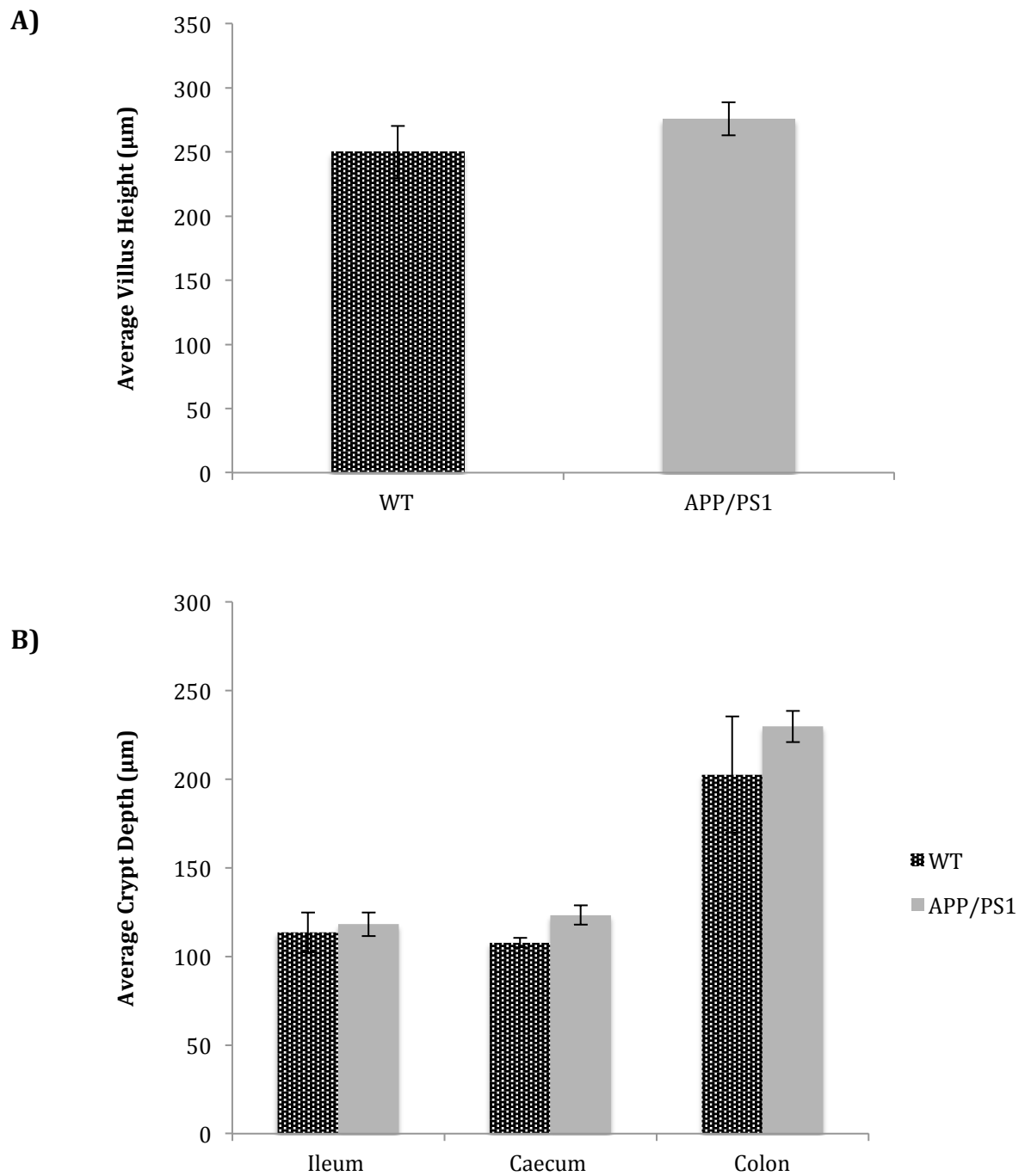


Figure 7: Histological analysis of the gut in WT and APP/PS1 seven-month mice. Error bars indicate SEM. A) Average villus height in the ileum (WT n = 4, APP/PS1 n = 7, p = 0.29), B) Average crypt depth in the ileum (WT n = 4, APP/PS1 n = 7, p = 0.71), caecum (WT n = 4, APP/PS1 n = 7, p = 0.94) and distal colon (WT n = 5, APP/PS1 n = 7, p = 0.37).

There was a tendency for the number of goblet cells to be fewer in both the small and large intestine in seven-month APP/PS1 mice compared to WT littermates (figure 8A and 8B). The largest difference was observed in the caecum where APP/PS1 mice had 16% fewer goblet cells than WT littermates, however this was not significant ($p = 0.13$). In the ileum the number of goblet cells also tended to be fewer in the APP/PS1 mice by approximately 15.4% in the villi and 12.5% in the crypts, but similarly this was not statistically significant ($p = 0.21$). The number of goblet cells in the colonic crypts had a propensity to be 12.1% fewer in the APP/PS1 mice compared to WT littermates, which was not significant ($p = 0.44$). Representative images of goblet cell numbers are shown in figure 9.

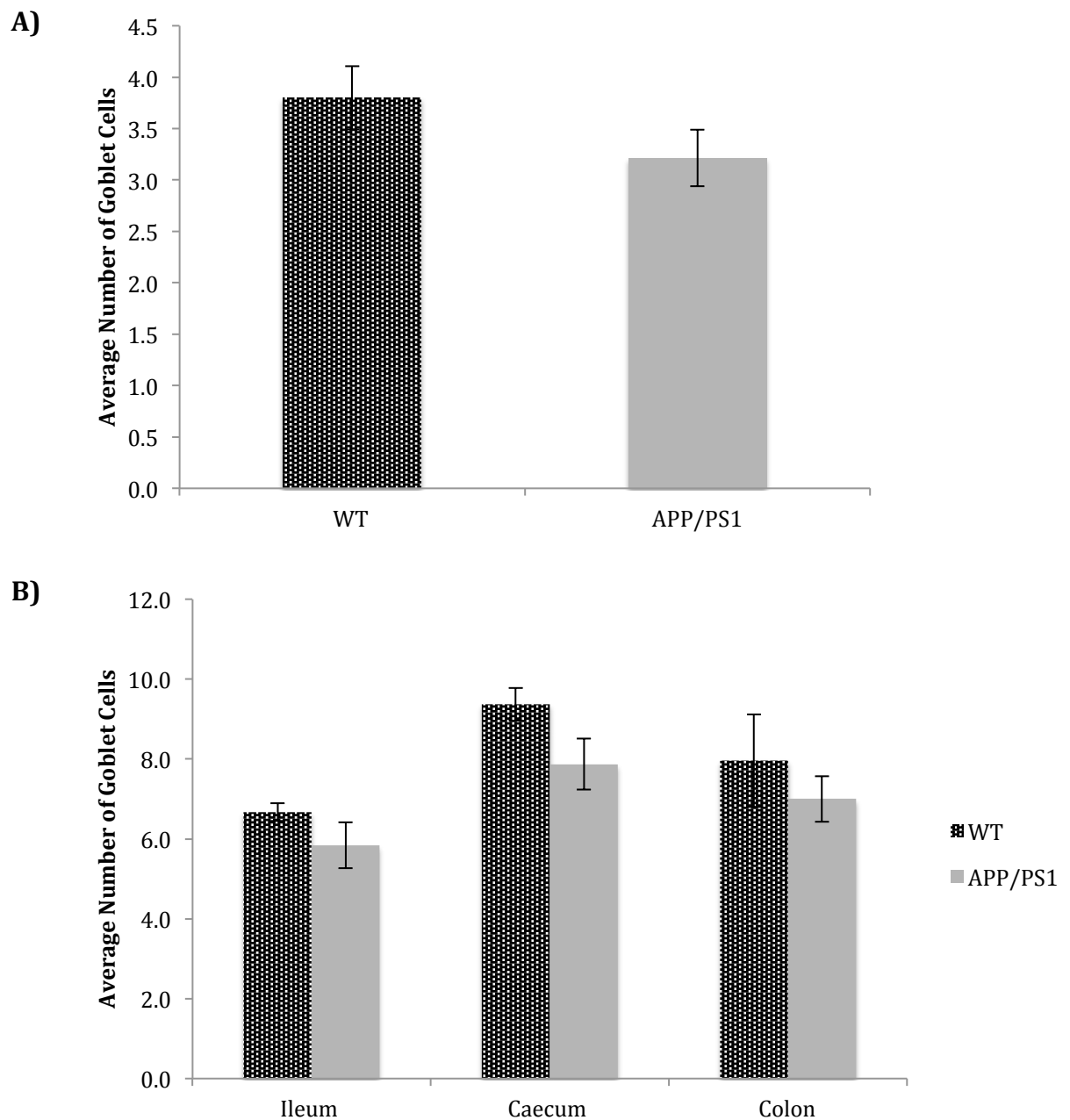


Figure 8: Average number of goblet cells in WT and APP/PS1 seven-month mice. Error bars indicate SEM. Ileum villus. A) Average number of goblet cells per 100 μm of villi in the ileum (WT $n = 4$, APP/PS1 $n = 7$, $p = 0.21$). B) Average number of goblet cells per 100 μm of crypt in the ileum (WT $n = 4$, APP/PS1 $n = 7$, $p = 0.21$), caecum (WT $n = 4$, APP/PS1 $n = 7$, $p = 0.13$) and distal colon (WT $n = 5$, APP/PS1 $n = 7$, $p = 0.44$).

To determine the proportions of acidic and neutral mucins, paraffin embedded sections were stained with PAS/AB. At pH 2.5, AB stains acidic mucins blue and PAS can subsequently differentiate the neutral mucins by staining them pink. Purple mucins indicate a combination of both acidic and neutral mucins produced by a goblet cell. The different types of mucins produced by the WT and APP/PS1 mice were assessed qualitatively.

As shown in figure 9, there were no observed differences in the types of mucins produced by the goblet cells in the ileum of WT and APP/PS1 mice. The neutral mucins tended to be located at the base of the crypts with the acidic and combination of acidic and neutral mucins located at the opening of the crypt. The goblet cells in the villi tended to produce acidic and a combination of acidic and neutral mucins. Furthermore, there was no obvious difference in the caecum or distal colon of WT and APP/PS1 mice. The goblet cells producing acidic mucins tended to reside at the base of the crypts and those producing neutral mucins located closer to the opening of the crypt.

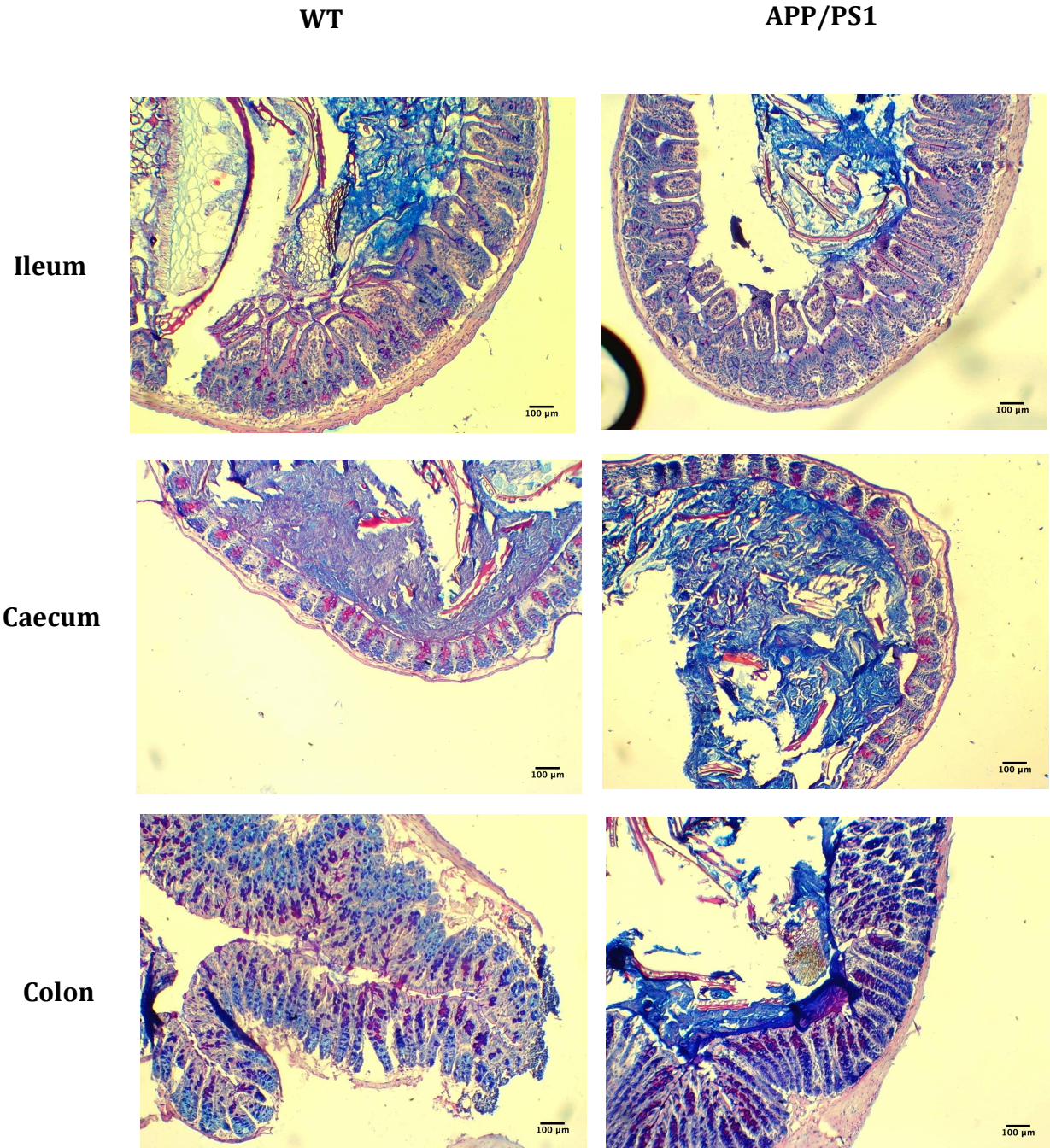


Figure 9: Representative PAS/AB stained sections in WT and APP/PS1 seven-month mice. Acidic mucins are stained blue by AB and neutral mucins are stained pink by PAS. Purple mucins indicate a combination of both acidic and basic mucins produced by a goblet cell. Scale bar = 100 μ m.

EECs are specialised cells found in the small and large intestine which secrete 5-HT and the peptide hormones: GLP-1, PPY, and CCK. CgA is a matrix soluble glycoprotein found on a type of secretory vesicle in EEC's known as a small synaptic like microvesicle (SLMV). (Gunawardene, Corfe & Staton, 2011). A rabbit polyclonal primary antibody raised against CgA was used to identify EECs. Isotype controls using a normal rabbit IgG are shown in figure 10.

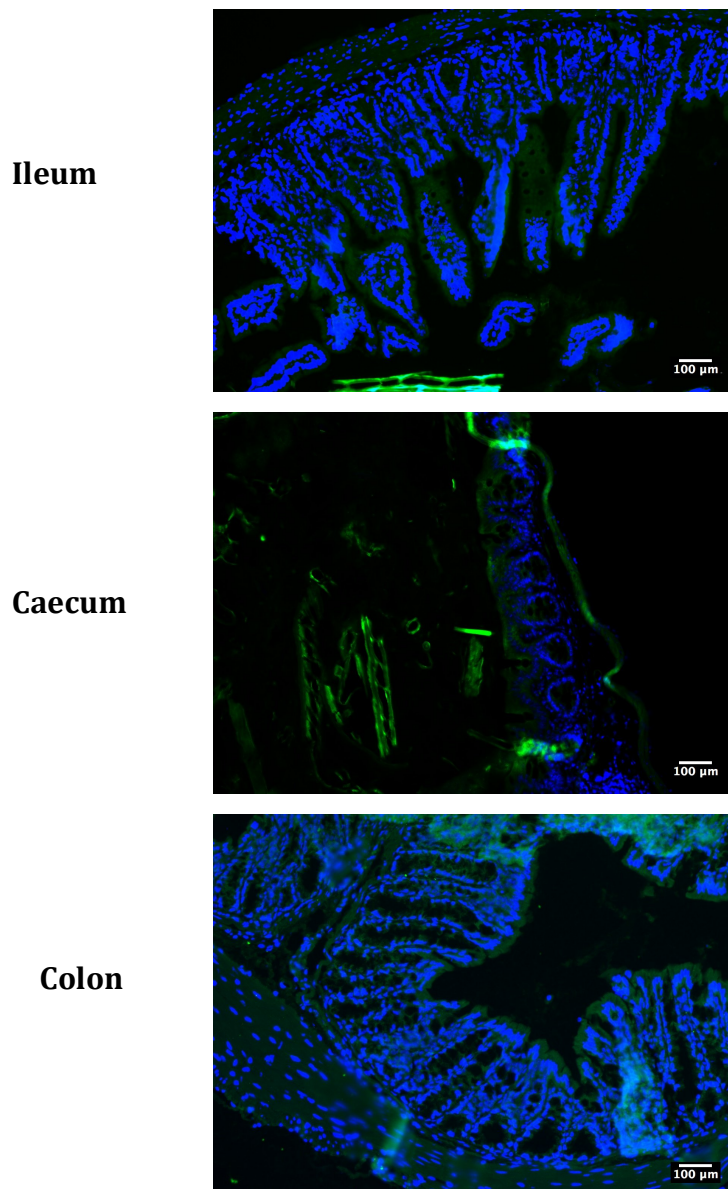


Figure 10: Normal rabbit IgG isotype controls for CgA. CgA = green, DAPI = blue.
Scale bar = 100 µm

As shown in figure 11A, the villi of the ileum had a propensity to have 28.4% fewer EECs in APP/PS1 compared to WT mice, however this was not statistically significant ($p = 0.21$). A similar observation was also made in the crypts of the ileum, as highlighted in figure 11B, with 21% fewer EECs present in the APP/PS1 mice compared to WT ($p = 0.40$). There was also no difference in the number of EEC's in the caecum of WT and APP/PS1 mice ($p = 0.44$), with both genotypes tending to have 0.44 EEC's per 100 μm of crypt. In contrast, there was a statistically significant 40.1% decrease in the number of EEC's in the distal colon ($p = 0.04$) as indicated in figure 11B. APP/PS1 mice averaged 0.31 ± 0.02 EEC's per 100 μm of colonic crypt, compared to 0.52 ± 0.10 in the WT littermates. Representative images are shown in figure 12.

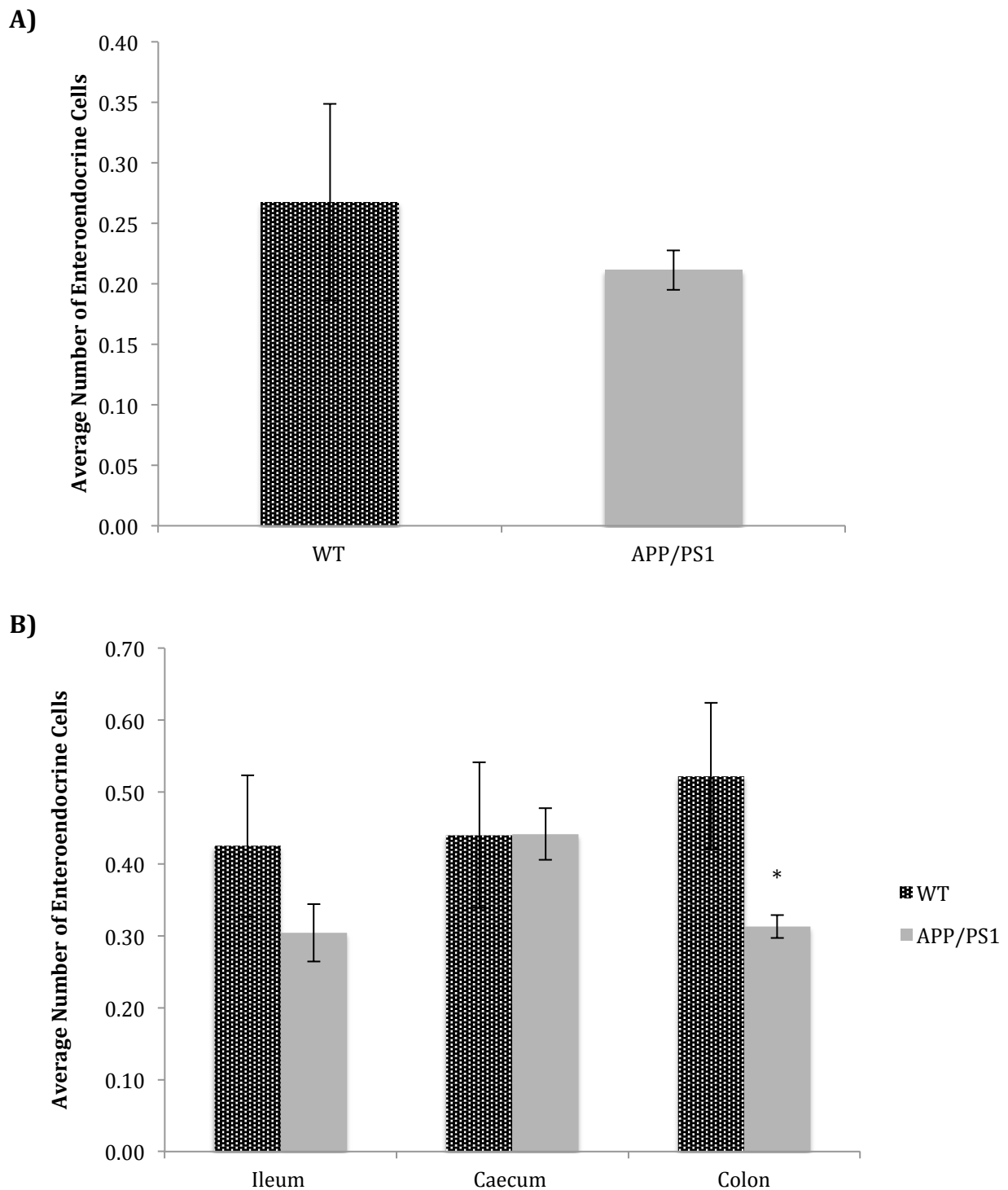


Figure 11: Average number EEC's in WT and APP/PS1 seven-month mice. Error bars indicate SEM. A) Average number of EECs per 100 μm of villi in the ileum (WT n = 4, APP/PS1 n = 7, p = 0.40). B) Average number of EEC's per 100 μm of crypt in the ileum (WT n = 4, APP/PS1 n = 7, p = 0.21), caecum (WT n = 4, APP/PS1 n = 7, p = 0.99) and distal colon (WT n = 5, APP/PS1 n = 7, p = 0.04). * p \leq 0.05.

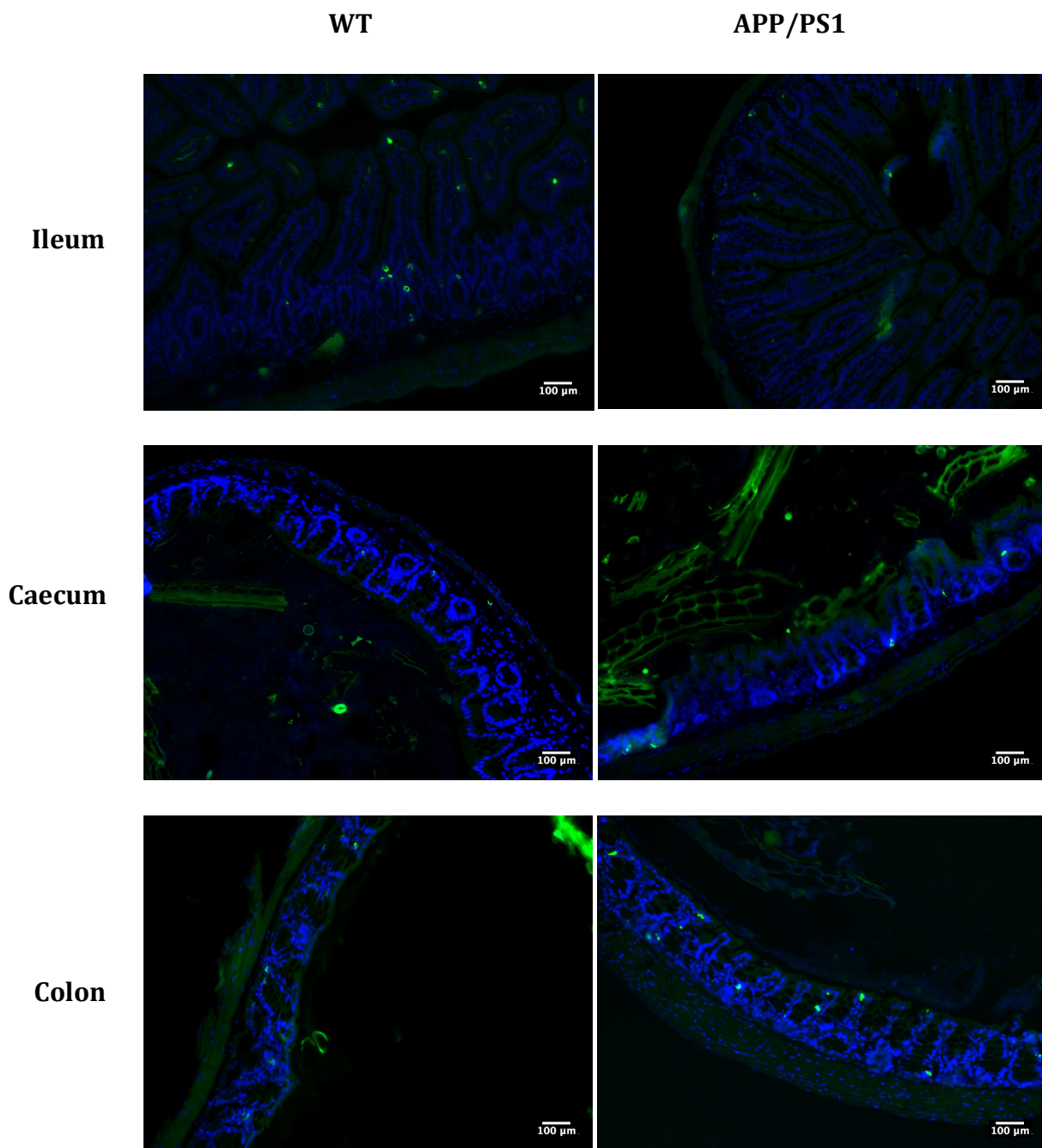


Figure 12: Representative fluorescent IHC images of the number of EEC's in seven-month WT and APP/PS1 mice. CgA = green, DAPI = blue. Scale bar = 100 μ m

Sex specific differences in the number of EEC's in the distal colon of seven-month mice were assessed by comparing WT and APP/PS1 male and female mice (figure 13). Although statistical analysis could not be performed due to a small n number, there was a tendency for male APP/PS1 mice to have greater decrease in EEC numbers than female APP/PS1 mice, however male WT mice displayed a large variation in EEC numbers.

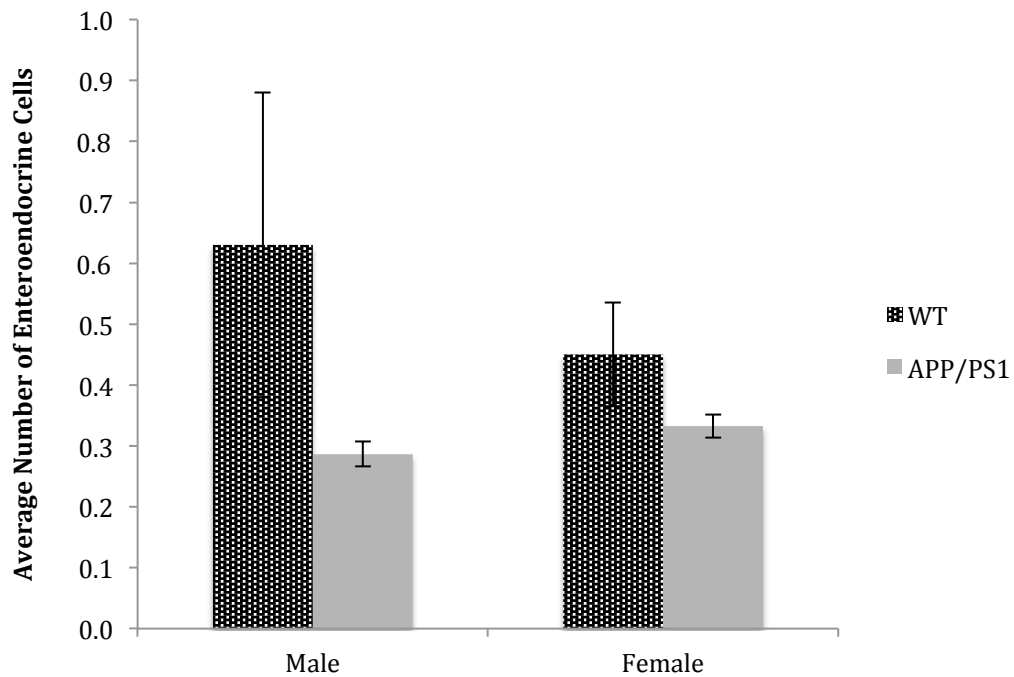


Figure 13: Average number of EEC's in male and female WT and APP/PS1 seven-month mice. Average number of EEC's per 100 μm of villus height and/or crypt depth. Error bars indicate SEM. Male (WT n = 2, APP/PS1 n = 3), female (WT n = 3, APP/PS1 n = 4).

5.1.2 A decrease in the phylum Firmicutes was observed in seven-month APP/PS1 mice

Broad changes in the diversity of the microbiota between subjects, known as beta diversity, in the mucosal-associated microbiota were assessed by qRT-PCR for the two major phyla: Firmicutes and Bacteroidetes, in the ileum, caecum and distal colon in seven and fifteen-month mice (Goodrich et al., 2014).

The abundance of Firmicutes in APP/PS1 mice was significantly decreased in the colon by $49\% \pm 12\%$ relative to WT mice ($p = 0.05$) as indicated in figure 14. A similar trend was seen in the ileum with a decrease of $26\% \pm 29\%$, however this did not reach statistical significance ($p = 0.20$). In contrast, there was no significant difference in the abundance of Firmicutes with the abundance being $17\% \pm 14\%$ greater in the caecum of compared to WT littermates ($p = 0.92$).

In both the small and large intestine, there was a propensity for Bacteroidetes to be more abundant in APP/PS1 mice. The greatest difference tended to be in the ileum and caecum with a $48\% \pm 13\%$ and $38\% \pm 28\%$ increase, however this was not statistically significant ($p = 0.33$ and $p = 0.68$ respectively). A smaller increase tended to occur in the colon of around $8\% \pm 13\%$, but similarly was not statistically significant ($p = 0.92$).

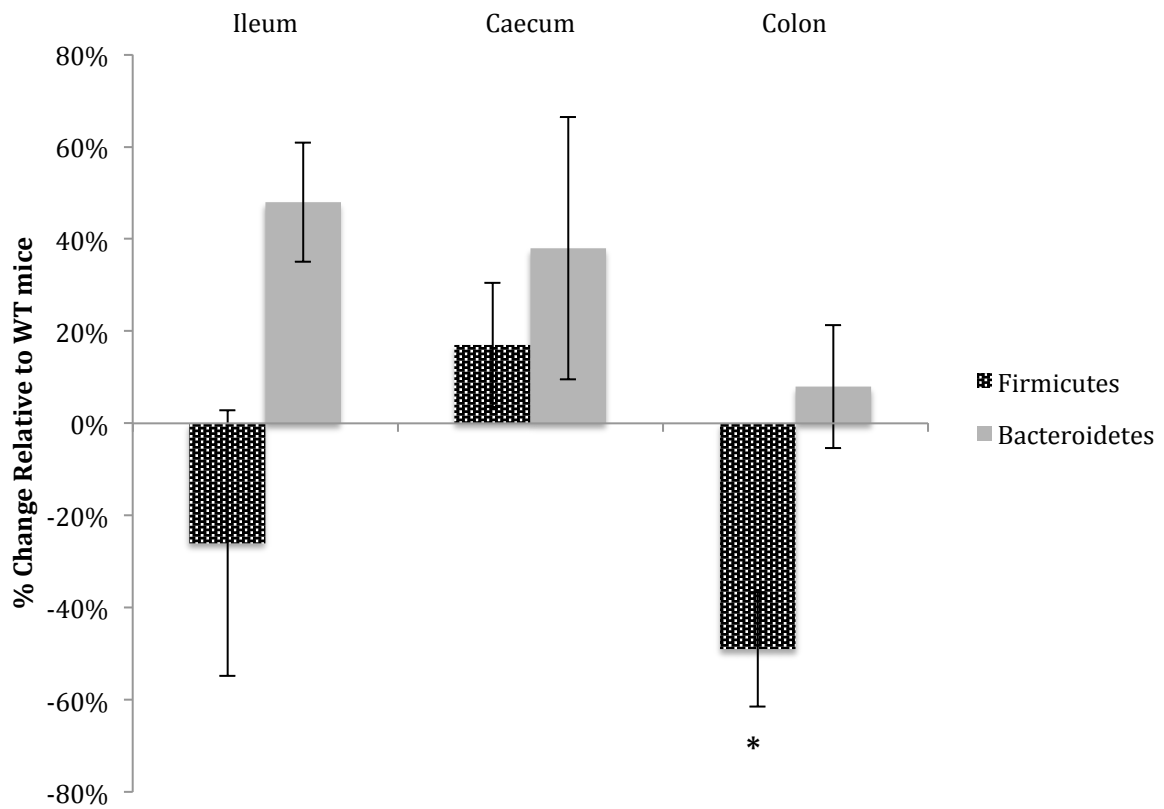


Figure 14: Relative percentage change of predominant mucosal-associated phyla in seven-month mice. Percentage change of the phyla Firmicutes and Bacteroidetes in the mucosal-associated microbiota of seven-month APP/PS1 mice relative to age matched WT littermates. Error bars indicate SEM. Firmicutes: ileum (WT n = 5, APP/PS1 n = 6, p = 0.20), caecum (WT n = 5, APP/PS1 n = 6, p = 0.92), distal colon (WT n = 4, APP/PS1 n = 7, p = 0.05). Bacteroidetes: ileum (WT n = 5, APP/PS1 n = 5, p = 0.33), caecum (WT n = 5, APP/PS1 n = 7, p = 0.68), distal colon (WT n = 4, APP/PS1 n = 7, p = 0.92). * p ≤ 0.05.

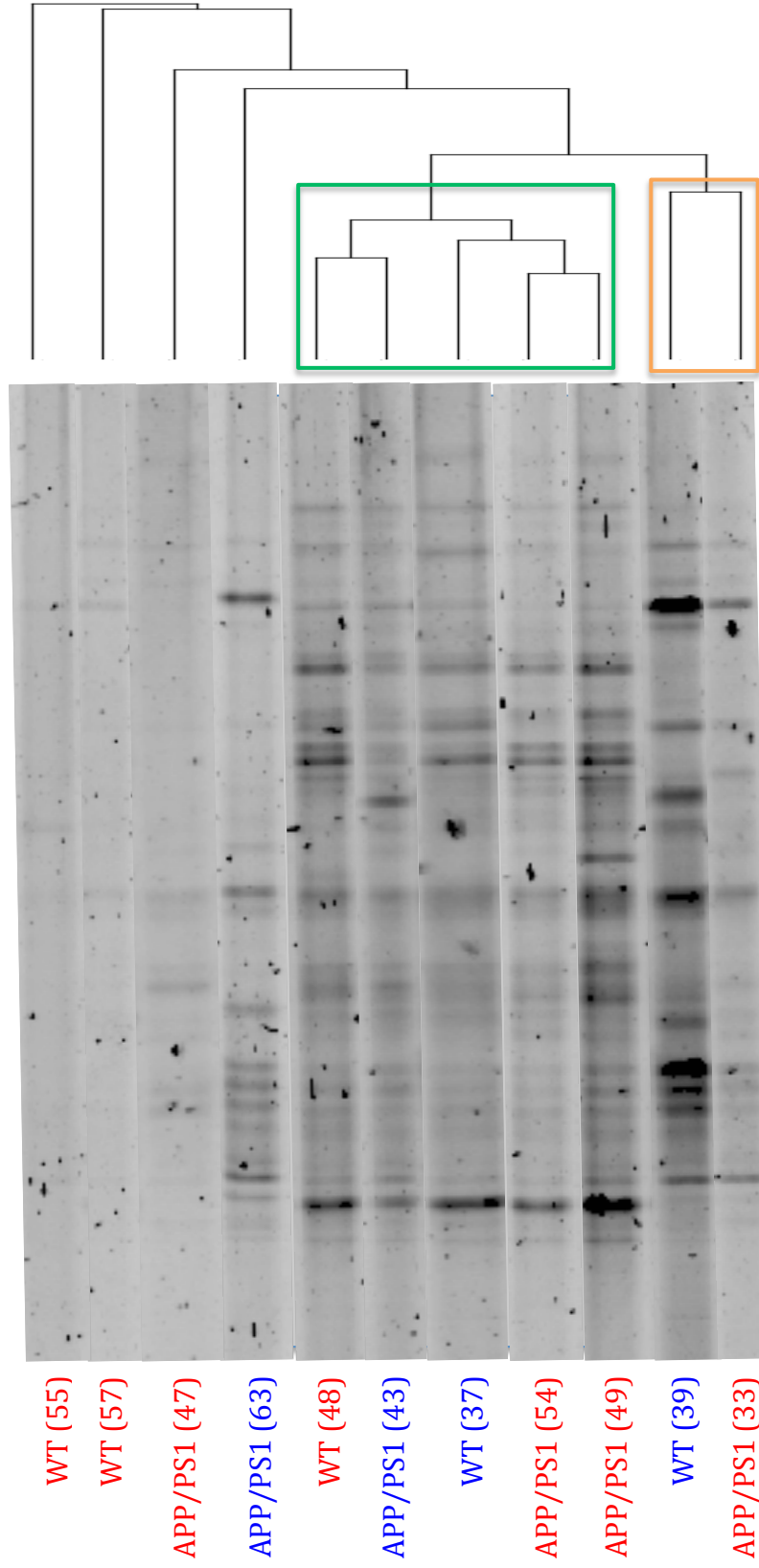
5.1.3 No difference in bacterial community was seen in seven-month APP/PS1 mice

As shifts in the major phyla are a very broad reflection of any changes, DGGE's were performed to assess differences in the beta diversity further. DNA extracted from the mucosal and luminal-associated microbiota was amplified via PCR and purified, before being run overnight on a gradient gel. Each band on the gel represents one or more closely related bacterial species. Therefore, differences in the microbiota can be assessed by comparing the presence and absence of bands across the samples. Variation in band profiles may indicate differences in community composition and increases in total number of bands may indicate a greater beta diversity. UPGMA phylogenetic trees and NMDS plots were used to visualise and assess these differences. UPGMA phylogenetic trees were chosen as they assume no time related differences in the relationship.

Ileum

There was no statistically significant difference in the mucosal-associated microbiota profiles if the ileum of seven-month WT and APP/PS1 mice ($p = 0.82$). There did appear to be some clustering as highlighted by the green and orange boxes in the phylogenetic tree shown in figure 15A, and also in the NMDS plot in figure 15B, however there was no correlation between genotype and clustering. In addition, the microbiota profiles that were distant from the clustered profiles were WT and APP/PS1 mice, indicating no relationship between genotype and distant microbiota profiles.

A)



B)

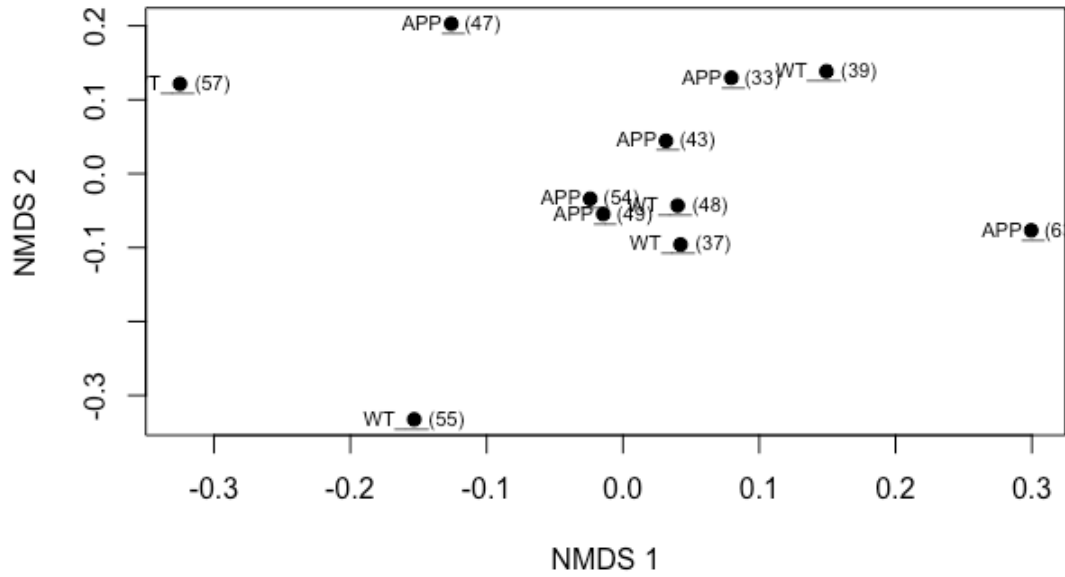


Figure 15: Mucosal bacterial community profiling from the ileum of WT and APP/PS1 seven-month mice. A) 16S rDNA DGGE profile and UPGMA phylogenetic tree. No difference in community profiles was observed (WT n = 5, APP/PS1 n = 6, $p = 0.82$). Blue = male, red = female. Orange and green boxes = clustered microbiota profiles. B) NMDS analysis. Stress value = 0.1 indicating good quality fit of data. Numbers in brackets depicts sample identification number. Abbreviation: APP = APP/PS1.

The beta diversity of the microbiota profiles can be broadly assessed by quantifying the average total number of bands in WT and APP/PS1 mice, with a greater number of bands being indicative of greater diversity. As shown in figure 16, there was no difference in the total number of bands present in the microbiota profiles of WT and APP/PS1 mice (26 ± 7.2 and 27.4 ± 4.8 respectively), suggesting no difference in the beta diversity of the mucosal-associated microbiota in the seven-month caecum ($p = 0.69$).

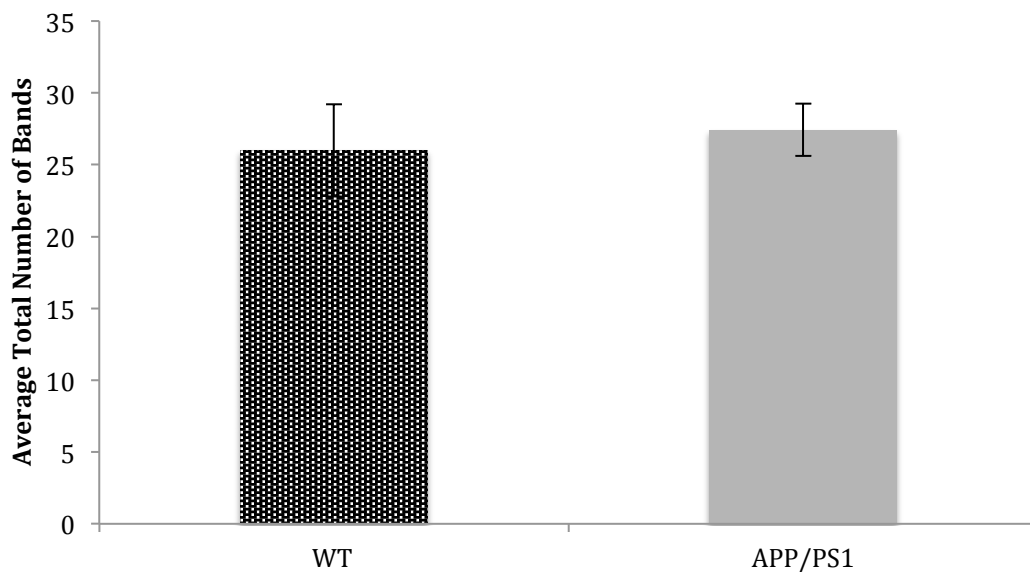
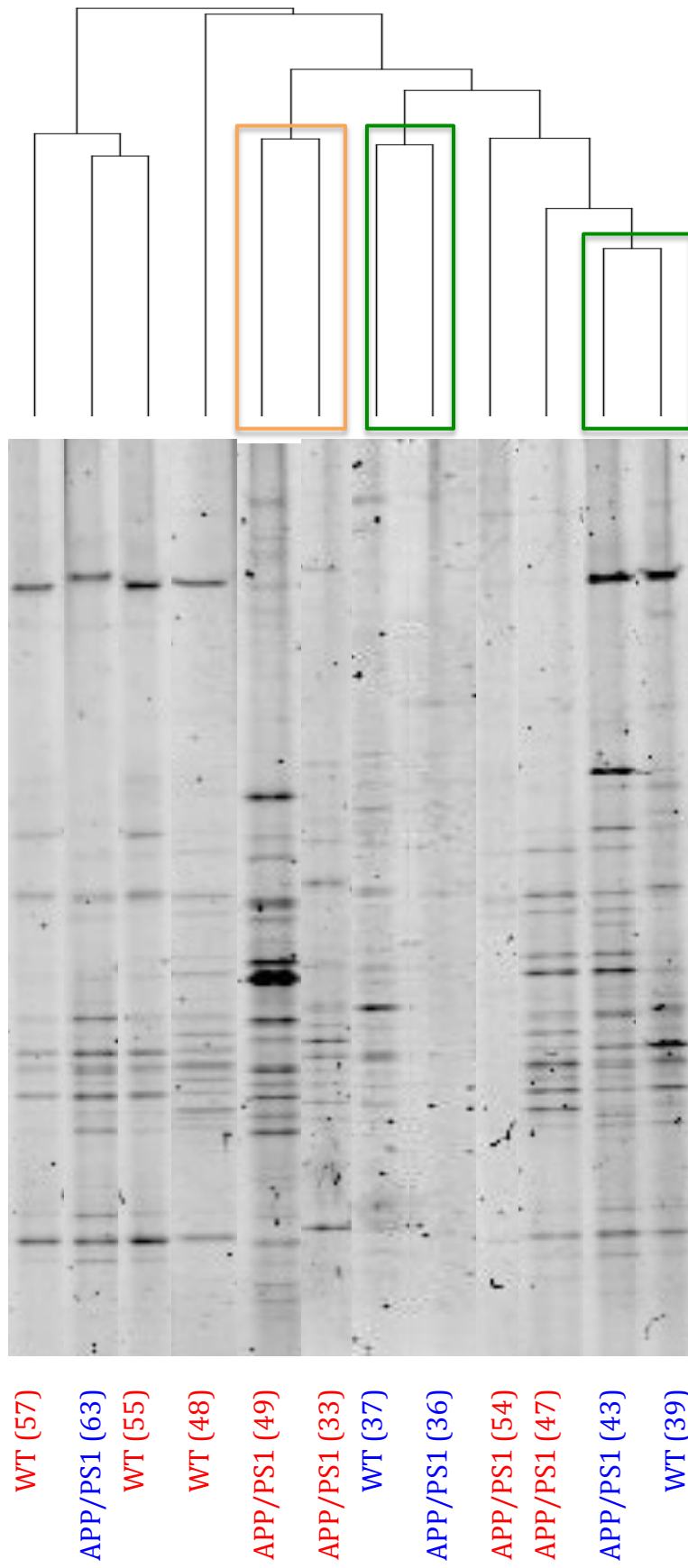


Figure 16: Average total number of bands from a 16S rDNA DGGE of the mucosal bacterial community from the ileum of seven-month WT and APP/PS1 mice. Error bars indicate SEM. (WT n = 5, APP/PS1 n = 6, $p = 0.69$).

A DGGE was also performed on the luminal-associated microbiota of the ileum and revealed no difference in the microbiota profiles of WT and APP/PS1 seven-month mice ($p = 0.67$). The clustering patterns displayed in the phylogenetic tree and NMDS plot indicated in figure 17A and 17B showed no relationship between microbiota profiles and genotype. However there did appear to be a correlation of sex specific clustering that was not based on genotype, as indicated by the green (male) and orange (female) boxes.

A)



B)

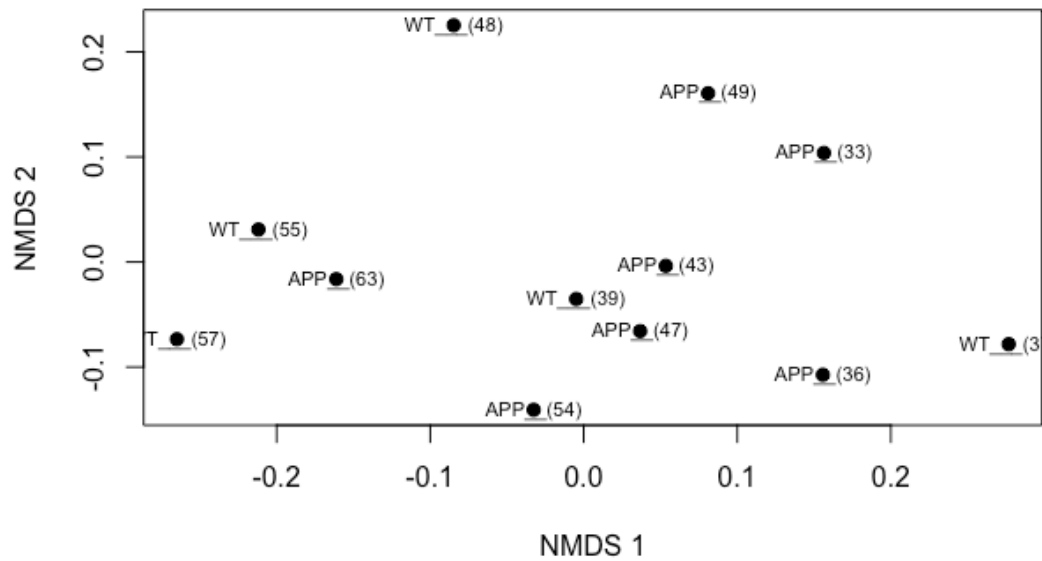


Figure 17: Luminal bacterial community profiling from the ileum of WT and APP/PS1 seven-month mice. A) 16S rDNA DGGE profile and UPGMA phylogenetic tree. No difference in community profiling was observed (WT n = 5, APP/PS1 n = 7, p = 0.67). Blue = male, red = female. Green box = clustered males, orange box = clustered females. B) NMDS analysis. Stress value = 0.1 indicating good quality fit of data. Numbers in brackets depicts sample identification number. Abbreviation: APP = APP/PS1.

As shown in figure 18, there was a propensity for the APP/PS1 mice to have a greater number of total bands in their DGGE profile than their WT littermates (34.6 ± 5.1 compared to 31.8 ± 5.8 respectively). However, this was not statistically significant suggesting no overall difference in beta diversity ($p = 0.40$).

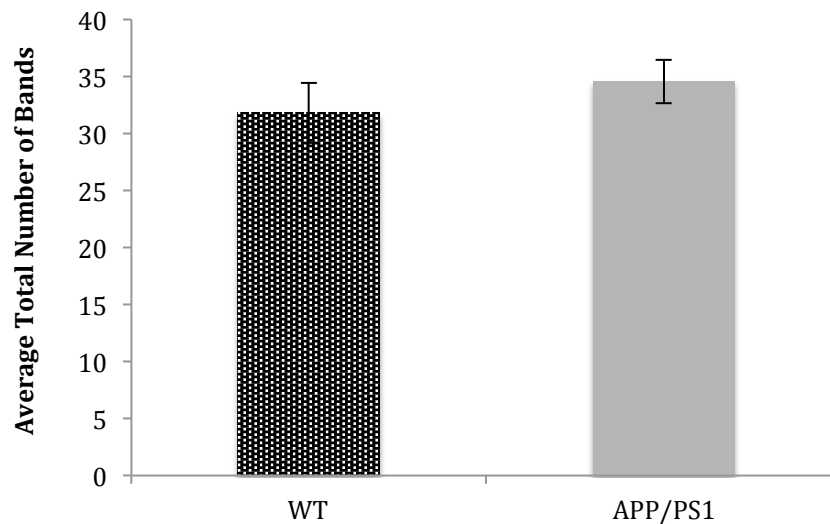
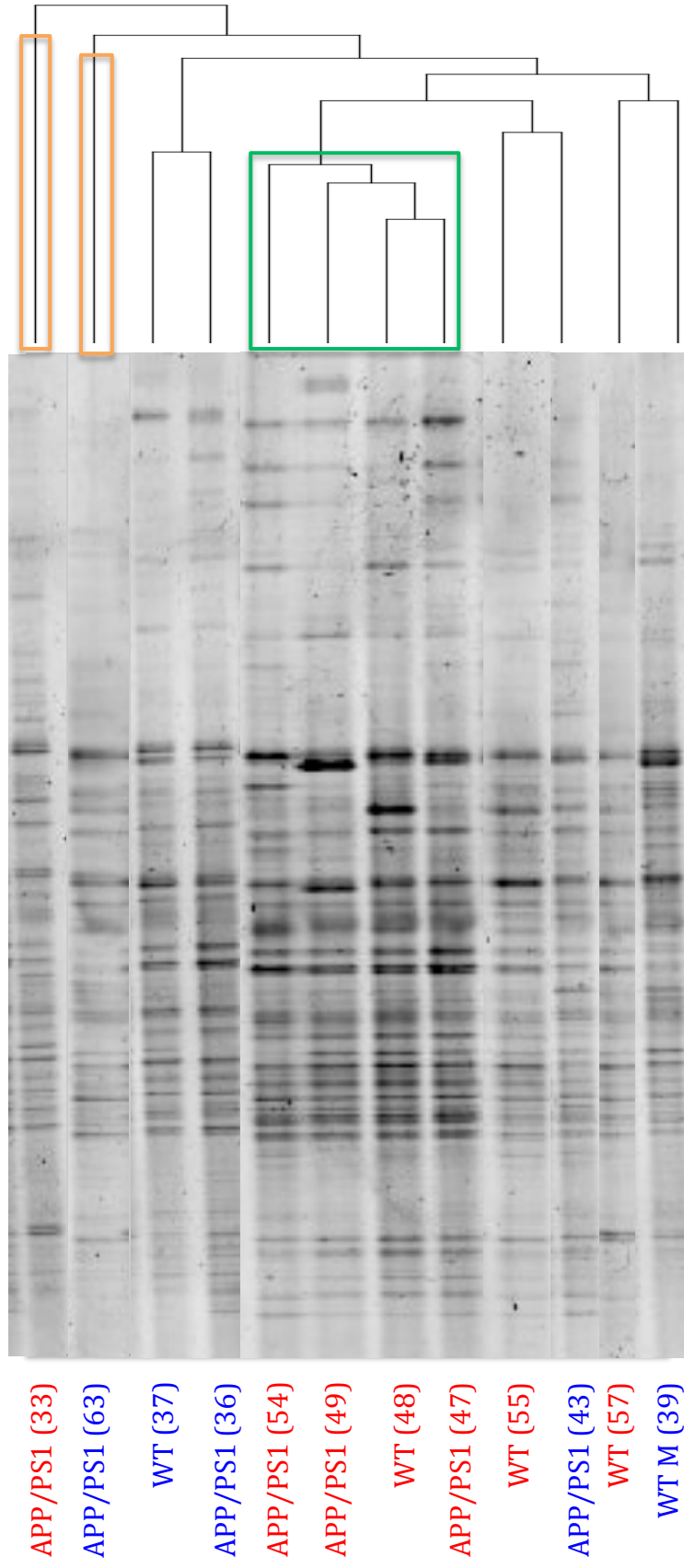


Figure 18: Average total number of bands from 16S rDNA DGGE of the luminal bacterial community from the ileum of seven-month WT and APP/PS1 mice. Error bars indicate SEM. (WT $n = 5$, APP/PS1 $n = 7$, $p = 0.40$).

Caecum

There was no statistically significant difference in the mucosal-associated microbiota profiles of the caecum in seven-month WT and APP/PS1 mice ($p = 0.82$). As indicated in the phylogenetic tree and NMDS plot in figure 19A and 19B, there are some microbiota profiles that appeared clustered (highlighted in green), and others that appear distant (highlighted in orange). Despite the distant microbiota profiles being APP/PS1 mice, the remaining APP/PS1 microbiota profiles appear to be clustered to the WT mice as shown in the NMDS plot. This suggests there is no relationship between genotype and microbiota profiles between WT and APP/PS1 mice.

A)



B)

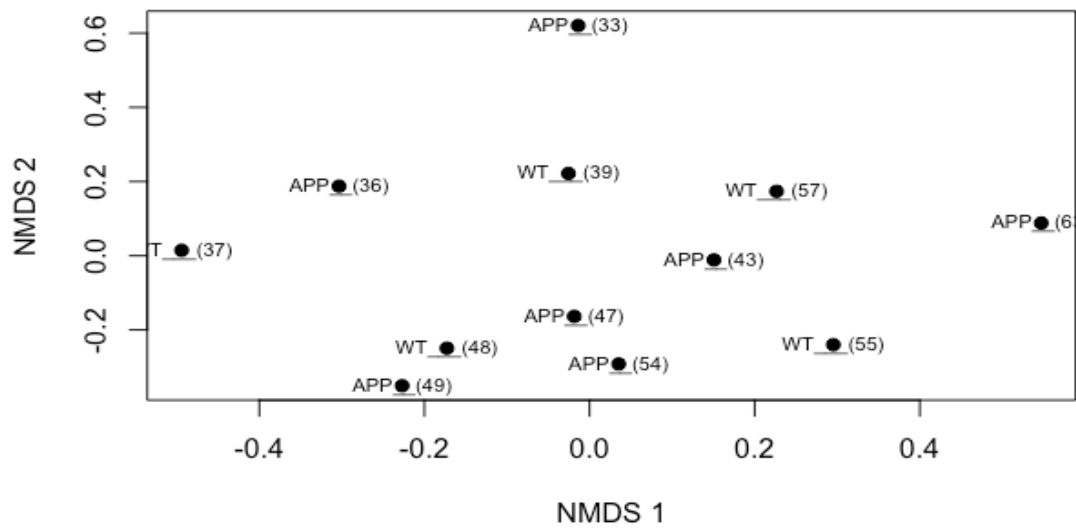


Figure 19: Mucosal bacterial community profiling from the caecum of WT and APP/PS1 seven-month mice. A) 16S rDNA DGGE profile and UPGMA phylogenetic tree. No difference in community profiling was observed (WT n = 5, APP/PS1 n = 7, p = 0.82). Blue = male, red = female. Green box = clustered microbiota profiles, orange box = distant microbiota profiles. B) NMDS analysis. Stress value = 0.2 indicating good quality fit of data. Numbers in brackets depicts sample identification number. Abbreviation: APP = APP/PS1.

There was no difference in the average total number of DGGE bands in the mucosal-associated microbiota profiles from the caecum of WT and APP/PS1 seven-month mice (40.6 ± 3 and 42.3 ± 3.1 respectively), indicating no overall difference in beta diversity ($p = 0.38$) as shown in figure 20.

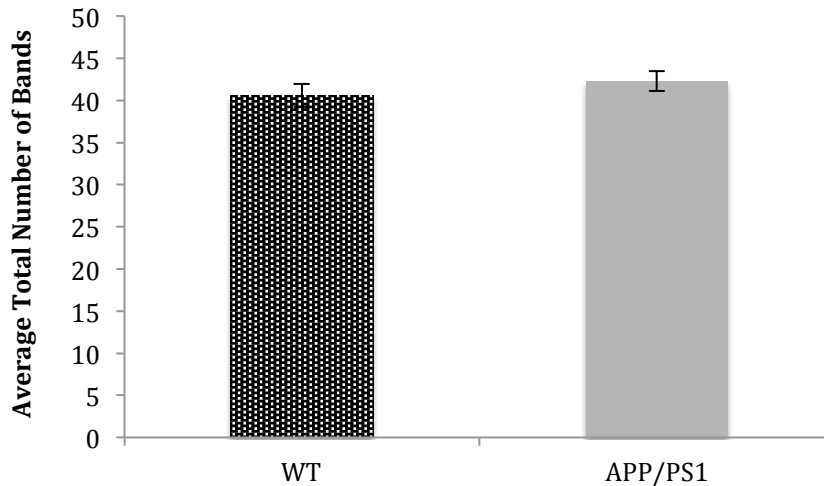
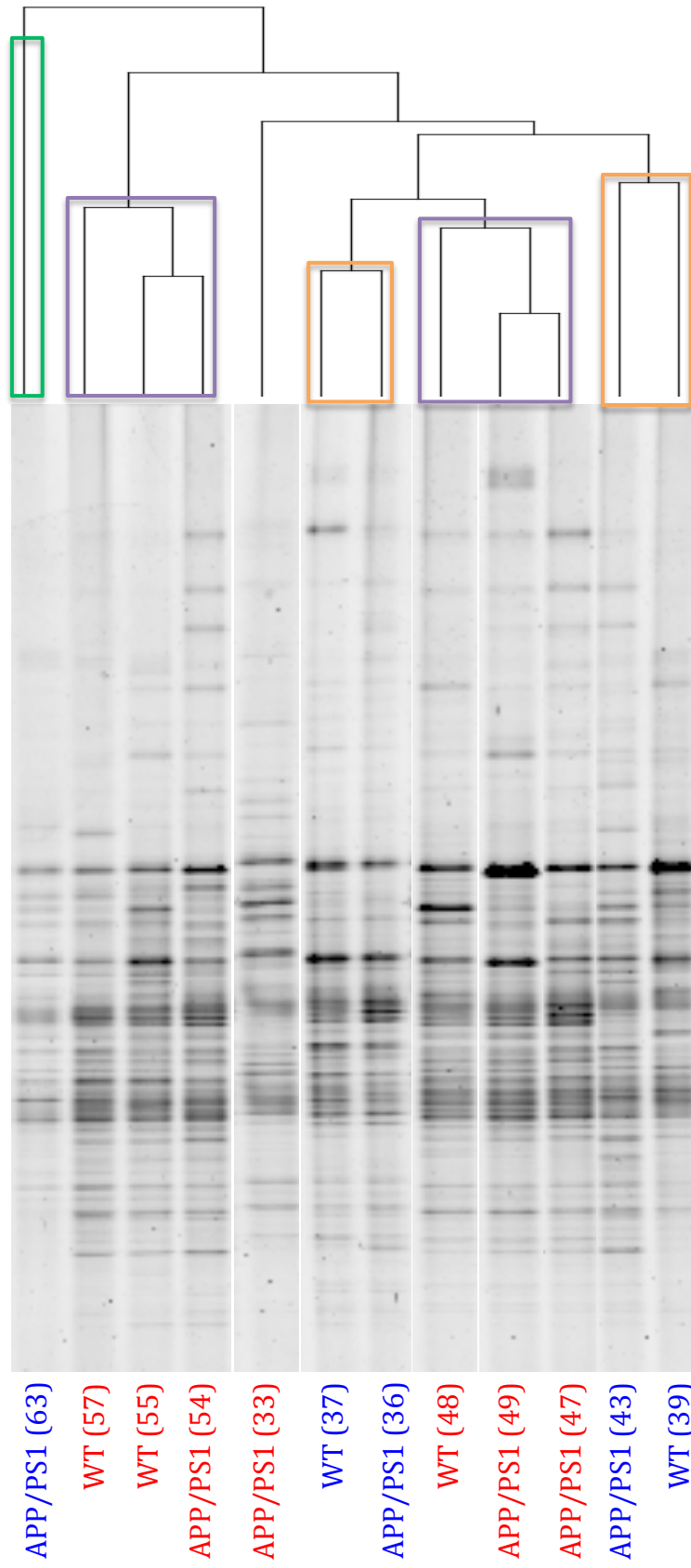


Figure 20: Average total number of bands from 16S rDNA DGGE of mucosal bacterial community from the caecum of seven-month WT and APP/PS1 mice. Error bars indicate SEM. (WT $n = 5$, APP/PS1 $n = 7$, $p = 0.38$).

There was also no significant difference in the luminal-associated microbiota profiles of the caecum in seven-month WT and APP/PS1 mice ($p = 0.81$). Both the phylogenetic tree and NMDS plot shown in figure 21A and 21B, indicate that all but one of the microbiota profiles are closely related, with the profile highlighted in green being distant from the others. The remaining WT and APP/PS1 microbiota profiles are shown to be clustered on the NMDS plot therefore suggesting there is no difference microbiota composition.

However, there did appear to be a trend in the clustering between sexes (males highlighted in orange, females in purple) suggesting sex determined the closest related microbiota profiles.

A)



B)

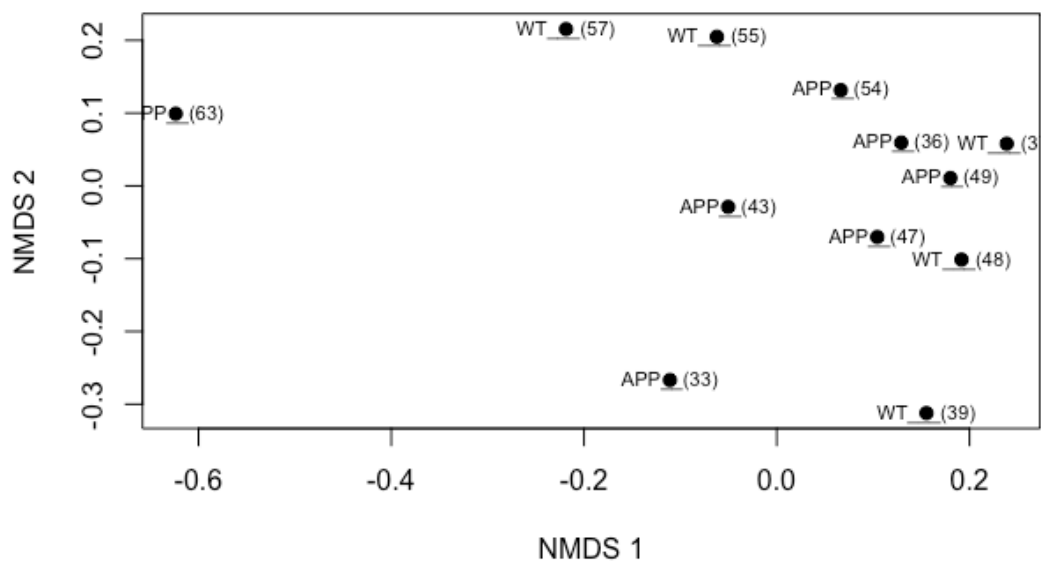


Figure 21: Luminal bacterial community profiling from the caecum of WT and APP/PS1 seven-month mice. A) 16S rDNA DGGE profile and UPGMA phylogenetic tree. No difference in community profiling was observed (WT n = 5, APP/PS1 n = 7, p = 0.81). Blue = male, red = female Green box = distant microbiota profile, orange box = clustered male microbiota profiles, purple = clustered female microbiota profiles. B) NMDS analysis. Stress value = 0.1 indicating good quality fit of data. Numbers in brackets depicts sample identification number. Abbreviation: APP = APP/PS1.

There was a tendency for the luminal-associated microbiota profiles from the caecum of seven-month APP/PS1 mice to have fewer bands than the WT littermates (35.1 ± 8.7 , 39.2 ± 3.3 respectively) as shown in figure 22. However this was not statistically significant, suggesting no overall difference in beta diversity ($p = 0.35$).

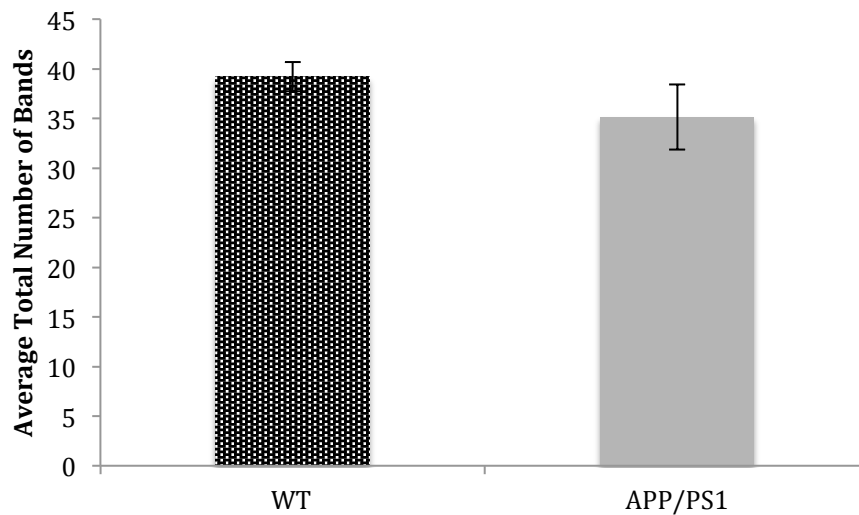
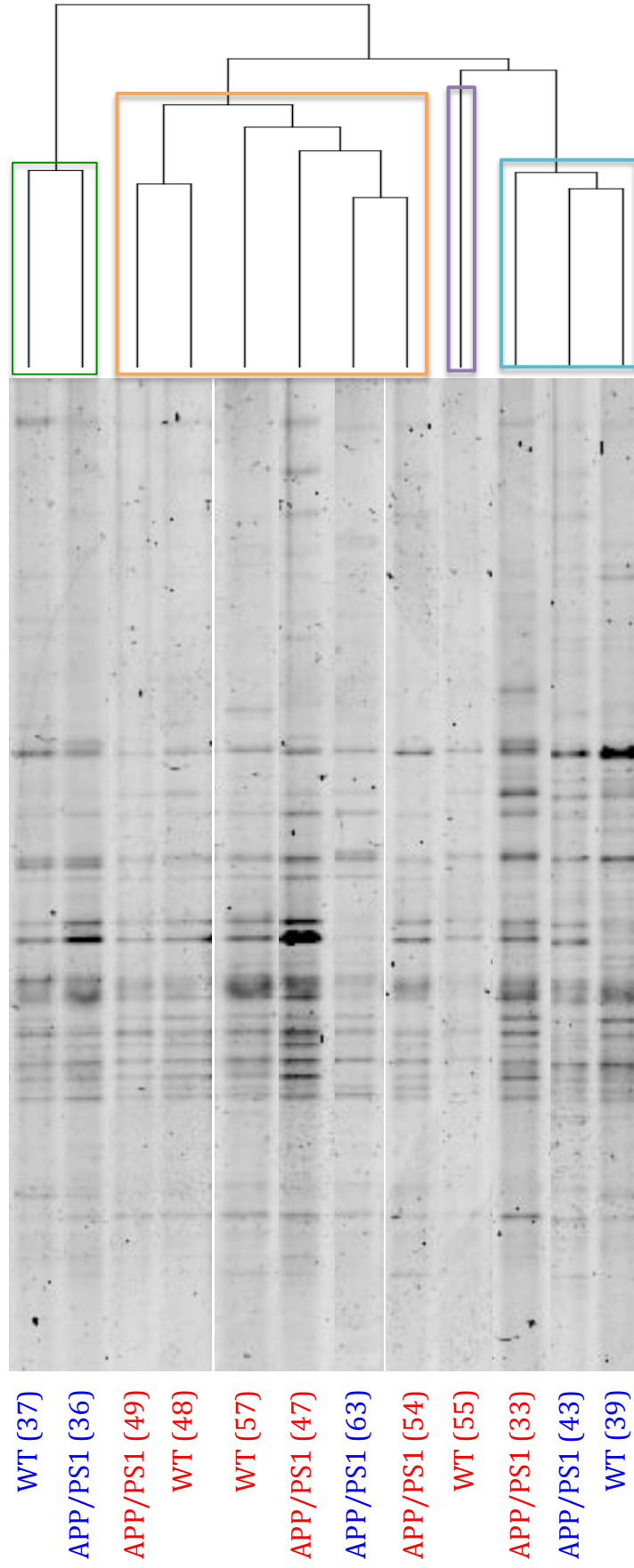


Figure 22: Average total number of bands from 16S rDNA DGGE of the luminal bacterial community from the caecum of seven-month WT and APP/PS1 mice. Error bars indicate SEM. (WT $n = 5$, APP/PS1 $n = 7$, $p = 0.35$).

Distal Colon

There was no statistically significant difference in the mucosal-associated microbiota from the distal colon of seven-month WT and APP/PS1 mice ($p = 0.44$). The phylogenetic tree and NMDS plot shown in figure 23A and 23B suggest that the microbiota profiles are divided into four distinct groups which each have closely related microbiota profiles, as highlighted by the green, orange, purple and blue boxes. However there is no observed correlation between clustering and genotypes, indicating no difference community composition in WT and APP/PS1 mice.

A)



B)

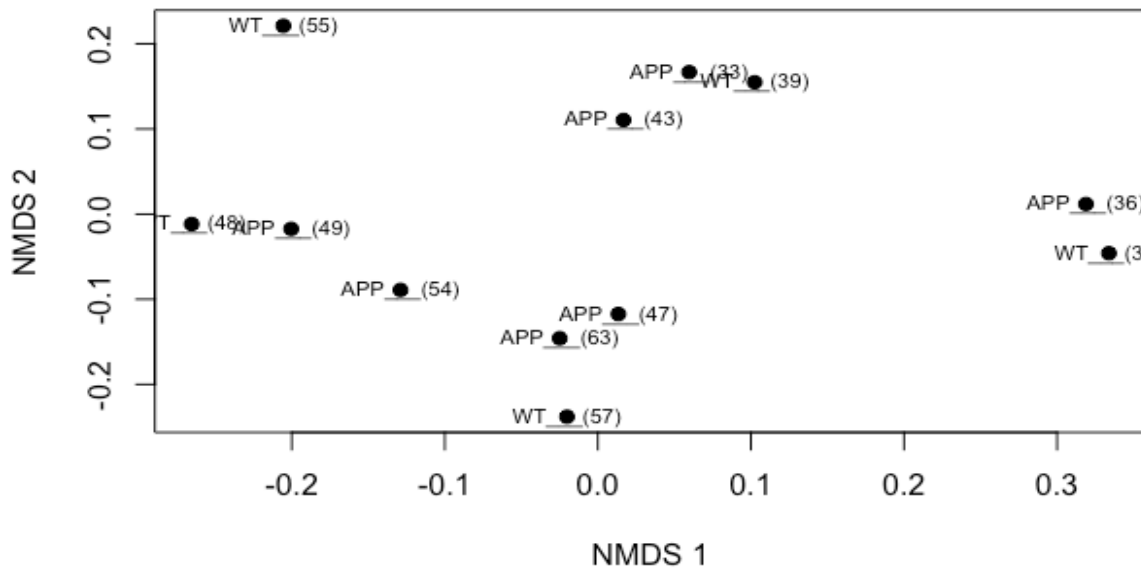


Figure 23: A) Mucosal bacterial community profiling from the distal colon of WT and APP/PS1 seven-month mice. A) 16S rDNA DGGE profile and UPGMA phylogenetic tree. No difference in community profiling was observed (WT n = 5, APP/PS1 n = 7, p = 0.44). Blue = male, red = female. Green, orange, purple and blue boxes = each indicate a group of clustered microbiota profiles. B) NMDS analysis. Stress value = 0.1 indicating good quality fit of data. Numbers in brackets depicts sample identification number. Abbreviation: APP = APP/PS1.

As shown in figure 24, there was no difference in the average total number of bands in the DGGE profile of the WT and APP/PS1 mucosal-associated microbiota (29.6 ± 5.9 and 31.4 ± 5.1 respectively) in the distal colon of seven-month mice indicating no overall difference in beta diversity ($p = 0.58$).

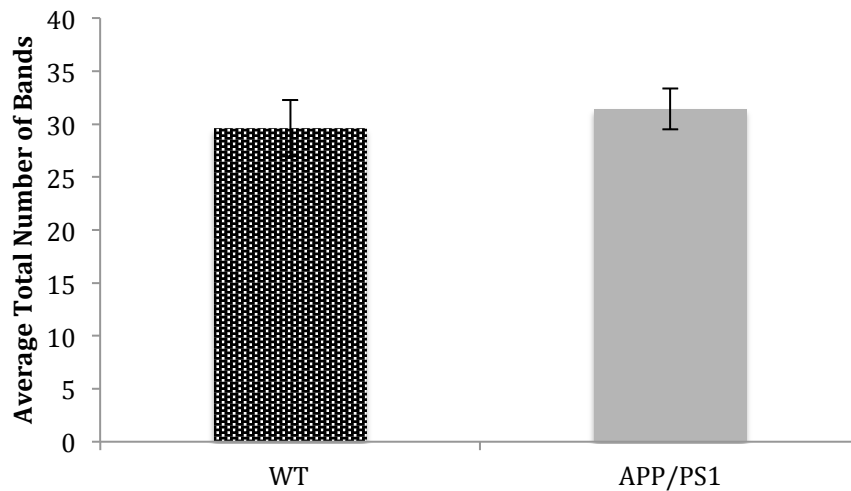
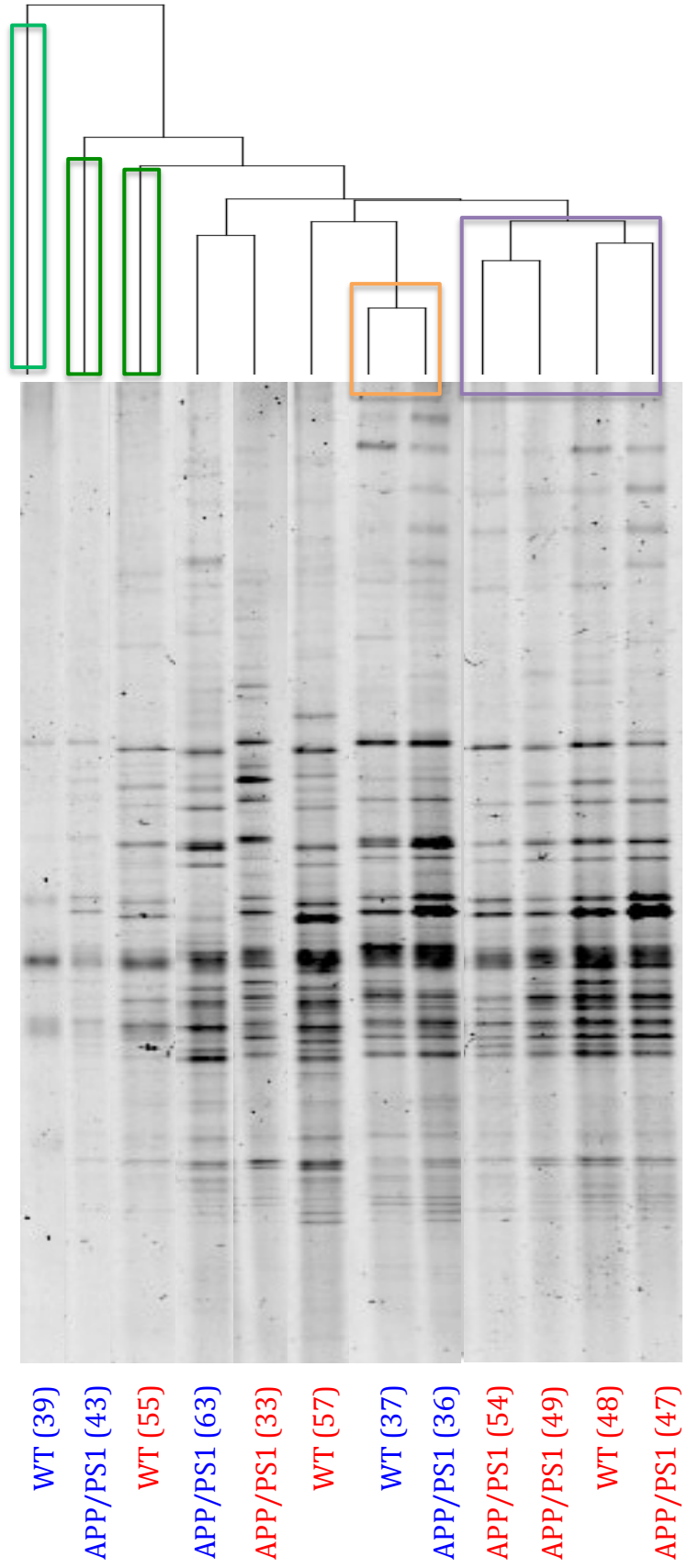


Figure 24: Average total number of bands from 16S rDNA DGGE profile of mucosal bacterial community from the distal colon of seven-month WT and APP/PS1 mice Error bars indicate SEM. (WT n = 5, APP/PS1 n = 7, $p = 0.58$).

There was no significant difference in the luminal-associated microbiota of the distal colon between WT and APP/PS1 seven-month mice ($p = 0.49$). The phylogenetic tree and NMDS plot as shown in figure 25A and 25B revealed three distinct microbiota profiles, highlighted in green, however this was not specific to a single genotype. The remaining microbiota profiles appear closely related with no trend in the clustering of genotypes. However, there did appear to be clustering of male microbiota profiles and female profiles as highlighted by the orange and purple boxes.

A)



B)

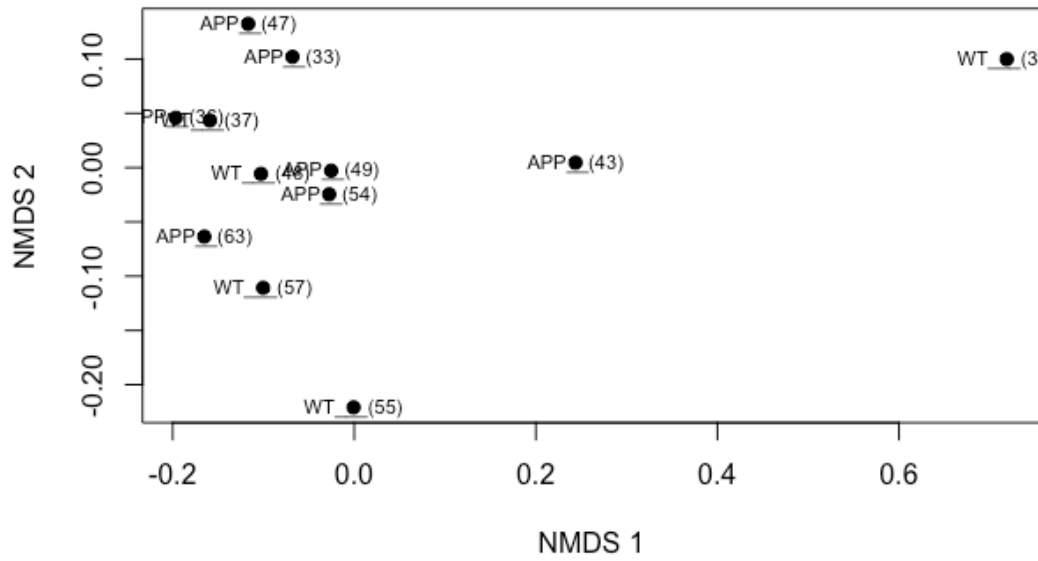


Figure 25: Luminal bacterial community profiling from the distal colon of WT and APP/PS1 seven-month mice. A) 16S rDNA DGGE profile and UPGMA phylogenetic tree. No difference in community profiling was observed (WT n = 5, APP/PS1 n = 7, p = 0.49). Blue = male, red = female. Green boxes = distant microbiota profiles, orange box = clustered male microbiota profiles, purple box = clustered female microbiota profiles. B) NMDS analysis. Stress value = 0.1 indicating good quality fit of data. Numbers in brackets depicts sample identification number. Abbreviation: APP = APP/PS1.

As indicated in figure 26, in the distal colon of seven-month mice there was no difference in the average total number of bands in the luminal-associated microbiota profiles between WT and APP/PS1 mice (43.4 ± 6 and 45.4 ± 3.1 respectively) indicating no overall difference in beta diversity ($p = 0.75$).

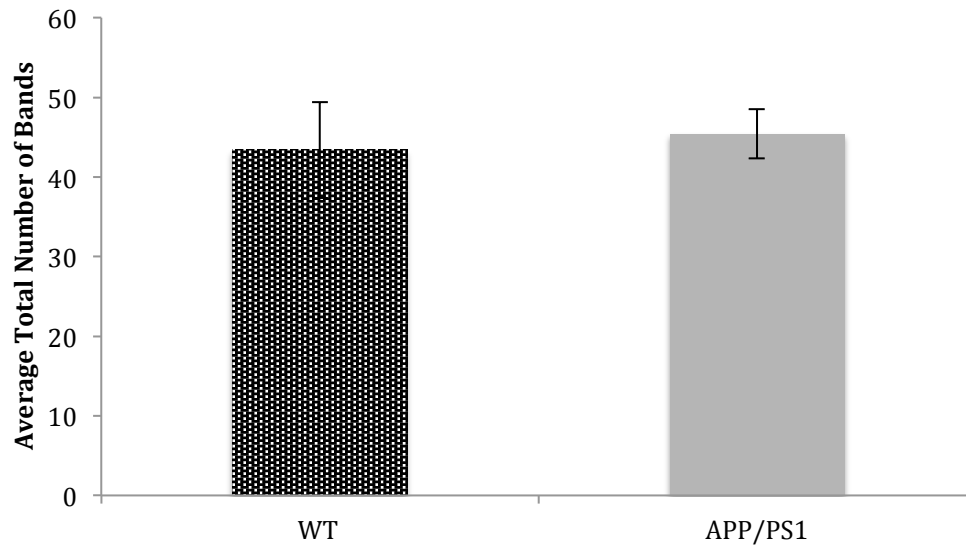


Figure 26: Average total number of bands from 16S rDNA DGGE profile of luminal-bacterial community from the distal colon of seven-month WT and APP/PS1 mice. Error bars indicate SEM. (WT = 5, APP/PS1 n = 7, $p = 0.75$).

5.2 Fifteen-month old APP/PS1 mice

5.2.1 A decrease in goblet cell numbers was observed in the ileum of fifteen-month APP/PS1 mice

Fifteen-month APP/PS1 mice were utilised as a model of late A β associated AD pathology. As shown in figure 27A, there was a propensity for the villus height in the ileum to be 14.8% greater in APP/PS1 mice compared to WT littermates, however this did not reach statistical significance ($p = 0.17$).

A similar observation was seen in the crypts of the ileum, as shown in figure 27B, with the APP/PS1 crypts tending to be 16.6% larger than the WT mice, however this was not statistically significant ($p = 0.19$). In contrast, there was a tendency for shorter crypts in the caecum and colon by approximately 7.3% and 2%, however this was also not statistically significant ($p = 0.38$ and $p = 0.82$ respectively).

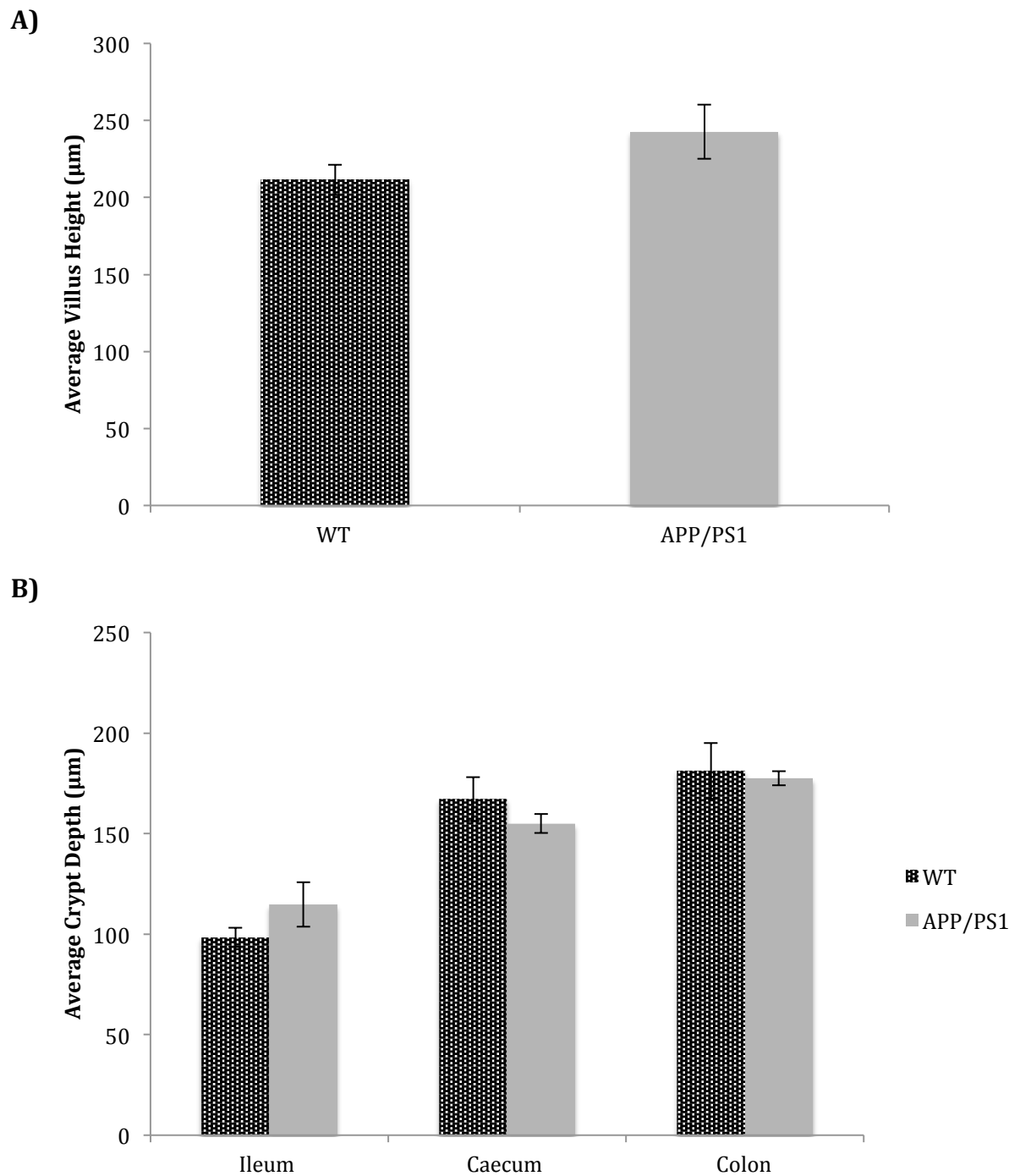


Figure 27: Histological analysis of the gut in fifteen-month mice. Error bars indicate SEM. A) Average villus height in the ileum (WT n = 4, APP/PS1 n = 4, p = 0.17). B) Average crypt depth in the ileum (WT n = 5, APP/PS1 n = 4, p = 0.19), caecum (WT n = 5, APP/PS1 n = 4, p = 0.38) and distal colon (WT n = 5, APP/PS1 n = 4, p = 0.82).

The average number of goblet cells in the ileum of fifteen-month mice was significantly lower in the APP/PS1 mice compared to the WT littermates as shown in figure 28A and 28B. The villi and crypts of APP/PS1 mice averaged 31.5% and 34.9% fewer goblet cells per 100 μm compared to WT littermates ($p = 0.01$ and $p = 0.001$ respectively).

In contrast, the average number of goblet cells in the caecum and distal colon had a propensity to be greater in the APP/PS1 mice than the WT littermates. An 11.8% increase in goblet cells was observed in the APP/PS1 colon, compared to 9.1% in the caecum, however neither result was significant ($p = 0.40$ and $p = 0.34$ respectively). Representative images are shown in figure 29.

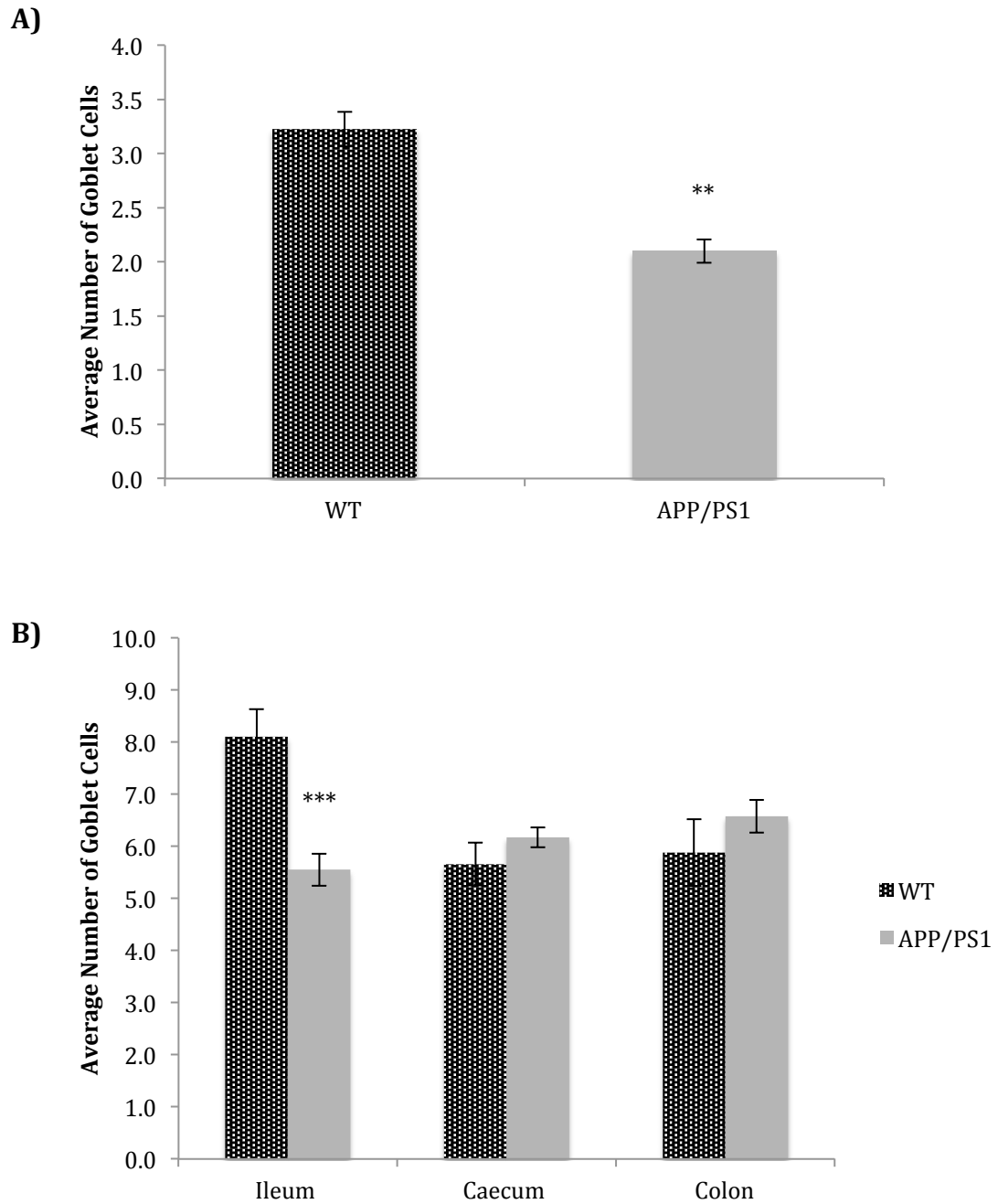


Figure 28: Average number of goblet cells in fifteen-month mice. Error bars indicate SEM. A) Average number of goblet cells per 100 μm of villi in the ileum (WT n = 4, APP/PS1 n = 4, p = 0.001). B) Average number of goblet cells per 100 μm of crypt in the ileum (WT n = 5, APP/PS1 n = 4, p = 0.01), caecum (WT n = 5, APP/PS1 n = 4, p = 0.34) and distal colon (WT n = 5, APP/PS1 n = 4, p = 0.40). ** p \leq 0.01; *** p \leq 0.001.

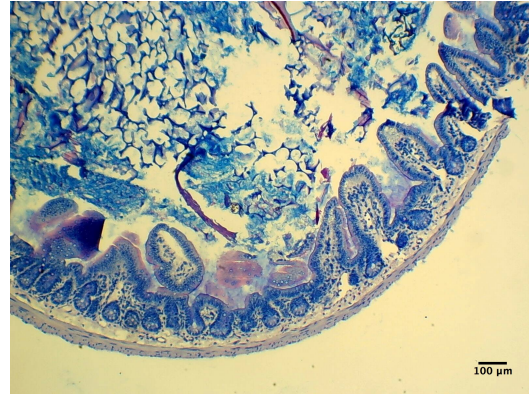
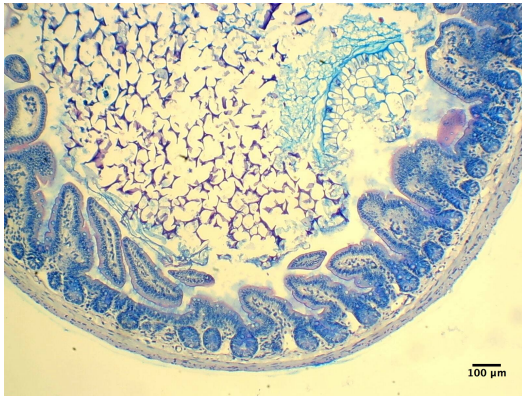
Despite fewer goblet cell numbers in the ileum of APP/PS1 mice, there were no observational differences in the types of mucins produced as shown in figure 29. The goblet cells that produced neutral mucins tended to be located at the base of the crypts, and those that produced acidic mucins were found at the opening of the crypt and along the villi in both WT and APP/PS1 mice.

Similarly, there was no difference in the types of mucins produced by goblet cells in the caecum. In both WT and APP/PS1 mice the acidic mucins tended to be located at the base of the crypts whereas the neutral mucins were located at the opening of the crypts. The same was observed in the distal colon, except there was a tendency for a greater number of goblet cells producing neutral mucins towards the opening of the crypt in the APP/PS1 mice.

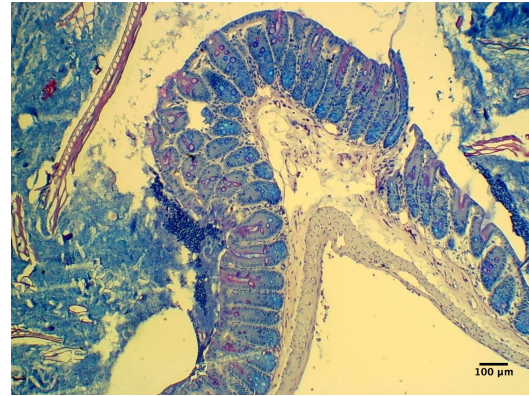
WT

APP/PS1

Ileum



Caecum



Colon

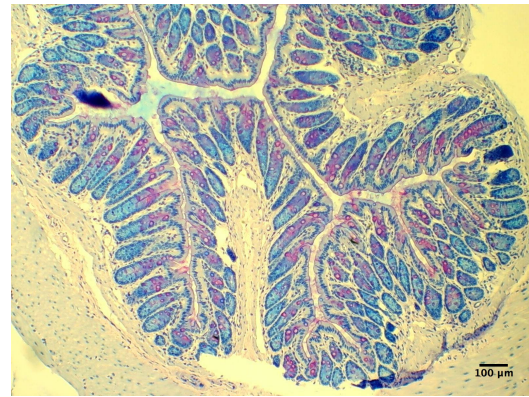
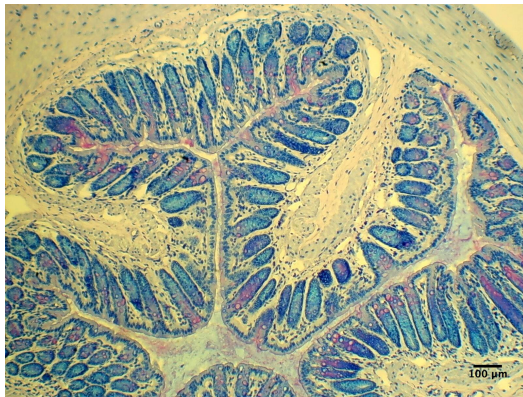


Figure 29: Representative PAS/AB stained sections in fifteen-month mice.

Acidic mucins are stained blue by AB and neutral mucins are stained pink by PAS. Purple mucins indicate a combination of both acidic and basic mucins produced by a goblet cell. Scale bar = 100 μ m.

Sex specific differences in the number of goblet cells present in the ileum of fifteen-month mice were investigated as shown in figure 30A and 30B. Although statistical analysis could not be performed due to a small n number, there was no observed differences between the sex of the mice and decreased goblet cell numbers in the villi and crypts of the ileum.

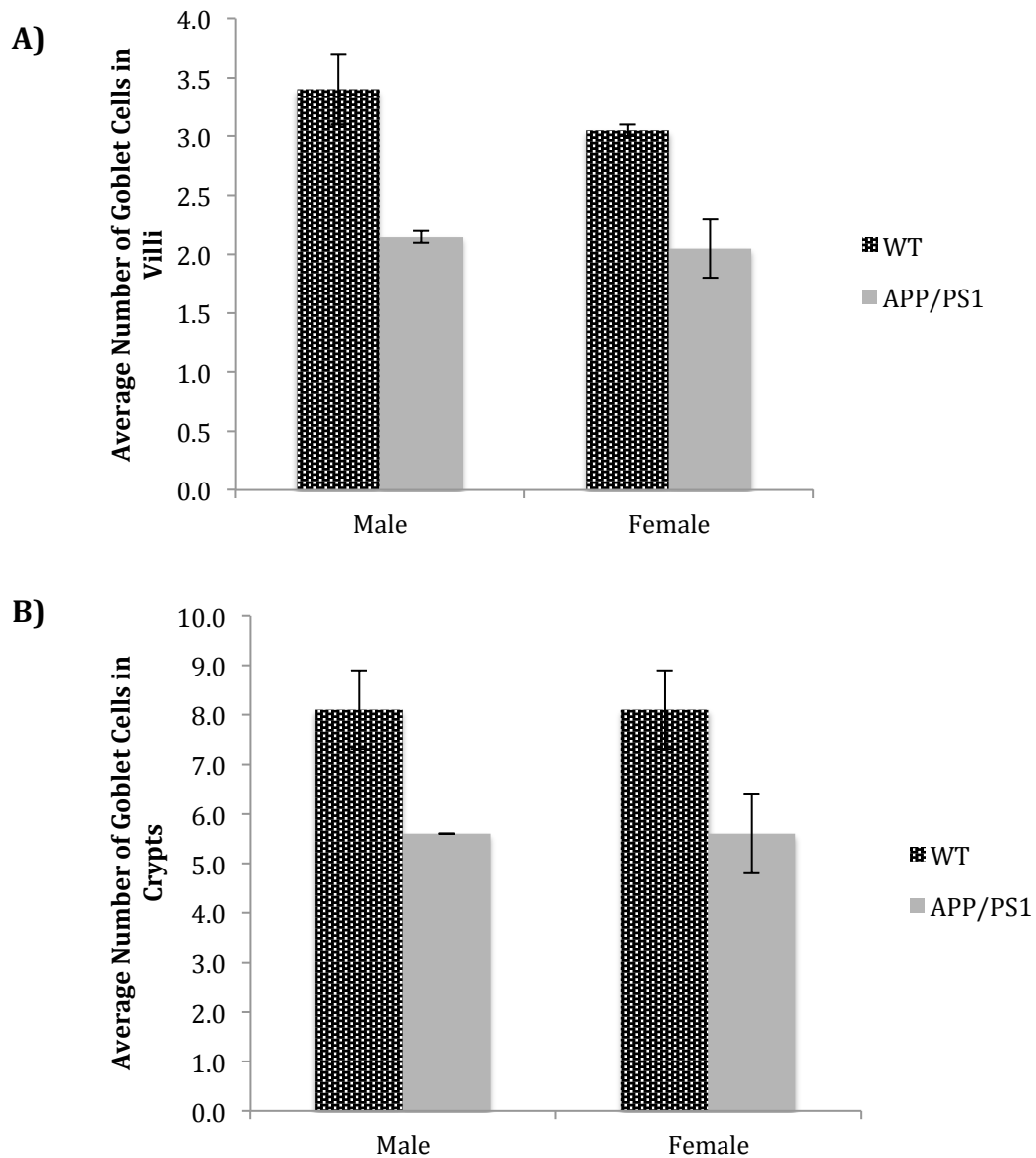


Figure 30: Average number of goblet cells in the ileum of male and female fifteen-month mice. Average number of goblet cells per 100 μm of villus height and/or crypt depth Error bars indicate SEM. A) Male villus (WT n = 2, APP/PS1 n = 2), female villus (WT n = 2, APP/PS1 n = 2). B) Male crypt (WT n = 2, APP/PS1 n = 2), female crypt (WT n = 3, APP/PS1 n = 2).

As indicated in figure 31A , there was no difference in the number of EEC's in the ileum of fifteen-month APP/PS1 mice. There was a propensity for 21.9% more EECs in the villi, however this was not statistically significant ($p = 0.25$).

Likewise, in figure 31B, there was no difference in the number of EEC's observed in the crypts of the ileum, with 16.1% fewer in the APP/PS1 mice, which was not statistically significant ($p = 0.61$). There was also no difference observed in the large intestine of APP/PS1 mice, although there was a propensity for 17.7% fewer EECs in the caecum in contrast to a 39.4% greater abundance in the colon, however similarly neither result was significant ($p = 0.54$ and $p = 0.25$ respectively).

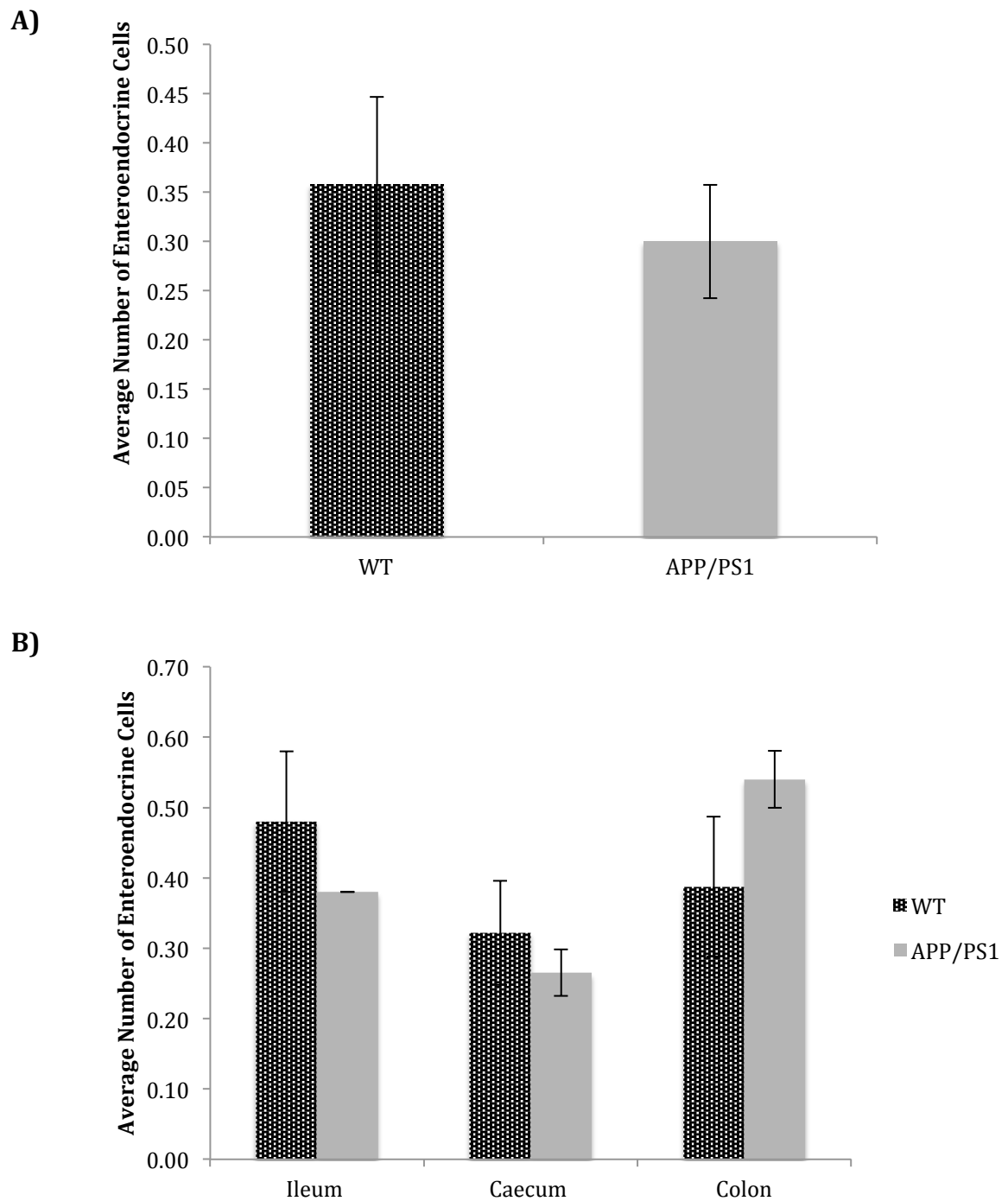


Figure 31: Average number of EEC's in fifteen-month mice. Error bars indicate SEM. A) Average number of EECs per 100 μm of villi in the ileum (WT n = 4, APP/PS1 n = 4, p = 0.61). B) Average number of EECs per 100 μm of crypt in the ileum (WT n = 5, APP/PS1 n = 4, p = 0.25), caecum (WT n = 5, APP/PS1 n = 4, p = 0.54) and distal colon (WT n = 4, APP/PS1 n = 4, p = 0.25).

5.2.2 No difference in bacterial community was observed in fifteen-month APP/PS1 mice.

The phylum Firmicutes had a tendency to be less abundance in the small and large intestine of fifteen-month APP/PS1 compared to WT littermates as indicated in figure 32. The large intestine saw a similar decrease of $20\% \pm 11\%$ and $21\% \pm 23\%$ in the caecum and colon, however this was not statistically significant ($p = 0.27$ and $p = 0.80$ respectively). Furthermore, a smaller but variable decrease of $10\% \pm 38\%$ tended to occur in the ileum, which was not statistically significant ($p = 0.58$).

The opposite was observed with Bacteroidetes, with the greatest increase tending to occur in the caecum and colon at $49\% \pm 21\%$ and $33\% \pm 21\%$ respectively, however this was not statistically significant ($p = 0.31$ and $p = 0.47$). The decrease in the ileum tended to be smaller but with a larger amount of variability than the large intestine with a $12\% \pm 47\%$ decrease which was not statistically significant ($p = 0.82$).

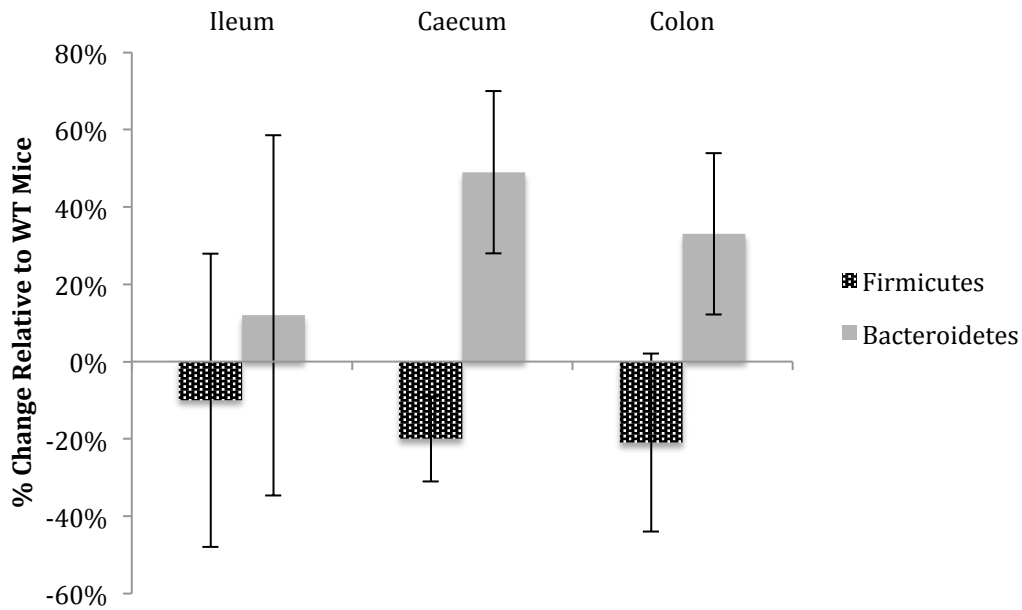


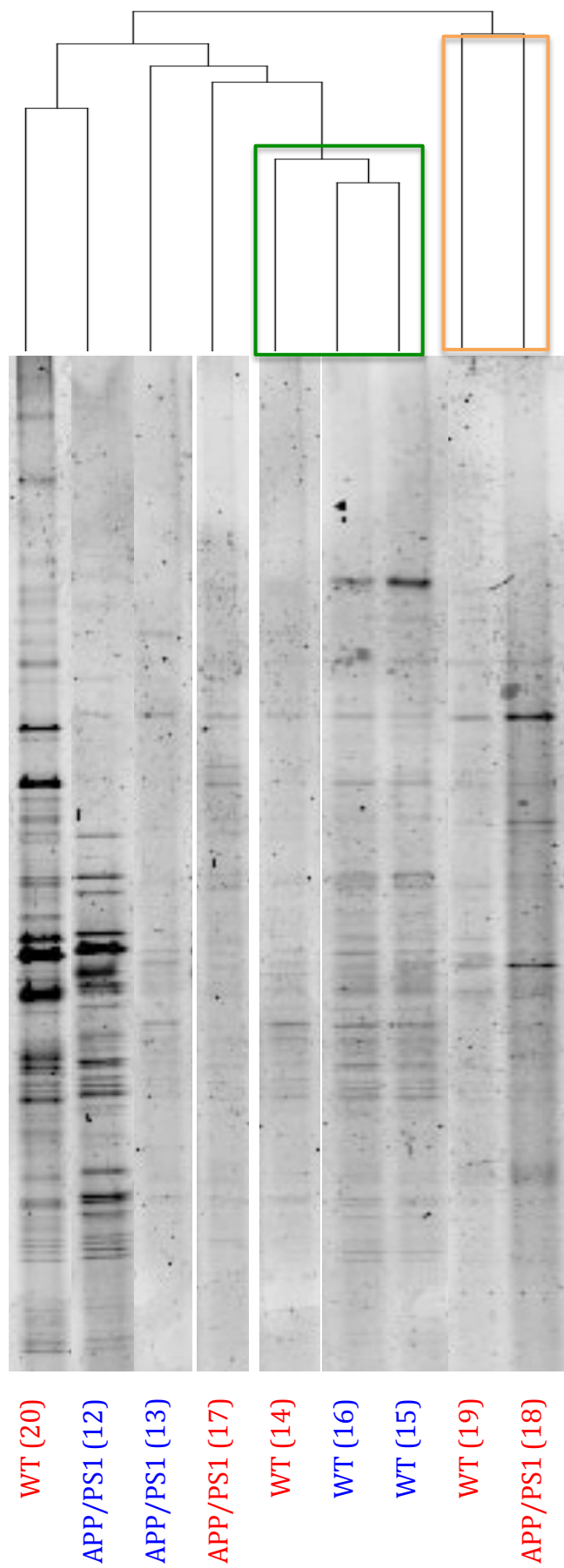
Figure 32: Relative percentage change of predominant mucosal-associated phyla in fifteen-month mice. Percentage change of the phyla Firmicutes and Bacteroidetes in the mucosal-associated microbiota of fifteen-month APP/PS1 mice relative to age matched WT littermates. Error bars indicate SEM. Firmicutes: ileum (WT n = 5, APP/PS1 n = 4, p = 0.58), caecum (WT n = 5, APP/PS1 n = 4, p = 0.27), distal colon (WT n = 5, APP/PS1 n = 4, p = 0.80). Bacteroidetes: ileum (WT n = 5, APP/PS1 n = 4, p = 0.82), caecum (WT n = 5, APP/PS1 n = 4, p = 0.31), distal colon (WT n = 5, APP/PS1 n = 4, p = 0.47).

DGGE Ileum

There was no difference in the mucosal-associated bacteria community profiles in the ileum of fifteen-month WT and APP/PS1 mice (p = 0.54). Several of the microbiota profiles appeared similar, as shown in the phylogenetic tree in figure 33A. In particular, the clade highlighted in green is shown to strongly cluster in the NMDS plot in figure 33B. The most distant related microbiota profiles belong to the clade highlighted in orange, which are also shown to be distant from each other on the NMDS plot.

Although the clustered microbiota profiles, highlighted in green are all WT genotypes, the remaining microbiota profiles are distant from one another and represent both WT and APP/PS1 mice.

A)



B)

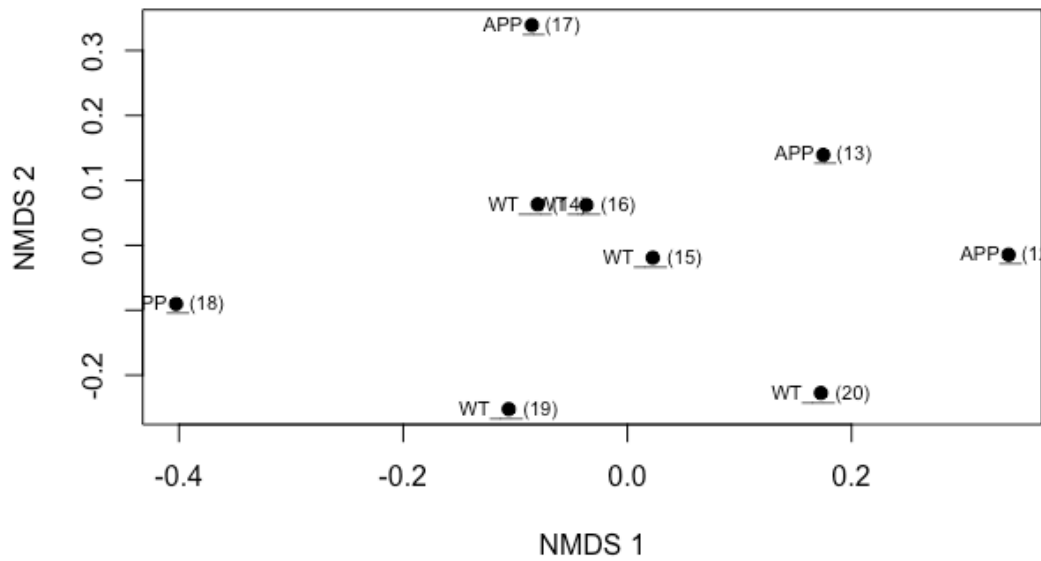


Figure 33: Mucosal bacterial community profiling from the ileum of WT and APP/PS1 fifteen-month mice. A) 16S rDNA DGGE profile and UPGMA phylogenetic tree. No difference in community profiling was observed (WT n = 5, APP/PS1 n = 4, p = 0.54). Blue = male, red = female. Green box = clustered microbial profiles, orange box = distant microbiota profiles. B) NMDS analysis. Stress value = 0.1 indicating good quality fit of data. Numbers in brackets depicts sample identification number. Abbreviation: APP = APP/PS1.

As shown in figure 34, there was a tendency for the mucosal-associated microbiota profiles from the ileum of fifteen-month APP/PS1 mice to have a slightly lower total number of bands (37.8 ± 3.9) compared to the WT littermates (40.8 ± 3.2), however the difference was not significant ($p = 0.56$), suggesting no difference in beta diversity.

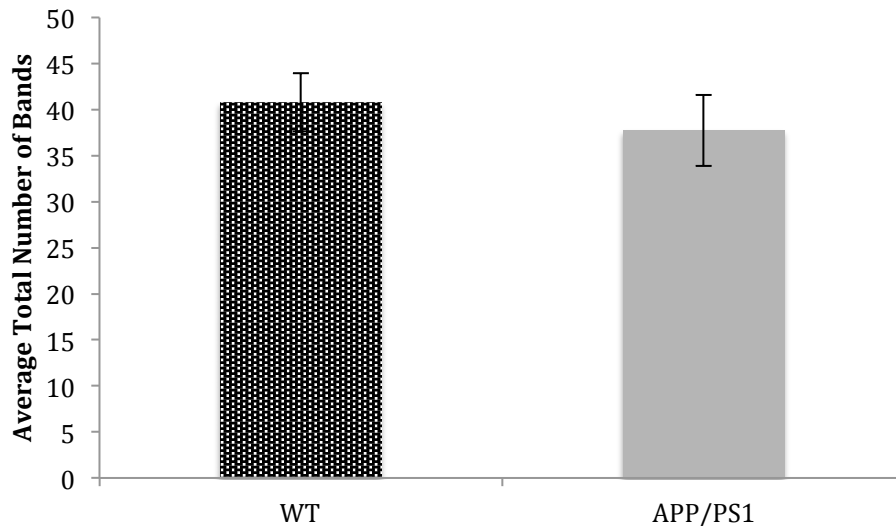
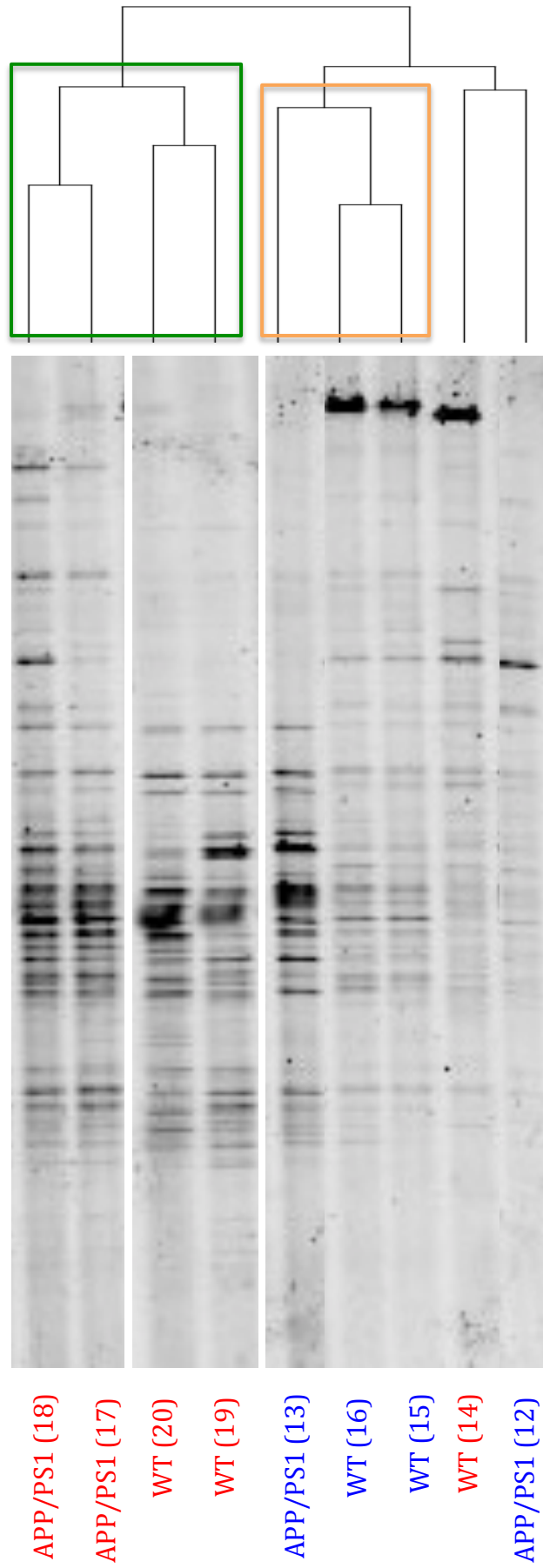


Figure 34: Average total number of bands from 16S rDNA DGGE profile of mucosal- bacterial community from the ileum of fifteen-month WT and APP/PS1 mice. Error bars indicate SEM. (WT n = 5, APP/PS1 n = 4, $p = 0.56$).

There was no significant difference in the microbial profiles of the luminal-associated microbiota from the ileum of fifteen-month WT and APP/PS1 mice ($p = 0.78$). As shown in the phylogenetic tree and NMDS plot in figure 35A and 35B there is no clustering of WT and APP/PS1 genotypes therefore suggesting no difference in community composition of the two genotypes.

However, there does appear to be clustering between same sexes regardless of genotype. The male dominated clade highlighted in green appears distant from the female dominated clade highlighted in orange, suggesting there may be sex specific differences.

A)



B)

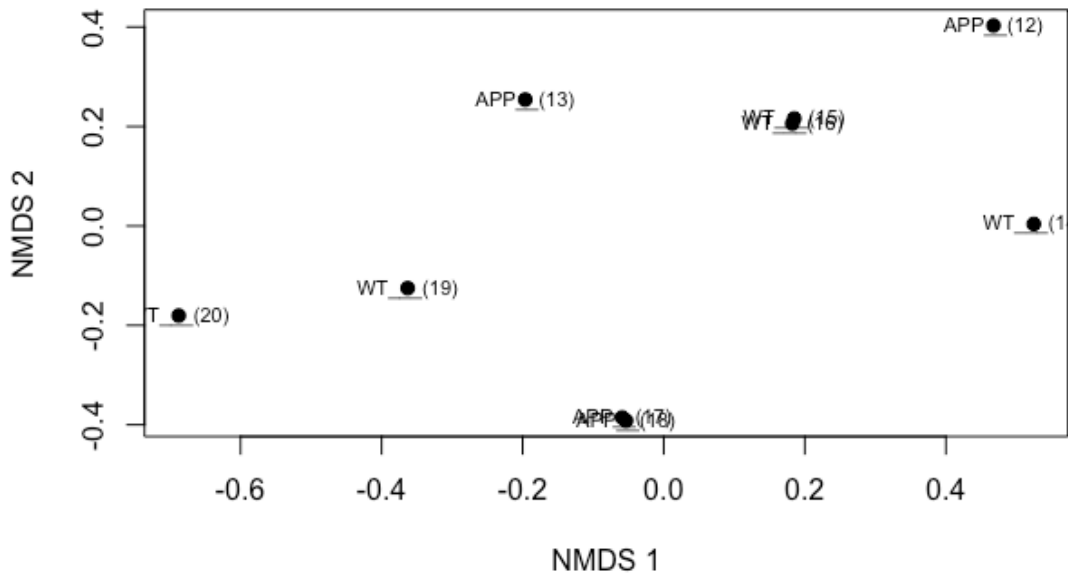


Figure 35: Luminal bacterial community profiling from the ileum of WT and APP/PS1 fifteen-month mice. A) 16S rDNA DGGE profile and UPGMA phylogenetic tree. No difference in community profiling was observed (WT n =5, APP/PS1 n = 4, p = 0.78). Blue = male, red = female. Green box = male microbiota profiles, orange = female microbiota profiles. B) NMDS analysis. Stress value = 0.03 indicating good quality fit of data. Numbers in brackets depicts sample identification number. Abbreviation: APP = APP/PS1.

Average total number of bands in the microbiota profiles were investigated as shown in figure 36, although statistical analysis was not performed due to low n number. There appeared to be no difference in the average total number of bands of each genotype in the luminal-associated microbiota from the ileum of fifteen-month WT and APP/PS1 mice, suggesting no difference in beta diversity.

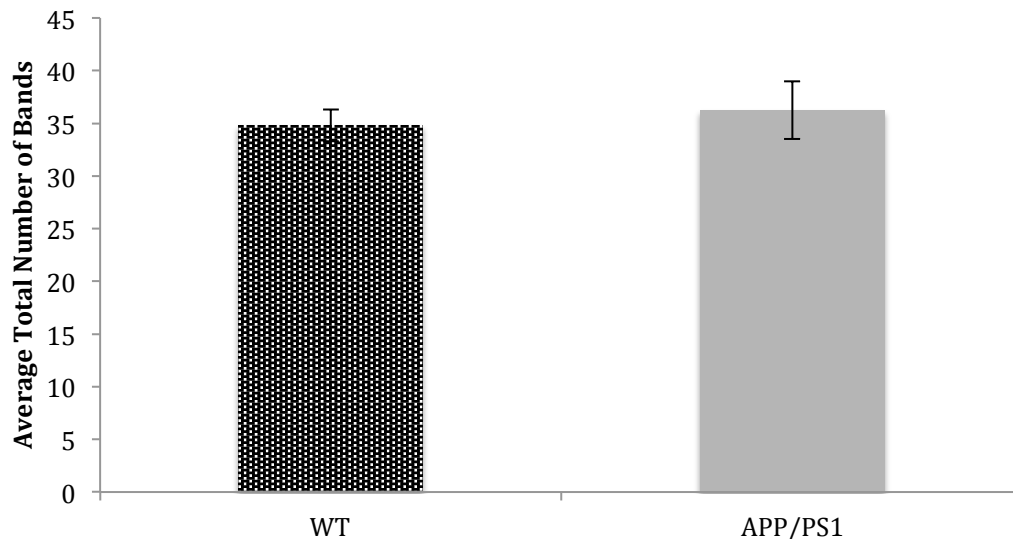
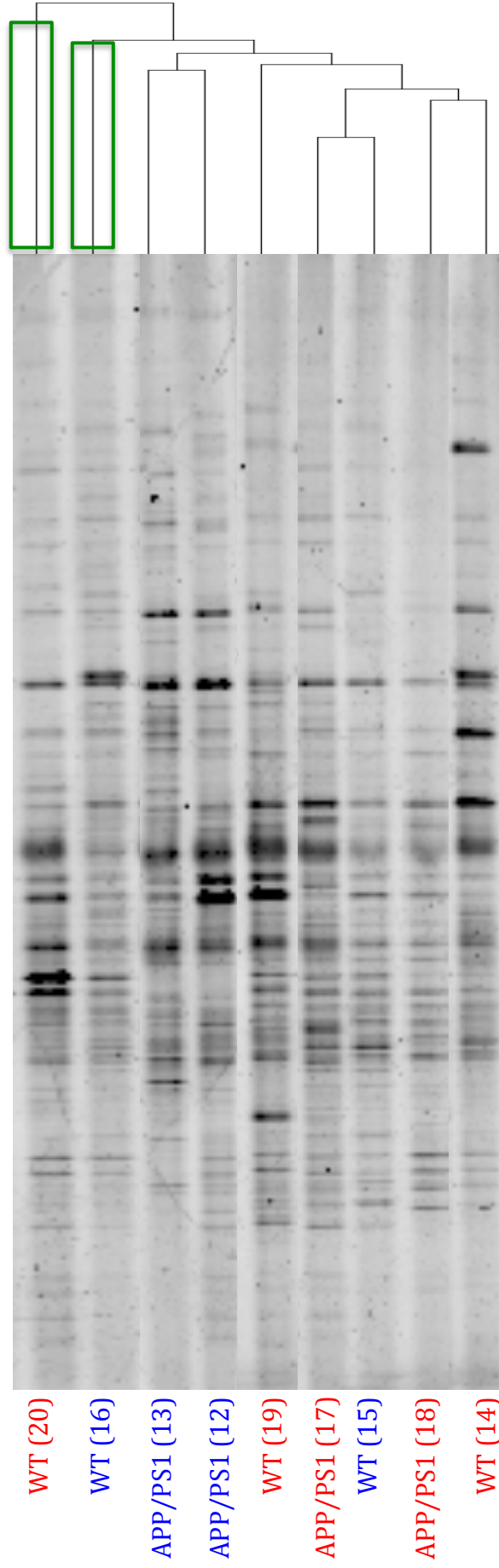


Figure 36: Average total number of bands from 16S rDNA DGGE profile of luminal-bacterial community from the ileum of fifteen-month WT and APP/PS1 mice. Error bars indicate SEM. (WT n = 5, APP/PS1 n = 4, p = 0.64).

Caecum

There was no statistically significant difference in the mucosal-associated microbiota profiles in the caecum of fifteen-month WT and APP/PS1 mice (p = 0.24). As shown in the phylogenetic tree in Figure 37A, the majority of the microbiota profiles appear closely related, with two distant profiles as highlighted by the green boxes. The random distribution of the microbiota profiles in the NMDS plot shown in figure 37B indicates no clustering between WT and APP/PS1 mice, and therefore no differences in the community composition between the genotypes.

A)



B)

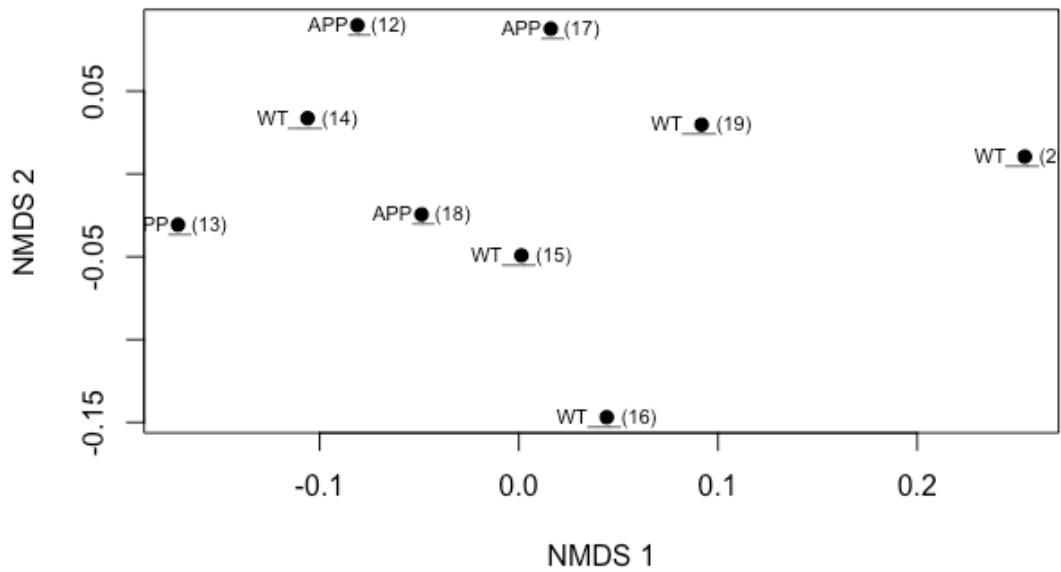


Figure 37: Mucosal bacterial community profiling from the caecum of WT and APP/PS1 fifteen-month mice. A) 16S rDNA DGGE profile and UGMA phylogenetic tree. No difference in community profiling was observed (WT n = 5, APP/PS1 n = 4, p = 0.24). Blue = male, red = female. Green box = distant microbiota profiles. B) NMDS analysis. Stress value = 0.1 indicating good quality fit of data. Numbers in brackets depicts sample identification number. Abbreviation: APP = APP/PS1.

There was no difference in the average total number of bands in the DGGE profiles of mucosal-associated bacteria of WT (39.4 ± 1.5) and APP/PS1 (41.3 ± 2.4) from the fifteen-month caecum, indicating no difference in beta diversity ($p = 0.52$) as shown in figure 38.

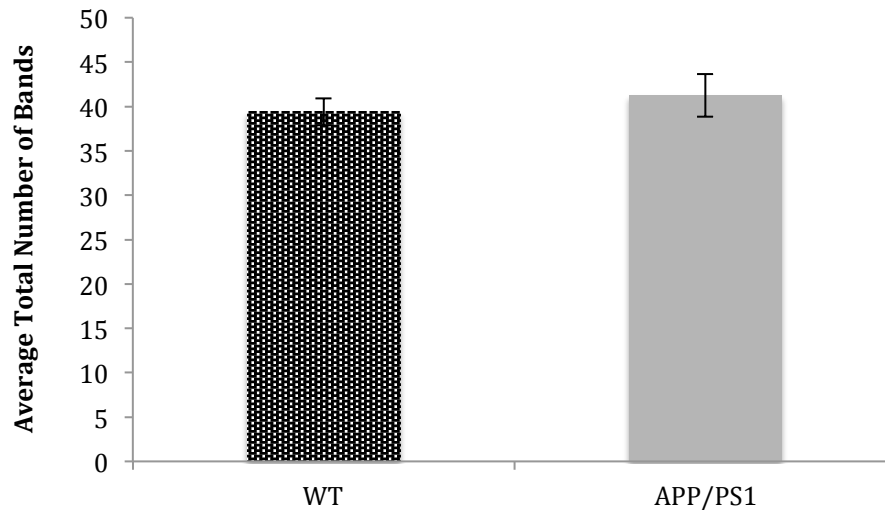
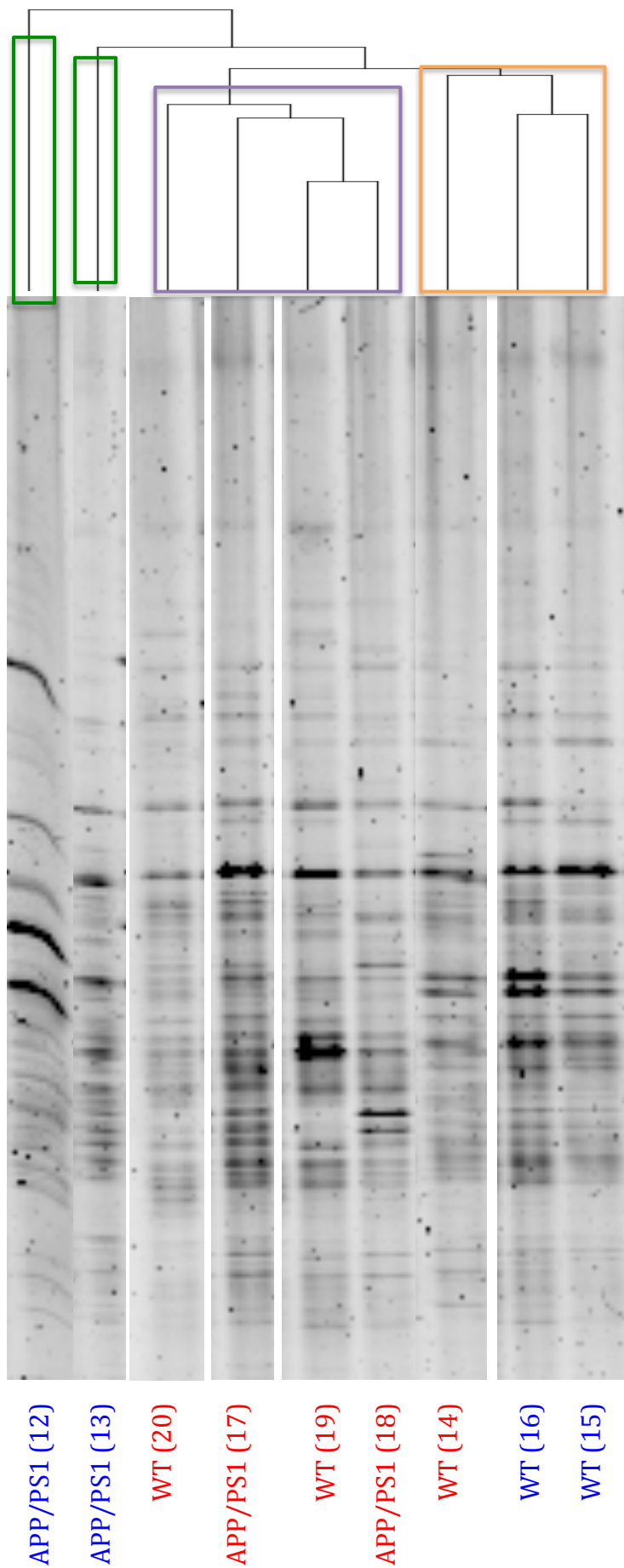


Figure 38: Average total number of bands from 16S rDNA DGGE profile of the mucosal bacterial community from the caecum of fifteen-month WT and APP/PS1 mice. Error bars indicate SEM. (WT $n = 5$, APP/PS1 $n = 4$, $p = 0.52$).

There was no difference in the luminal-associated microbiota from the caecum of fifteen-month WT and APP/PS1 mice ($p = 0.87$). The most distinct microbiota profiles are highlighted in the green boxes in the phylogenetic tree shown in figure 39A. The remaining microbiota profiles appear closely related and are shown to be clustered on the NMDS plot in figure 39B. However, there was no genotype associated clustering suggesting that there is no difference in microbiota profiles between the WT and APP/PS1 mice.

However, as highlighted by the orange and purple boxes in figure 39A, there appears a strong tendency for the clustering of male WT and APP/PS1 mice and female WT and APP/PS1 mice, suggesting that sex specific differences may be present.

A)



B)

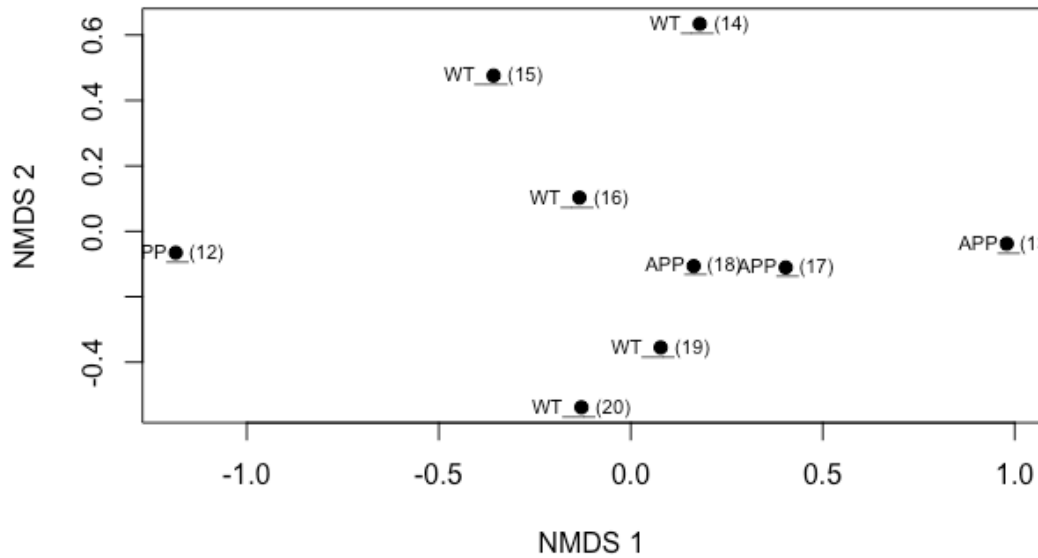


Figure 39: Luminal bacterial community profiling from the caecum of WT and APP/PS1 fifteen-month mice. A) 16S rDNA DGGE profile and UPGMA phylogenetic tree. No difference in community profiling was observed (WT n = 5, APP/PS1 n = 4, p = 0.87). Blue = male, red = female. Green boxes = distant microbiota profiles, orange box = clustered male microbiota profiles, purple box = clustered female microbiota profiles. B) NMDS analysis. Stress value = 0.1 indicating good quality fit of data. Numbers in brackets depicts sample identification number. Abbreviation: APP = APP/PS1.

There was no difference between the average total number of bands in the DGGE profiles of the luminal-associated microbiota in the caecum of fifteen-month WT and APP/PS1 mice as shown in figure 40. APP/PS1 mice exhibited 37.8 ± 3.8 bands compared to 37.2 ± 1.4 in the WT littermates, which was not statistically significant suggesting no difference in beta diversity ($p = 0.89$).

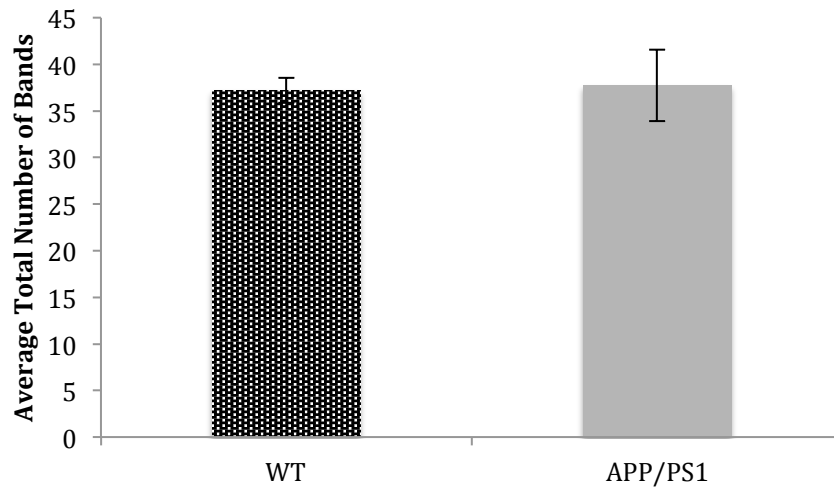
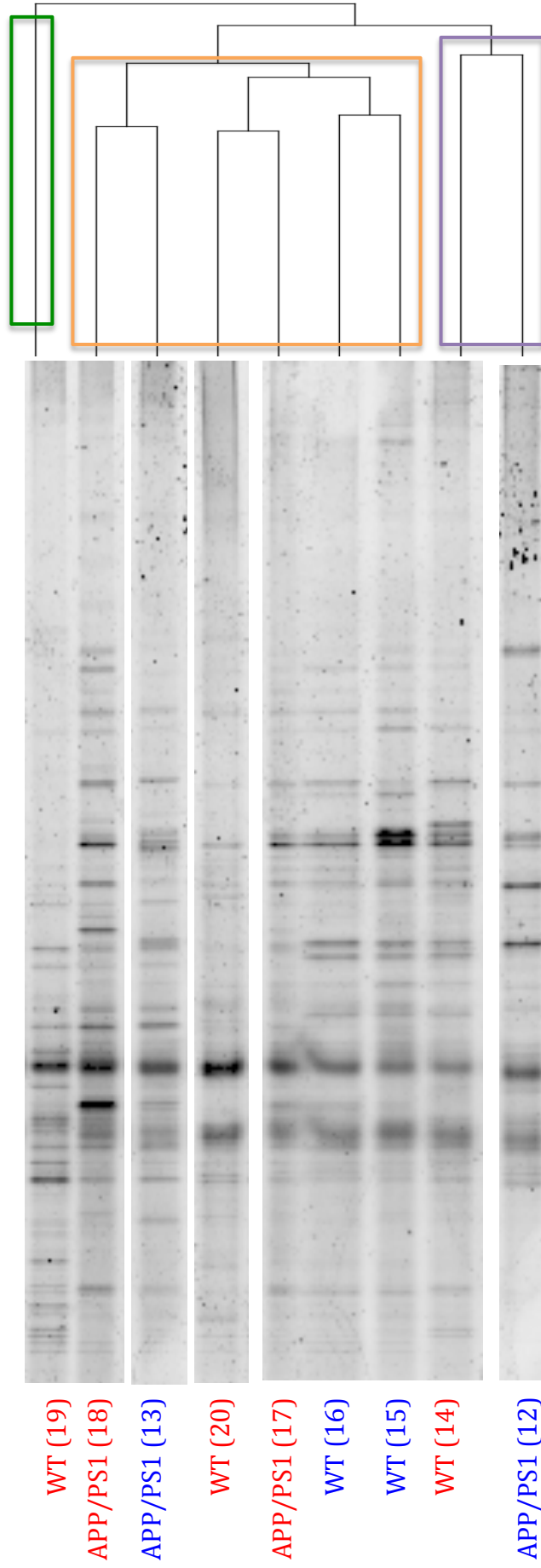


Figure 40: Average total number of bands from 16S rDNA DGGE profile of luminal-bacterial community from the caecum of fifteen-month WT and APP/PS1 mice. Error bars indicate SEM. (WT $n = 5$, APP/PS1 $n = 4$, $p = 0.89$).

Distal Colon

There was no statistically significant difference between the mucosal-associated microbiota profiles between WT and APP/PS1 mice in the distal colon of fifteen-month mice ($p = 0.83$). As shown in the phylogenetic tree in figure 41A, the microbiota profiles can be roughly divided into three groups, indicated by the green, orange and purple boxes. However there appears no correlation between clustering and genotypes, which can also be seen in the NMDS plot in figure 41B. This suggests there is no difference in the microbiota profiles between WT and APP/PS1 mice.

A)



B)

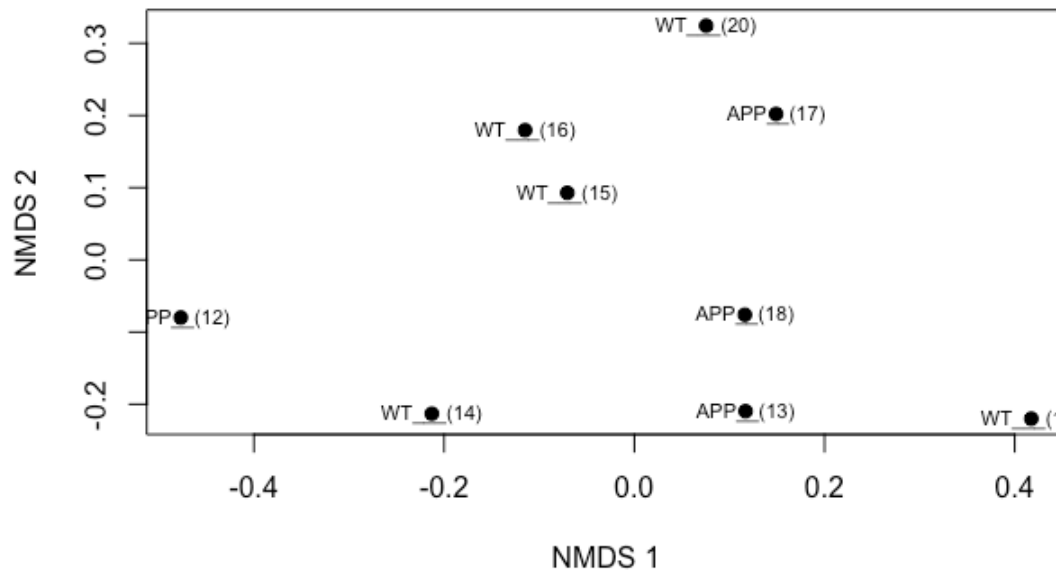


Figure 41: Mucosal bacterial community profiling from the distal colon of WT and APP/PS1 fifteen-month mice. A) 16S rDNA DGGE profile and UPGMA phylogenetic tree. No difference in community profiling was observed (WT n = 5, APP/PS1 n = 4, p = 0.83). Blue = male, red = female. Green, orange and purple boxes = clustered microbiota profiles. B) NMDS analysis. Stress value = 0.1 indicating good quality fit of data. Numbers in brackets depicts sample identification number. Abbreviation: APP = APP/PS1.

There was no difference in the number of bands present in the mucosal-associated microbiota of the distal colon in the fifteen-month WT and APP/PS1 mice suggesting no difference in beta diversity ($p = 0.91$). The APP/PS1 mice however displayed a greater amount of variation in the number of bands with 35.5 ± 5 bands present, compared to 36 ± 0.4 bands in the WT mice as shown in figure 42.

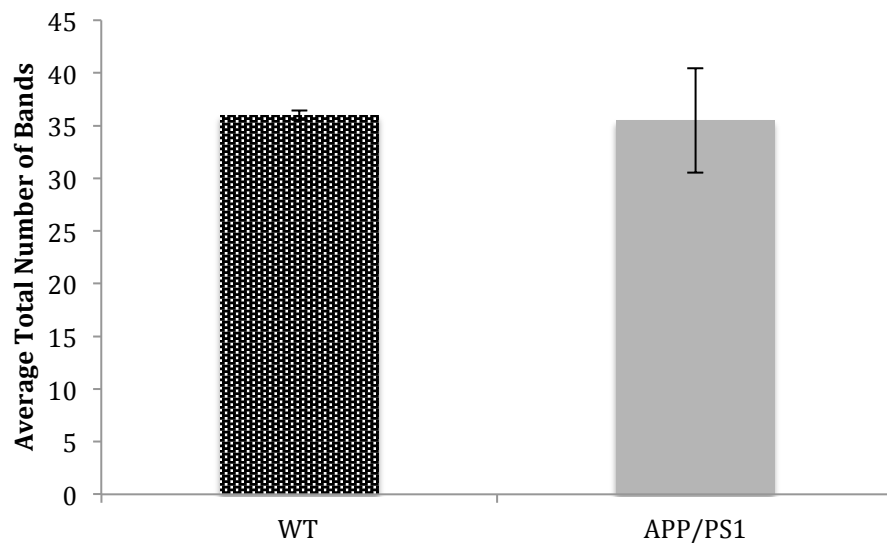
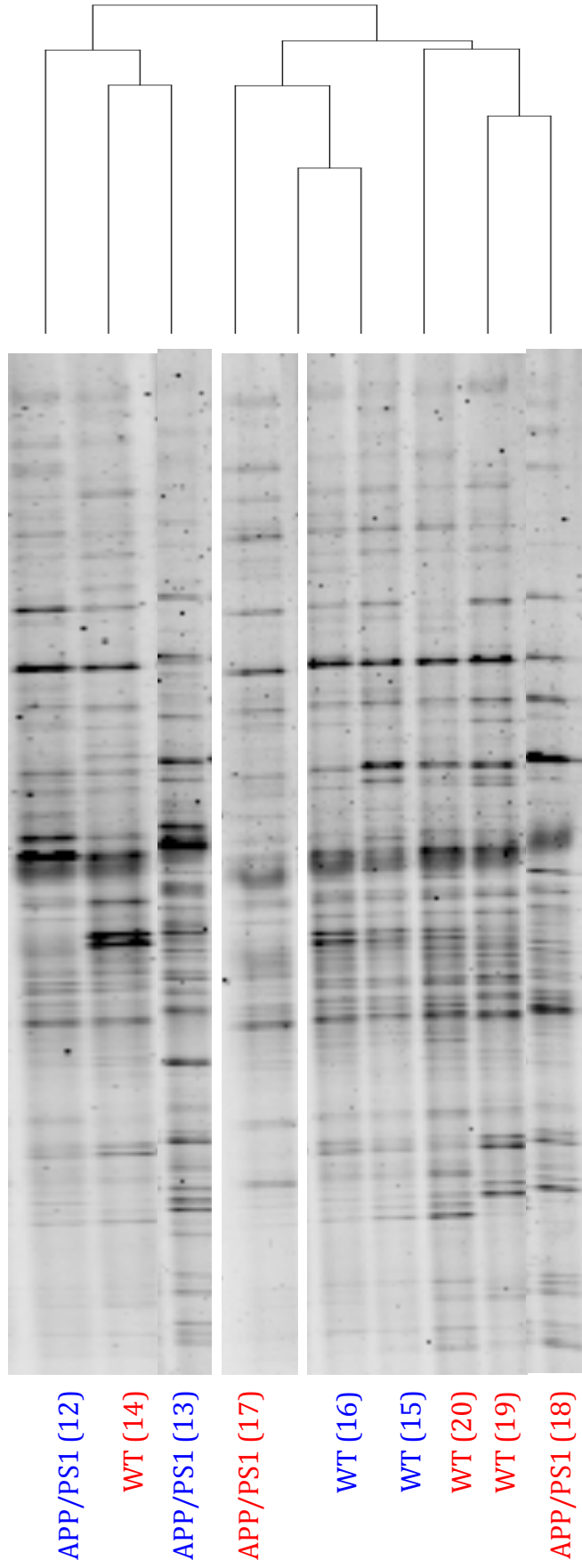


Figure 42: Average total number of bands from 16S rDNA DGGE profile of mucosal- bacterial community from the distal colon of fifteen-month WT and APP/PS1 mice. Error bars indicate SEM. (WT $n = 5$, APP/PS1 $n = 4$, $p = 0.91$).

There was no difference in the luminal-associated microbiota of the distal colon in fifteen-month WT and APP/PS1 mice ($p = 0.22$). Similarly to the mucosal associated microbiota of the colon, the luminal microbiota profiles can be roughly divided into three distinct mixed genotype groups as shown in the phylogenetic tree in Figure 43A. However, the NMDS plot in figure 43B shows there is no strong clustering between microbiota profiles indicating no difference between community composition in WT and APP/PS1 mice.

A)



B)

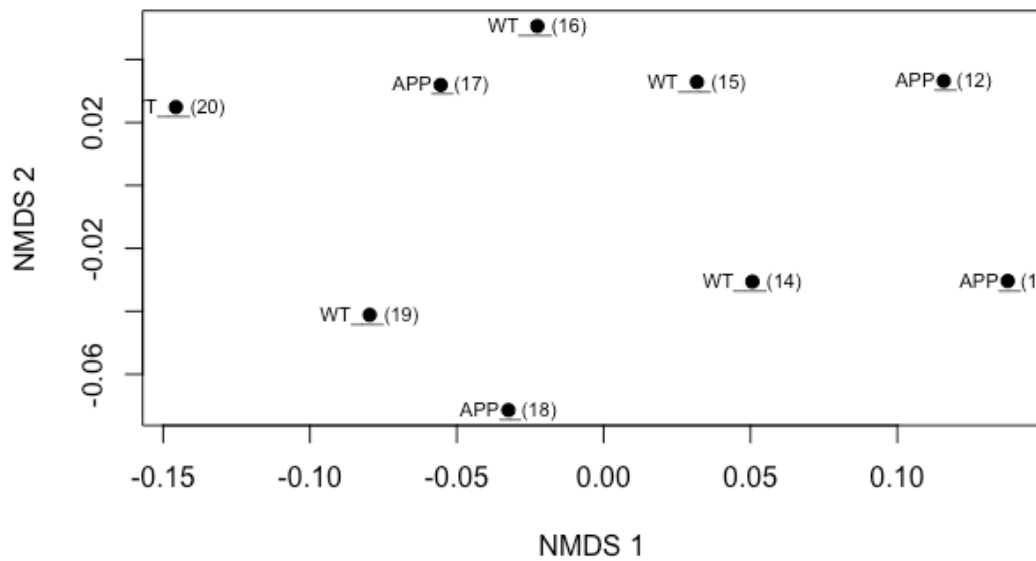


Figure 43: Luminal bacterial community profiling from the distal colon of WT and APP/PS1 fifteen-month mice. A) 16S rDNA DGGE profile and UPGMA phylogenetic tree. No difference in community profiling was observed (WT n = 5, APP/PS1 n = 4, p = 0.22). Blue = male, red = female. B) NMDS analysis. Stress value = 0.1 indicating good quality fit of data. Numbers in brackets depicts sample identification number. Abbreviation: APP = APP/PS1.

There was no difference in the average total number of bands present in the DGGE profile of the luminal-associated microbiota from the distal colon of fifteen-month mice as indicated in figure 44. APP/PS1 mice averaged 50.5 ± 0.6 bands compared to 49.4 ± 1.9 in the WT mice, which was not statistically significant and therefore indicating no difference in beta diversity ($p = 0.63$).

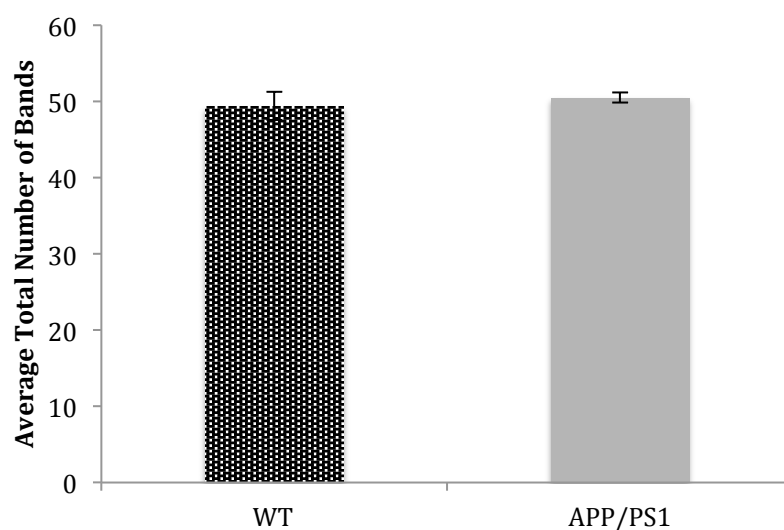


Figure 44: Average total number of bands from 16S rDNA DGGE profile of luminal-bacterial community from the distal colon of fifteen-month WT and APP/PS1 mice. Error bars indicate SEM. (WT n = 5, APP/PS1 n = 4, $p = 0.63$).

5.3 Three-month APP/PS1 mice

Despite observed alterations in gut phenotype in the early and late models of AD pathology, based on previous literature (Harach et al., 2017) we were surprised that our data suggested little difference in microbiota profiles between APP/PS1 and WT mice. Therefore we hypothesised that microbiota differences may be occurring prior to the seven-month time point, i.e. earlier in the pathology progression, and therefore we analysed a group of three-month old WT and APP/PS1 mice.

5.3.1 Crypt depth is decreased in the colon of three-month APP/PS1 mice

As shown in figure 45A, there was a tendency for the villus height to be 10.5% greater in the ileum of APP/PS1 mice compared to WT littermates, however this was not statistically significant ($p = 0.31$). Similarly in figure 45B, there was no significant difference in crypt depth of the ileum between APP/PS1 and WT mice, with the former presenting crypts that were 5.1% greater than the WT ($p = 0.17$).

In contrast, the colonic crypt depth was significantly decreased in APP/PS1 mice compared to the WT littermates as indicated in figure 45B ($p = 0.003$). APP/PS1 mice had an average crypt depth of $139.5 \pm 27.9 \mu\text{m}$, compared to $201.6 \pm 17.7 \mu\text{m}$ in the WT mice, equivalent to a 30.8% decrease. Representative images are shown in figure 46.

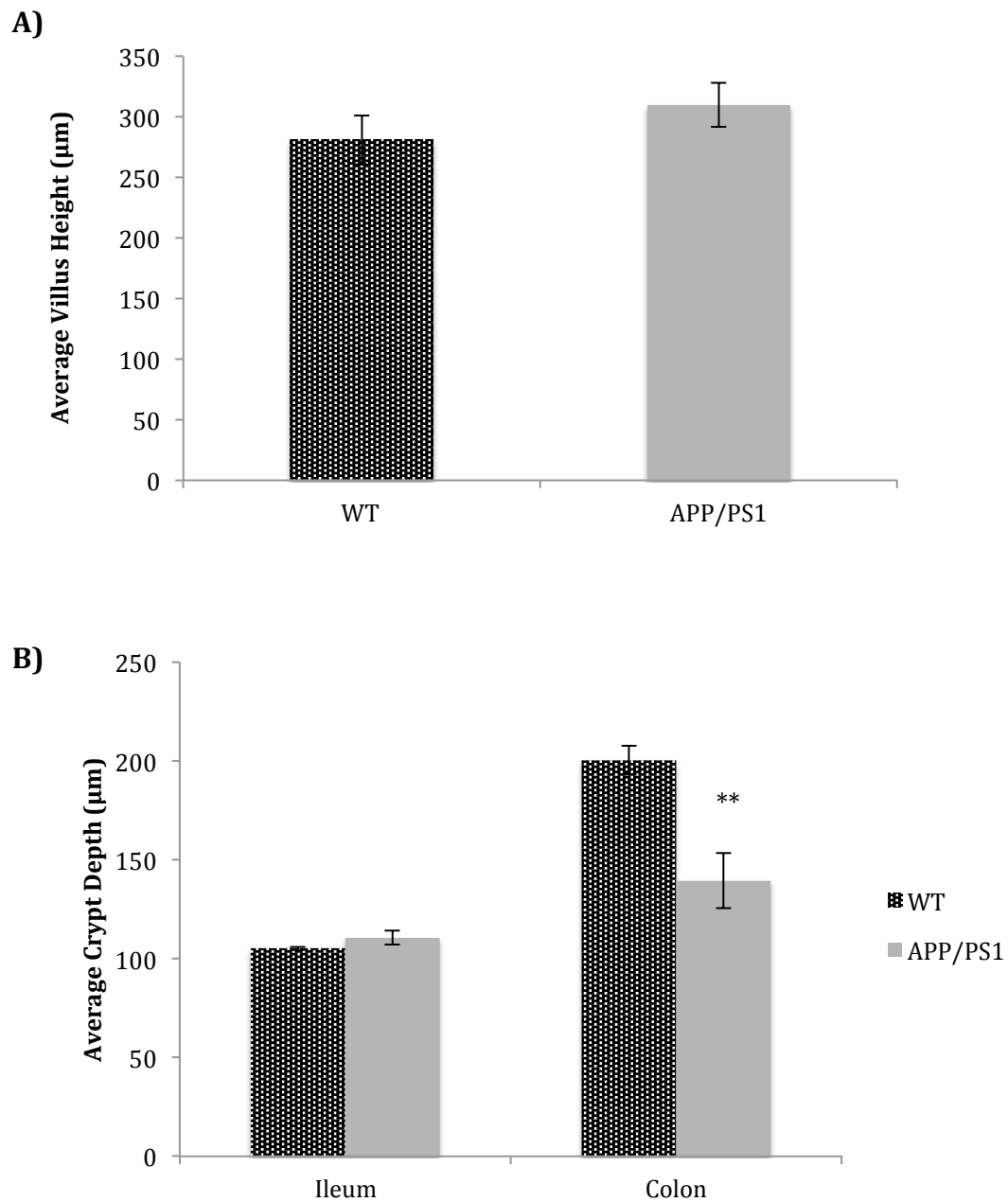


Figure 45: Histological analysis of the gut in WT and APP/PS1 three-month mice. Error bars indicate SEM. A) Average villus height in the ileum (WT n = 5, APP/PS1 n = 5, p = 0.31). B) Average crypt depth in the ileum (WT n = 5, APP/PS1 n = 5, p = 0.17) and distal colon (WT n = 6, APP/PS1 n = 4, p = 0.003). ** p ≤ 0.01.

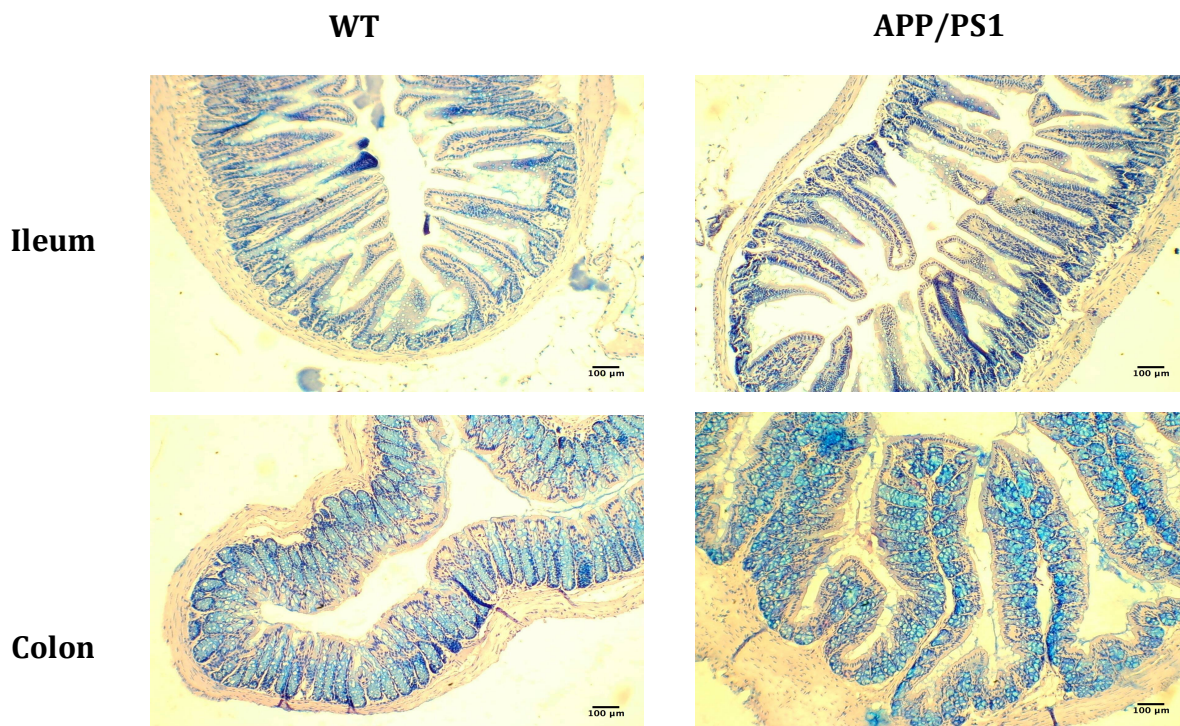


Figure 46: Representative images of WT and APP/PS1 three-month mice. Sections were stained with PAS/AB, although neutral mucins could not be identified due to fixation issues. Acidic mucins are stained blue by AB. Scale bar = 100 μm .

Sex specific differences were briefly investigated in the colonic crypt depth of three-month mice. Although statistical analysis could not be performed due to a small n number, the decrease in crypt depth tended to be greater in male mice at approximately 41.1% compared to 18.9% in female APP/PS1 mice (figure 47). Although male APP/PS1 mice tended to exhibit greater variation in the results than female APP/PS1 mice, an n=2 APP/PS1 males makes this difficult to confirm.

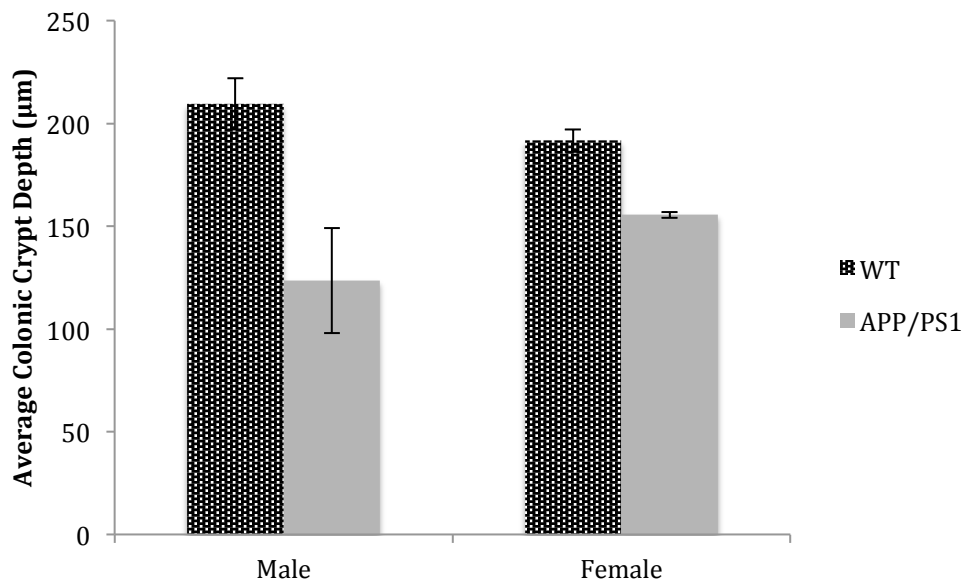


Figure 47: Average colonic crypt depth in male and female WT and APP/PS1 three-month mice. Error bars indicate SEM. Male (WT n = 3, APP/PS1 n = 2), female (WT n = 3, APP/PS1 n = 2).

As shown in figure 48A and 48B, there was no difference in the average number of goblet cells per 100 µm of villus height and/or crypt depth in the ileum or colon of three-month WT and APP/PS1 mice. The number of goblet cells in the ileum tended to be slightly lower in the villi and crypts by 4.2% and 5.7% in the APP/PS1 mice compared to WT littermates, however this was not statistically significant ($p = 0.61$ and $p = 0.63$ respectively). In contrast there was a propensity for 14.7% more goblet cells in the colon of APP/PS1 mice, however similarly this was not statistically significant ($p = 0.52$). Assessment of the proportion of acidic and neutral mucins was not possible in three-month mice due to issues during the fixation process.

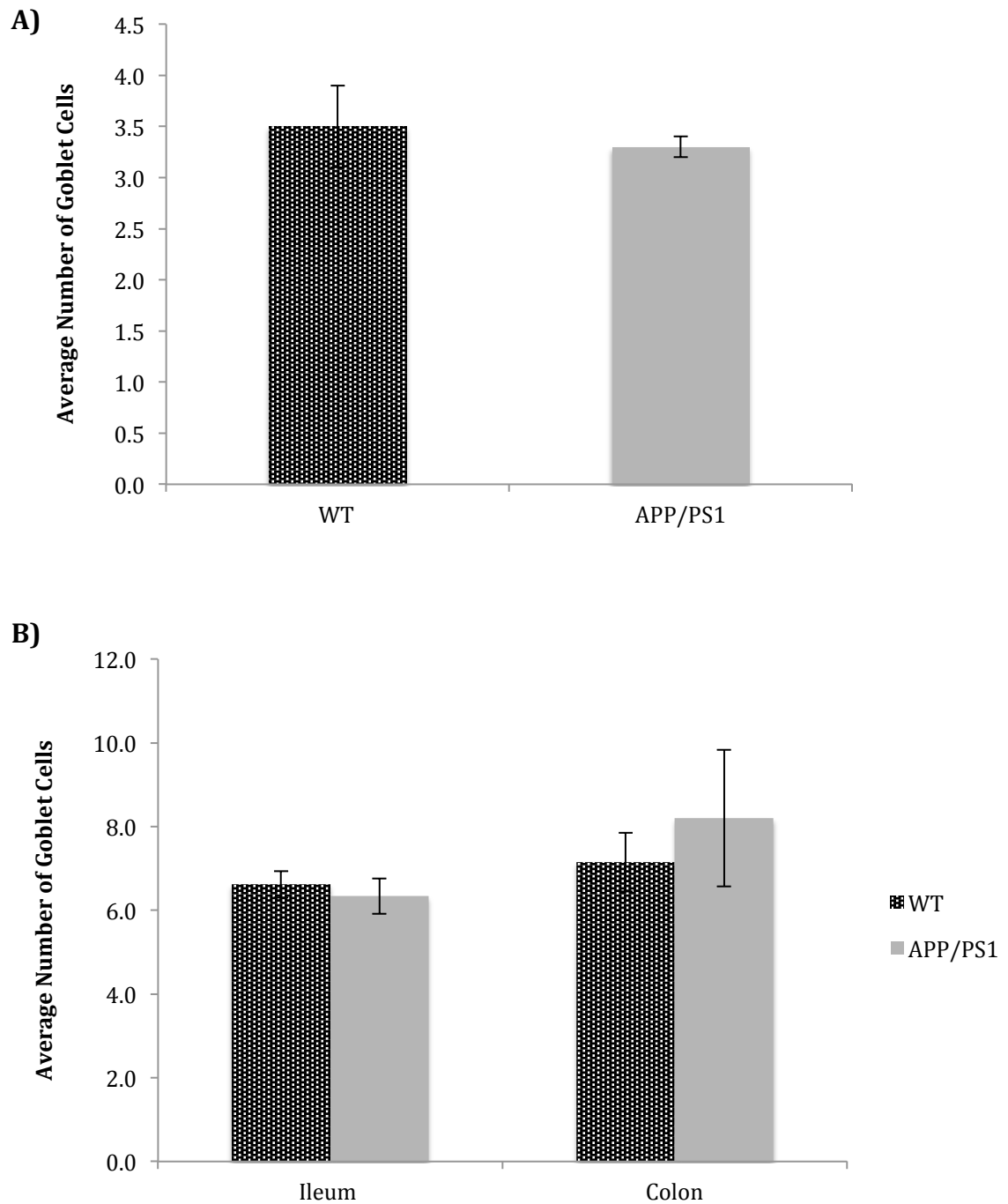


Figure 48: Average number of goblet cells in WT and APP/PS1 three-month mice.. Error bars indicate SEM. A) Average number of goblet cells per 100 μ m of villi in the ileum (WT n = 5, APP/PS1 n = 5, p = 0.63). B) Average number of goblet cells per 100 μ m of crypt in the ileum (WT n = 5, APP/PS1 n = 5, p = 0.61) and distal colon (WT n = 6, APP/PS1 n = 4, p = 0.52).

As shown in figure 49A, there was a tendency for the villi of the ileum to have 16.4% more EEC's in the APP/PS1 mice than the WT littermates, however this was not significant ($p = 0.56$). A similar observation was made in figure 49B, with the crypts of the ileum presenting 15.3% more EEC's in the APP/PS1 mice, however again this was not statistically significant ($p = 0.68$). In contrast, there was a statistically significant increase of 127.5% in the number of EEC's present in the distal colon of three-month APP/PS1 mice ($p = 0.002$). The APP/PS1 mice possessed 0.46 ± 0.08 EEC's per 100 μm of colonic crypt compared to 0.20 ± 0.09 in the WT littermates. Representative images are shown in figure 50.

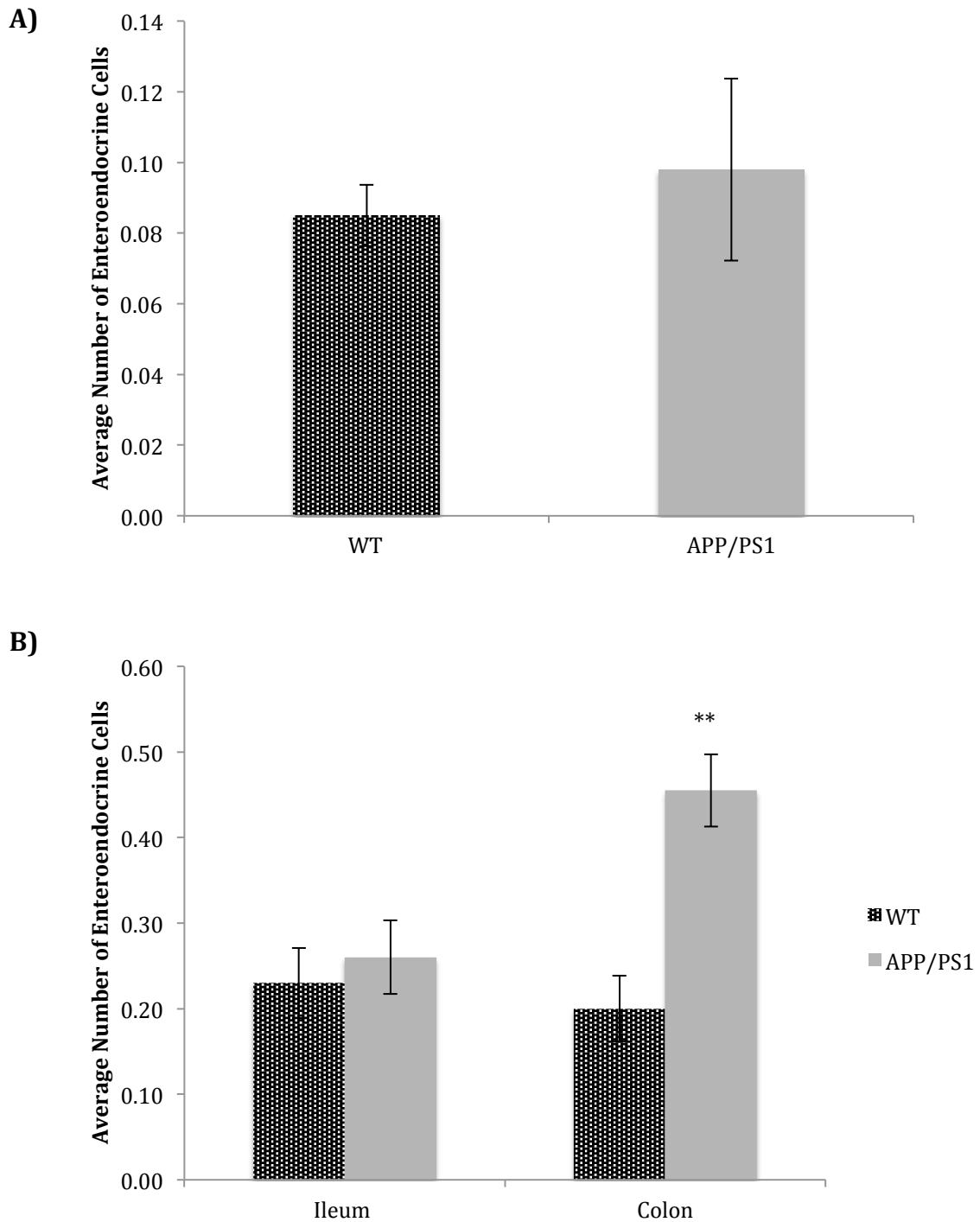


Figure 49: Average number of EEC's in WT and APP/PS1 three-month mice. Error bars indicate SEM. A) Average number of EECs per 100 μ m of villi in the ileum (WT n = 4, APP/PS1 n = 5, p = 0.68). B) Average number of EECs per 100 μ m of crypt in the ileum (WT n = 4, APP/PS1 n = 5, p = 0.56) and distal colon (WT n = 6, APP/PS1 n = 4, p = 0.002). ** p \leq 0.01.

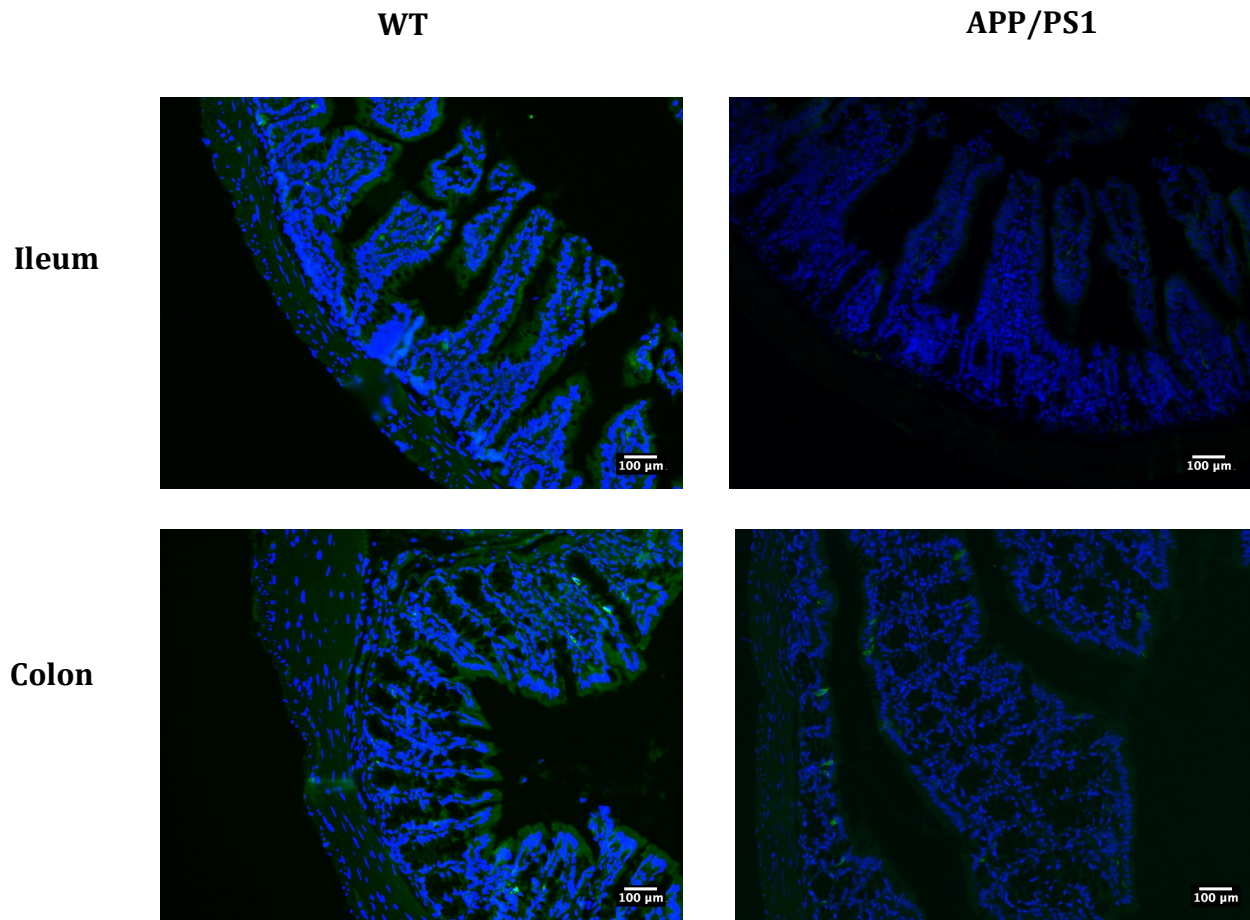


Figure 50: Representative fluorescent IHC images of the number of EEC's in three-month WT and APP/PS1 mice. CgA = green, DAPI = blue. Scale bar = 100 μ m

Sex specific differences of EEC numbers in the distal colon of three-month mice were investigated, although statistical analysis was not performed due to a low n number. However, there was a tendency for the increase in the number of EEC's to be greater in the male APP/PS1 (169.9%) than the female APP/PS1 mice (89.3%) as indicated in figure 51.

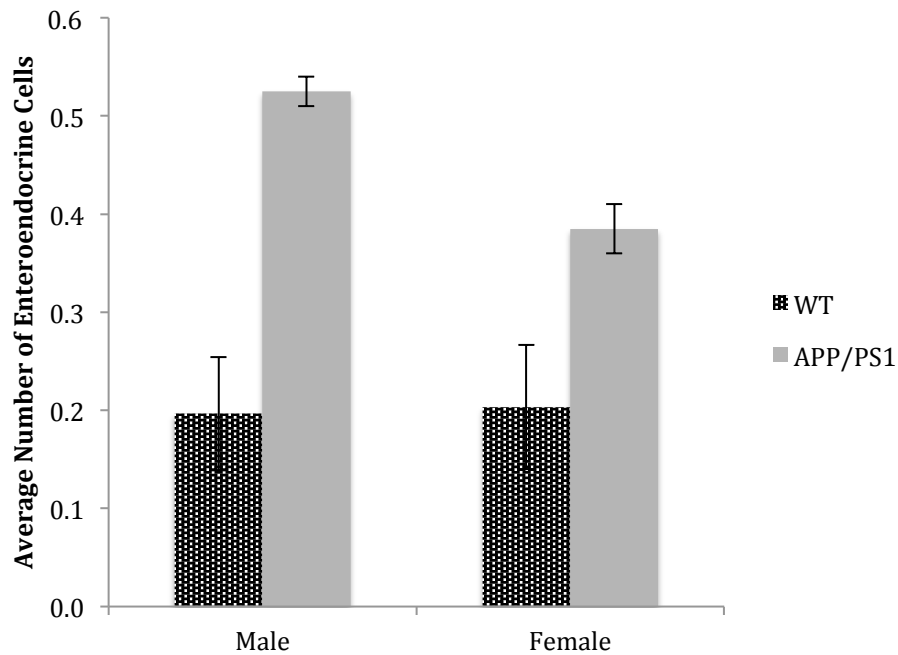


Figure 51: Average number of EEC's in male and female WT and APP/PS1 three-month mice. Average number of EECs per 100 μ m of villus height and/or crypt depth. Error bars indicate SEM. Male (WT n = 2, APP/PS1 n = 3), Female (WT n = 3, APP/PS1 n = 2).

5.3.2 Microbial diversity is altered in the caecum of three-month APP/PS1 mice

As shown in figure 52 there was a tendency for the phylum Firmicutes to be 32% \pm 38% more abundant in the APP/PS1 than WT mice, however this was not statistically significant ($p = 0.86$). In contrast, the phylum Bacteroidetes tended to be 57% \pm 17% less abundant in APP/PS1 than WT mice, but similarly was not statistically significant ($p = 0.27$) as shown in figure 52.

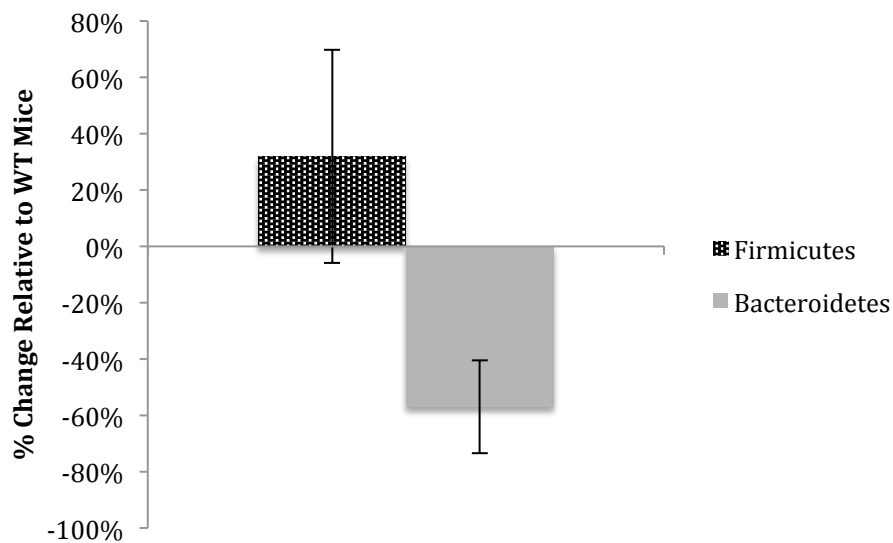
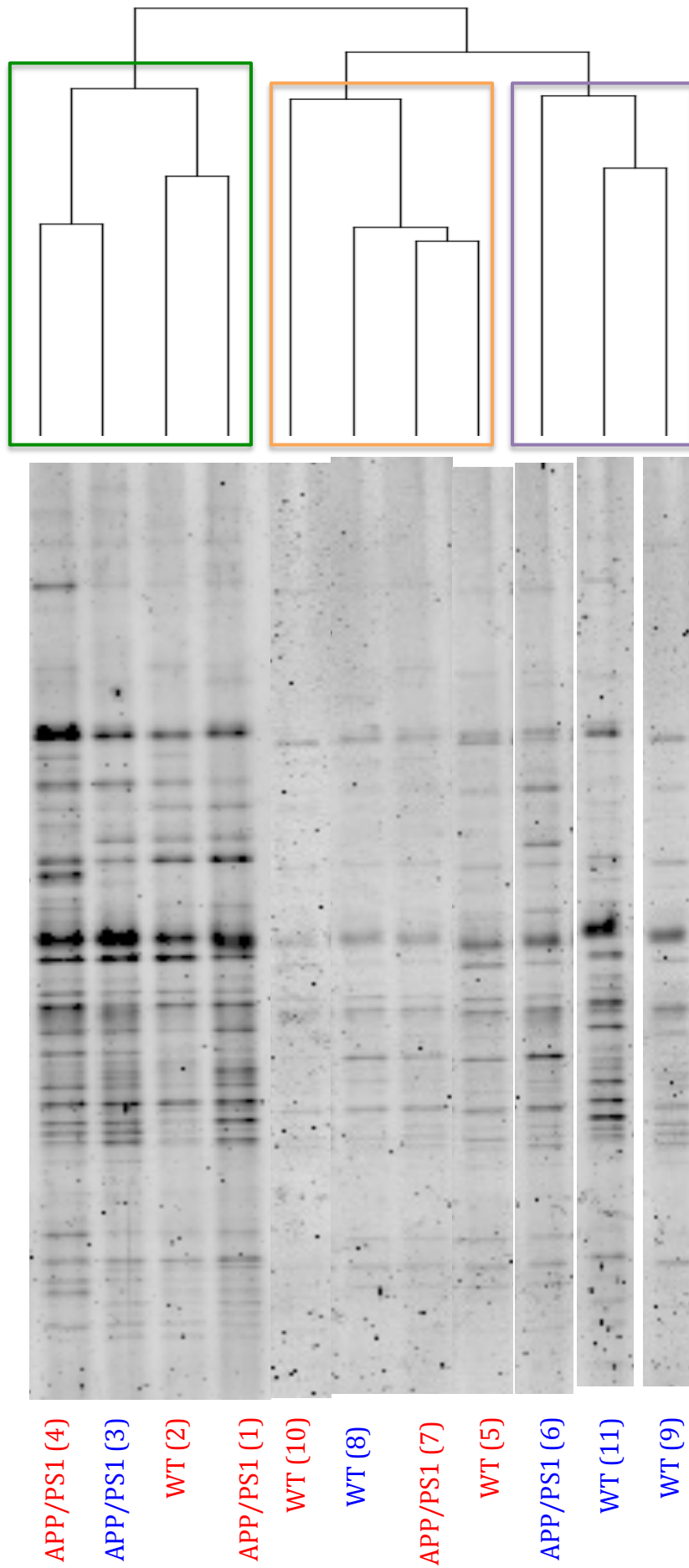


Figure 52: Relative percentage change of predominant mucosal-associated phyla in three-month mice. Percentage change of the phyla Firmicutes and Bacteroidetes in the mucosal-associated microbiota of three-month APP/PS1 mice relative to age matched WT littermates. Error bars indicate SEM. Firmicutes (WT $n = 6$, APP/PS1 $n = 5$, $p = 0.86$), Bacteroidetes (WT $n = 6$, APP/PS1 $n = 5$, $p = 0.27$).

A DGGE of the mucosal-associated microbiota from the caecum revealed a statistically significant difference between the microbiota in WT and APP/PS1 three-month mice ($p = 0.04$). As indicated in figure 53A, the clade highlighted in green on the phylogenetic tree is distant from the remaining microbiota profiles. Three-quarters of this clade are APP/PS1 mice, and as shown in the NMDS plot in figure 53B they appear to somewhat cluster together and away from the other microbiota profiles. The remaining WT in the clade is positioned away from the APP/PS1 microbiota profiles suggesting the microbiota profiles are relatively distinct.

The two remaining APP/PS1 microbiota profiles belong to two different clades as indicated by the orange and purple boxes. APP/PS1 7 appears closely related to WT 5, and APP/PS1 6 is most closely related to WT 11. Despite this, the remaining WT profiles appear distant from each other and the APP/PS1 samples, indicating distinct microbiota profiles.

A)



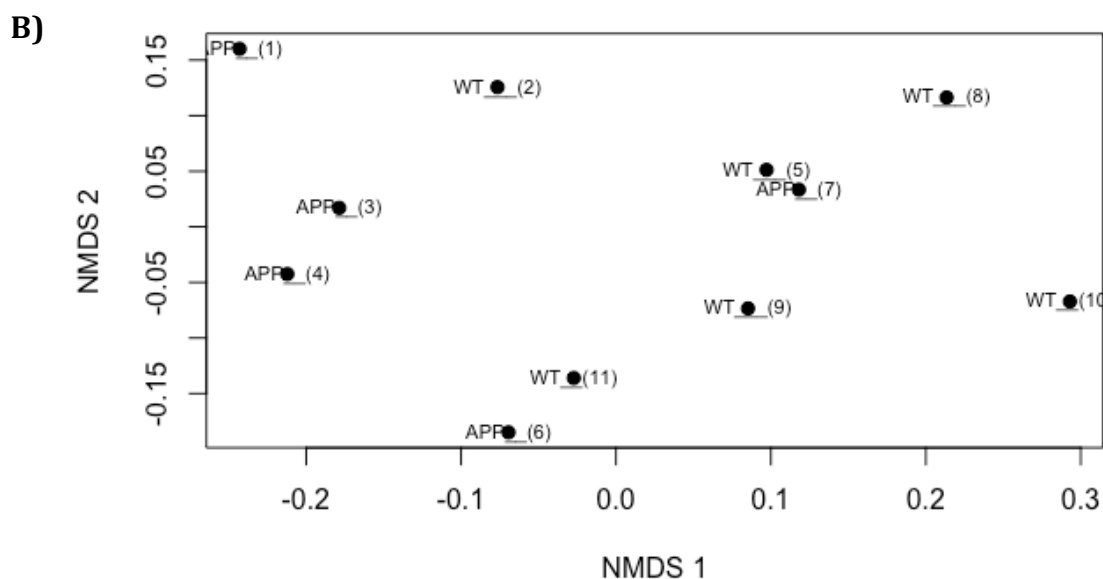


Figure 53: A) Mucosal bacterial community profiling from the caecum of WT and APP/PS1 three-month mice. A) 16S rDNA DGGE profile and UPGMA phylogenetic tree. A significant difference in community profiling was observed (WT n = 6, APP/PS1 n = 5, p = 0.04). Blue = male, Red = female. Green box = most distant microbiota profiles, orange and purple boxes = most closely related microbiota profiles. B) NMDS analysis. Stress value = 0.1 indicating good quality fit of data. Numbers in brackets depicts sample identification number. Abbreviation: APP = APP/PS1.

There was a significant increase in the total number of bands observed in the DGGE profile of the mucosal-associated microbiota from the three-month APP/PS1 mice (p = 0.03). The APP/PS1 mice averaged 38.8 ± 6.9 bands compared to WT's 30 ± 4.4 showing an increase in beta diversity in APP/PS1 mice (figure 54A)

Sex specific differences were also investigated as shown in figure 54B, although statistical analysis was not performed due to a small n number. However, female APP/PS1 mice appeared to show a greater difference in number of bands compared to female WT, suggesting that sex specific difference may be present.

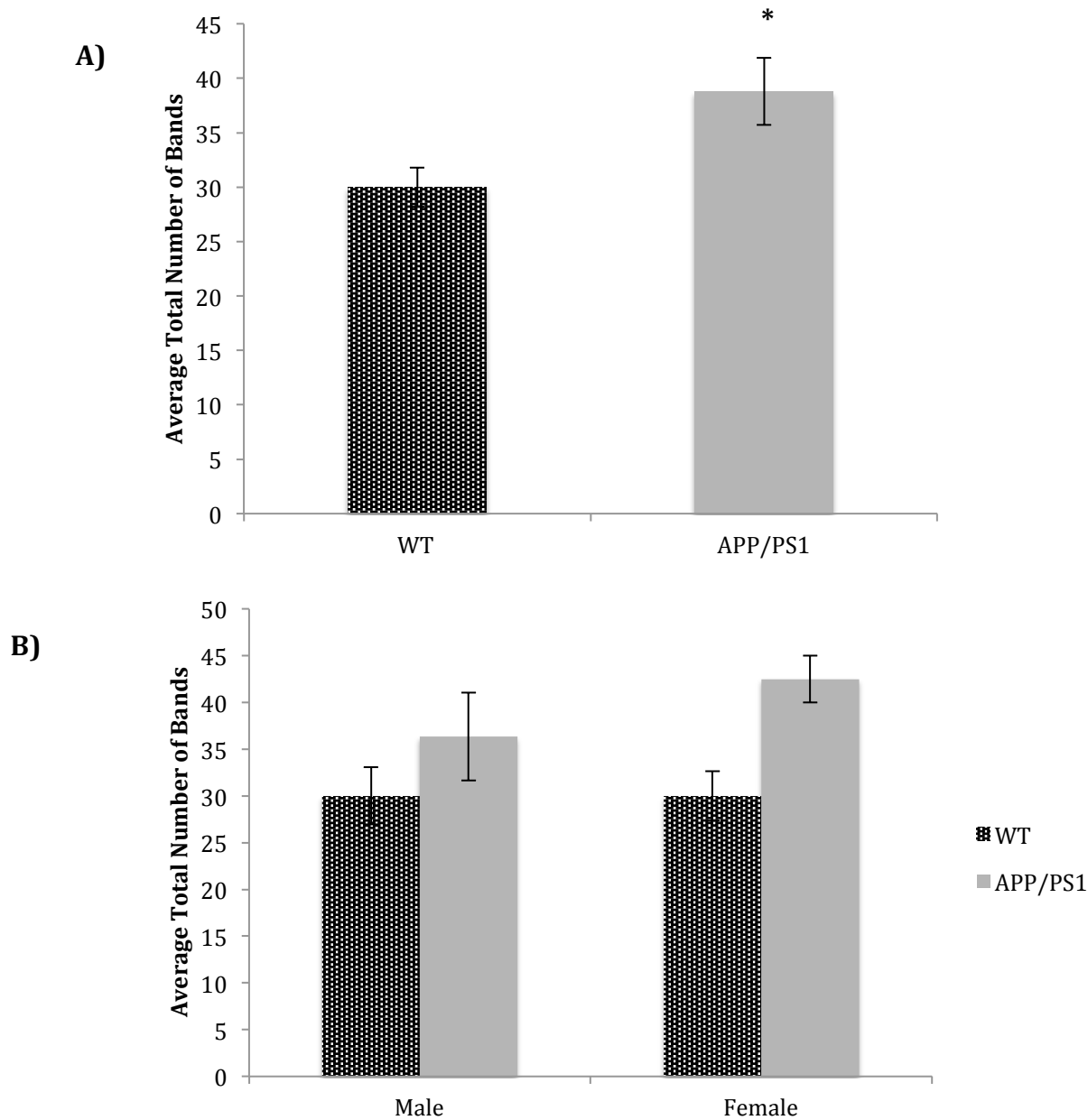


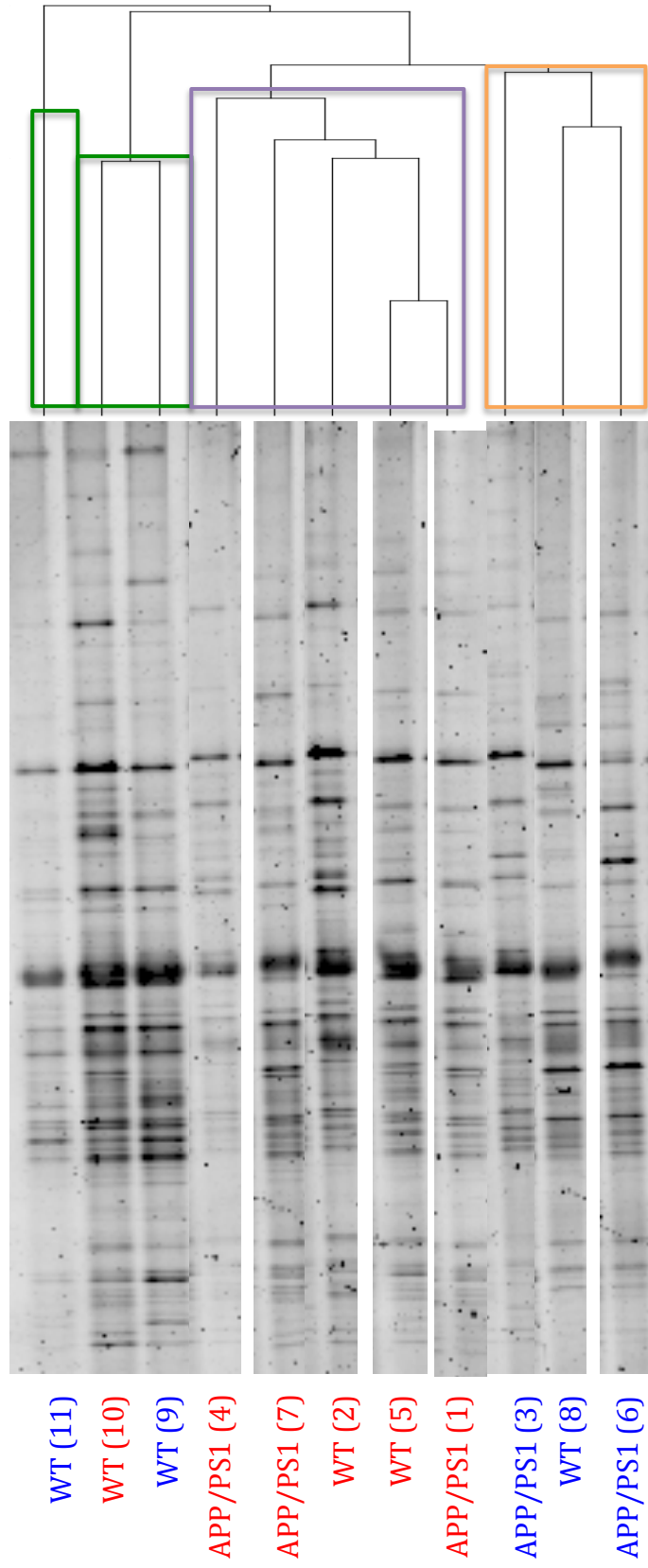
Figure 54: Average total number of bands of 16S rDNA DGGE associated with the mucosal bacterial community from the caecum of three-month WT and APP/PS1 mice A) Average total number of bands of 16S rDNA DGGE associated with the mucosal bacterial community from the caecum of three-month WT and APP/PS1 mice. Error bars indicate SEM. (WT n = 6, APP/PS1 n = 5, p = 0.03). * p ≤ 0.05. B) male and female WT and APP/PS1 three-month mice. Error bars indicate SEM. Male (WT n = 3, APP/PS1 n = 2), female (WT n = 3, APP/PS1 n = 3).

There were no differences in the luminal microbiota profiles between WT and APP/PS1 mice ($p = 0.66$) indicating that dysbiosis observed in the caecum of three-month mice is specific to the mucosal layer.

The most distinct microbiota profiles are indicated by the green boxes shown in the phylogenetic tree in Figure 55A. The NMDS plot in figure 55B shows that whilst appearing distinct from the rest of the microbiota profiles, they are also distinct from each other. Whilst these distinct profiles are all WT mice, the remaining WT microbiota profiles appear closely related to APP/PS1 microbiota profiles suggesting no overall difference in community composition.

The clade represented by the orange box consists of a mixture of male WT and APP/PS1 mice, and the clade represented by the purple box consists solely of female WT and APP/PS1 mice suggesting there may be sex specific differences.

A)



B)

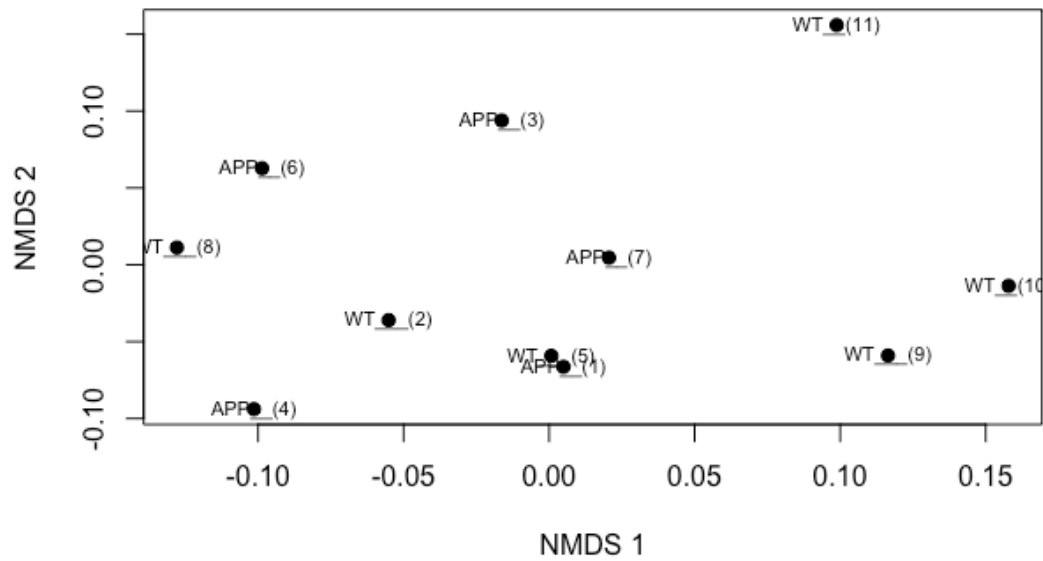


Figure 55: Luminal bacterial community profiling from the caecum of WT and APP/PS1 three-month mice. A) 16S rDNA DGGE profile and UPGMA phylogenetic tree. No difference in community profiling was observed (WT n = 6, APP/PS1 n = 5, p = 0.66). Blue = male, red = female. Green boxes = distant microbiota profiles orange box = male dominated microbiota profiles, purple box = female dominated microbiota profile. **B) NMDS analysis.** Stress value = 0.1 indicating good quality fit of data. Numbers in brackets depicts sample identification number. Abbreviation: APP = APP/PS1.

There was no difference in the average total number of bands in the DGGE profiles of the luminal-associated bacteria in the caecum of three-month WT and APP/PS1 mice ($p = 0.85$). APP/PS1 microbiota profiles averaged 41.8 ± 1.3 compared to 42.0 ± 1.3 in the WT littermates indicating no difference in beta diversity (figure 56).

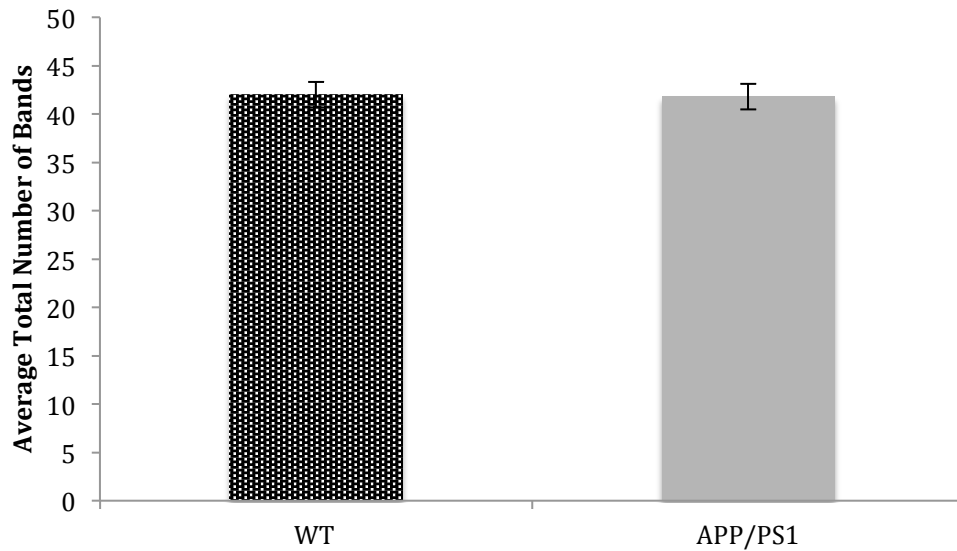


Figure 56: Average total number of bands of 16S rDNA DGGE associated with the luminal bacterial community from the caecum of three-month WT and APP/PS1 mice. Error bars indicate SEM. (WT $n = 6$, APP/PS1 $n = 5$, $p = 0.85$).

6. Summary of Results

6.1 Villus height and crypt depth

	Ileum (villus)	Ileum(crypt)	Caecum	Colon
3 Month	↑ p = 0.31	↑ p = 0.17		↓ p = 0.003
7 Month	↑ p = 0.17	↓ p = 0.71	↑ p = 0.38	↑ p = 0.82
15 Month	↑ p = 0.17	↑ p = 0.19	↓ p = 0.38	↓ p = 0.82

Table 8: Summary of statistical analysis of villus height and/or crypt depth

Average villus height and/or crypt depth in the ileum, caecum and distal colon in three, seven and fifteen month WT and APP/PS1 mice. ↑ = increase, ↓ = decrease in APP/PS1 compared to WT. Green box indicates statistically significant result. Black box indicates data not collected.

6.2 Goblet cell count

	Ileum (villus)	Ileum (crypt)	Caecum	Colon
3 Month	↓ p = 0.63	↓ p = 0.61		↑ p = 0.52
7 Month	↓ p = 0.21	↓ p = 0.21	↓ p = 0.13	↓ p = 0.44
15 Month	↓ p = 0.001	↓ p = 0.01	↑ p = 0.34	↑ p = 0.40

Table 9: Summary of statistical analysis of goblet cell numbers

Average number of goblet cells per 100 μm of villus height and/or crypt depth of the ileum, caecum and distal colon in three, seven and fifteen month WT and APP/PS1 mice. ↑ = increase, ↓ = decrease in APP/PS1 compared to WT. Green box indicates statistically significant result. Black box indicates data not collected.

6.3 EEC count

	Ileum (villus)	Ileum (crypt)	Caecum	Colon
3 Month	↑ p = 0.68	↑ p = 0.56		↑ p = 0.002
7 Month	↓ p = 0.40	↓ p = 0.21	/ p = 0.99	↓ p = 0.04
15 Month	↓ p = 0.61	↓ p = 0.25	↓ p = 0.54	↑ p = 0.25

Table 10: Summary of statistical analysis of EEC numbers

Average number of EEC's per 100 µm of villus height and/or crypt depth of the ileum, caecum and distal colon in three, seven and fifteen month WT and APP/PS1 mice. ↑ = increase, ↓ = decrease, / = no change in APP/PS1 compared to WT. Green box indicates statistically significant result. Black box indicates data not collected.

6.4 Microbial community diversity – qRT-PCR

		Ileum	Caecum	Colon
3 month	Firmicutes		↑ p = 0.86	
	Bacteroidetes		↓ p = 0.27	
7 month	Firmicutes	↓ p = 0.20	↑ p = 0.92	↓ p = 0.05
	Bacteroidetes	↑ p = 0.33	↑ p = 0.68	↑ p = 0.92
15 month	Firmicutes	↓ p = 0.58	↓ p = 0.27	↓ p = 0.80
	Bacteroidetes	↑ p = 0.82	↑ p = 0.31	↑ p = 0.47

Table 11: Summary of statistical analysis of qRT-PCR data

Relative percentage change in the abundance of the two main phyla, Firmicutes and Bacteroidetes from mucosal associated microbiota of the ileum, caecum and distal colon in three, seven and fifteen-month WT and APP/PS1 mice. ↑ = increase, ↓ = decrease in relative percentage change of phylum in APP/PS1 compared to WT. Green box indicates statistically significant result. Black box indicates data not collected.

6.5 Microbial community diversity – DGGE

Mucosal:

	Ileum	Caecum	Colon
3 Month		p = 0.04	
7 Month	p = 0.82	p = 0.82	p = 0.44
15 Month	p = 0.54	p = 0.24	p = 0.83

Luminal:

	Ileum	Caecum	Colon
3 Month		p = 0.66	
7 Month	p = 0.07	p = 0.81	p = 0.49
15 Month	p = 0.78	p = 0.87	p = 0.22

Table 12: Summary of statistical analysis of DGGE profile data

from the ileum, caecum and distal colon in three, seven and fifteen month WT and APP/PS1 mice in both A) mucosal-associated microbiota and B) luminal-associated microbiota. Green box indicates statistically significant result. Black box indicates data not collected.

6.6 Average total number of DGGE bands

Mucosal:

	Ileum	Caecum	Colon
3 Month		↑ p = 0.03	
7 Month	p = 0.69	p = 0.38	p = 0.58
15 Month	p = 0.56	p = 0.52	p = 0.91

Luminal:

	Ileum	Caecum	Colon
3 Month		p = 0.85	
7 Month	p = 0.40	p = 0.35	p = 0.75
15 Month	p = 0.64	p = 0.89	p = 0.63

Table 13: Summary of statistical analysis of the number of bands from 16S rDNA DGGE profiles. Average total number of bands from the ileum, caecum and distal colon in three, seven and fifteen-month WT and APP/PS1 mice in both A) mucosal bacterial community and B) luminal bacterial community. ↑ = increase in number of DGGE bands. Green box indicates statistically significant result. Black box indicates data not collected.

7. Discussion

7.1 Dysbiosis in the large intestine occurs in early AD pathology

To our knowledge, this is the first study that has investigated dysbiosis in the mucosal and luminal-associated microbiota in early and late A β associated models of AD. Dysbiosis was assessed in three, seven and fifteen-month APP/PS1 and WT mice using qRT-PCR and 16S rDNA DGGE. Analysis of the three-month DGGE's indicated that mucosal-associated dysbiosis was accompanied by increased microbial diversity in the caecum of APP/PS1 mice. In addition, the qRT-PCR results suggested no difference in the abundance of the phyla Firmicutes and Bacteroidetes. It is possible that the observed dysbiosis was due to an increase in diversity at the lower taxonomic levels of Firmicutes and/or Bacteroidetes, which had no overall impact on the abundance of the phyla. Alternatively, it may have been that the increase in diversity occurred within another phylum, such as Proteobacteria or Actinobacteria, which we have not investigated.

A limited number of studies have looked at dysbiosis in early models of AD pathology. In agreement with our study Shen, Liu & Ji, (2017) observed an increase in microbial diversity in three-month APP/PS1 mice, however they did not investigate changes in the phyla. In contrast, Harach et al. (2017) found no difference in diversity in three and a half month APP/PS1 mice, but in agreement with our study found no alteration in the abundance of the two major phyla. Brandscheid et al. (2017) utilised the 5xFAD mouse model and observed dysbiosis at nine weeks, however they also observed an increase in Firmicutes and a decrease in Bacteroidetes.

The lack of consistency between research groups may be due to the origin of the samples. We investigated the microbiota associated with the mucosal and luminal contents within specific regions of the gut. This method was selected due to distinct differences in the microbial composition in the mucosal and luminal contents, and also along the length of the GI tract (Sekirov et al. 2010; Simrén et

al. 2013). All previous studies in early models of AD sampled faecal pellets, which disregards the mucosal-associated microbiota and does not represent the microbiota from a specific region in the GI tract. Additionally, faecal pellets are more prone to environmental contamination that may impact the results.

In addition, different techniques were utilised. We employed qRT-PCR and DGGE as methods to assess differences in gut microbiota between genotypes. Harach et al. (2017) used Illumina sequencing and qRT-PCR, Shen, Liu & Ji (2017) used pyrosequencing and Brandscheid et al. (2017) used qRT-PCR. Sequencing the microbiota using Illumina or pyrosequencing provides a greater in-depth representation of the microbial populations, which our study lacks. However, similarities are apparent in our results and the studies that utilised sequencing based techniques, which supports our findings.

In addition to dysbiosis, an increase in the number of EEC's was observed in the colon of three-month APP/PS1 mice, suggesting differentiation of colonic stem cells is affected as a result of A β deposition in this model of early AD. In our study, EEC's were identified using an antibody raised against CgA, and therefore it was not possible to distinguish between EC and L cells in the colon. Although we have not elucidated the type of EEC affected, we have considered the potential downstream consequences for both L and EC cells.

A decrease in microbial diversity has been shown to cause a reduction in SCFA levels; therefore it is plausible that we have an increase in SCFA in our study due to an increased diversity (Zhang et al, 2017). SCFA rich conditions in the large intestine have been reported to increase the proliferation of L cells in rats, resulting in an increase in GLP-1 secretion (Kaji et al., 2011).

GLP-1 is able to bind to its receptor, GLP-1R on muscle cells and the myenteric plexus within the colon. This causes a reduction in the amplitude of smooth muscle contractions, resulting in a decrease in intestinal transit in a concentration dependent manner, known as the 'ileal brake' (Amato et al., 2014). Intestinal transit is important in ensuring a balance between digestion,

absorption of water and nutrients, preventing overgrowth of bacteria and excreting faeces (Greiner & Bäckhed, 2016).

A decrease in intestinal transit can result in the proliferation of fast growing microbiota species. Interestingly, a GLP-1 induced reduction in intestinal transit has been demonstrated *in vivo* resulting in an increase in microbial diversity in the proximal colon with no effect observed in the distal colon (Tottey et al., 2017). If L cells numbers and GLP-1 secretion were increased in our study, this could account for why dysbiosis was observed upstream of the distal colon in the caecum.

PYY is also secreted by L cells and has a similar role in the ileal brake. An increase in PYY reduces intestinal transit time and inhibits gastric emptying in a dose dependent manner (Savage et al., 1987). As described above, the inhibition of gastrointestinal transit in addition to gastric emptying could promote the growth of bacteria that may result in dysbiosis (Greiner & Bäckhed, 2016).

Levels of 5-HT and tryptophan have not been observed in the AD gut, but have been reported in the brain, with a decrease in 5-HT and increase in tryptophan (González-Domínguez, García-Barrera & Gómez-Ariza, 2015; Hendricksen et al., 2004; Lai et al., 2005; O'Mahony et al., 2015). 5-HT is synthesised via the same two step pathway in both the gut and the brain, although the synthesis in the brain involves tryptophan being absorbed from the gut and traveling in the circulation free or bound to albumin before crossing the BBB via an amino acid transporter (O'Mahony et al., 2015). With lower levels of 5-HT observed in the AD brain, we would be surprised to also find an increase in 5-HT in the three month mice. However, since we have not determined if EC cells are elevated in the three-month colon we cannot confirm this. Therefore, if an increase in 5-HT could was observed, this could suggest that depleted 5-HT signalling in the gut is not an early event in AD, however confirmation of this would be required using techniques such as gas chromatography coupled to mass spectrometry.

A high concentration of SCFA promotes the expression of TPH1 found on EC cells thereby enhancing 5-HT biosynthesis (Reigstad et al., 2015). 5-HT₃ receptor antagonists have shown to decrease intestinal transit suggesting that elevated levels of 5-HT have the opposing effect (Gregory & Ettinger, 1998). If EC cell numbers were increased, it would be unlikely that the dysbiosis observed in the colon was a consequence of elevated 5-HT and increased intestinal transit. However, this does not necessarily mean EC cells are not increased in the colon.

5-HT is also an immune modulator, with several of its receptors present on immune cells such as: macrophages, monocytes, dendritic cells and lymphocytes. This enables 5-HT to impact the immune system both locally in the gut and systemically in the circulation (O'Mahony et al., 2015; Shajib & Khan, 2014).

5-HT is able to control the production of both pro-inflammatory and anti-inflammatory cytokines and chemokines, influence activation of T cells, and also have chemotactic effects on several cells including: dendritic cells, mast cells and eosinophils (Ahern, 2011; Shajib & Khan, 2014). It is clear that AD, Crohn's disease and IBS are strongly associated with inflammation, however since there are extensive differences in the amounts of 5-HT present between the diseases, it is difficult to deduce whether elevated 5-HT could be an early trigger of localised inflammation in AD or make no significant impact as the inflammation is caused by another metabolite or signalling pathway. Therefore, additional work would need to be carried out to understand the effect of high 5-HT in the early pathology of AD.

The three-month APP/PS1 mice also displayed a significant decrease in colonic crypt depth. Since the gut microbiota are known to have a role in maintaining gut architecture (Nowacki, 1993), it was not surprising that dysbiosis in the large intestine was accompanied by a reduction in colonic crypt depth.

The SCFA butyrate acts an inhibitor of stem cell proliferation in the colonic crypts. It is the main energy source of the colonic enterocytes and is therefore metabolised at the opening of the crypts resulting in its concentration decreasing

to the stem cells at the base of the crypts (Donohoe et al., 2011; Kaiko et al., 2016). As already proposed, an increase in microbial diversity may result in the increase in SCFA production which could inhibit stem cell proliferation at above homeostatic levels causing a decrease in colonic crypt depth in the APP/PS1 mice (Zhang et al., 2017).

7.2 Firmicutes are decreased in the colon at seven-months

The seven-month APP/PS1 mice presented no difference in diversity in the ileum, caecum or distal colon of APP/PS1 and WT mice, indicating that the increased diversity in the caecum had normalised by seven-months. However, dysbiosis was observed in the colon with a significant decrease in the phylum Firmicutes and no difference in Bacteroidetes.

These findings partially agree with Harach et al. (2017) who reported a decrease in Firmicutes in eight-month APP/PS1 mice; however they also noted an increase in Bacteroidetes. Furthermore in partial agreement, Shen, Liu & Ji (2017) saw a decrease in microbiota diversity in six and eight-month APP/PS1 mice compared to the three-month. However, in the 5xFAD model Brandscheid et al. (2017) found the dysbiosis that occurred at nine weeks was absent by eighteen weeks. Zhang et al. (2017) reported an increase in richness in the faecal microbiota of APP/PS1 mice aged between five and six-months. The differences observed were due to an increase in the phyla Proteobacteria, which we did not investigate in this study.

In addition to dysbiosis, we found a significant decrease in the number of EEC's. Zhang et al. (2017) reported an increase in richness in faecal microbiota and a decrease in diversity in eight-month APP/PS1 mice, which was accompanied by a reduction in SCFA production, particularly butyric acid. Although Zhang et al. (2017) reported an increase in Proteobacteria, we observed a decrease in Firmicutes which contains several dominant butyrate producers. (Louis et al.,

2010). This in addition to a decrease in diversity from three to seven-months could suggest that there may be a decrease in SCFA, particularly butyrate, in the seven-month APP/PS1 mice in our study. As already discussed, a SCFA rich environment is able to increase proliferation both L cell and EC cell numbers, therefore it is plausible to assume the inverse in low SCFA environments (Kaji et al., 2011; Reigstad et al., 2015).

A decrease in the number of L cells in the colon is likely to cause a reduction in the amount of GLP-1 and PYY secreted. Since high levels of GLP-1 and PYY are associated with decreased intestinal transit and gastric emptying, it is reasonable to suggest that at low levels of the inverse is observed (Amato et al., 2014; Savage et al., 1987). An increase in intestinal transit and gastric emptying prevents the overgrowth of microbiota which may explain why a decrease in diversity is observed from three to seven months.

Secreted GLP-1 also has an important role in glucose homeostasis, by influencing the secretion of insulin and inhibiting glucagon release from the pancreas. Grasset et al., (2017) found that there is a decrease in GLP-1R on the ENS neurons and vagus nerve in AD which results in the deregulation of glucose homeostasis, leading to GLP-1 resistance. A decrease in GLP-1 levels may contribute to GLP-1 resistance, as less GLP-1 would be available to bind to the GLP-1R on the ENS neurons and vagus nerve. Deregulated insulin secretion induced by low GLP-1 levels could contribute to insulin resistance observed in the brain, disrupting brain metabolism and contributing to impaired neuronal survival and synaptic plasticity and a decrease in cognitive function (Dineley, Jahrling & Denner, 2014).

In support of our findings, a significant decrease in the genera *Akkermansia* and *Allobaculum* was reported in eight-month APP/PS1 (Harach et al., 2017). Interestingly, these two genera are correlated with dysbiosis induced by consumption of a HFD and insulin resistance suggesting that dysbiosis at seven to eight months may contribute to insulin resistance (Schneeberger et al., 2015; Shin et al., 2014; Zhang et al., 2015).

7.3 Dysbiosis is normalised by fifteen-months

At fifteen months there was no difference in the abundance of Firmicutes and Bacteroidetes or in the diversity of APP/PS1 mice compared to the WT littermates. This suggests that dysbiosis is isolated to the early stages of pathology and is restored as the disease progresses. However, our results disagree with the findings by Zhang et al., (2017) who found a decrease in diversity in 8-12 month APP/PS1 compared to WT mice.

There was no difference in the abundance of EEC's observed at fifteen-months which may be due to the absence of dysbiosis in the APP/PS1 mice. The normalisation of the microbiota may have stabilised SCFA production and returned the proliferation of L cells back to normal homeostatic levels. GLP-1R agonists are commonly used to treat type 2 diabetes, therefore an increase in GLP-1 secretion may to some extent recover the GLP-1 and insulin resistance in our fifteen-month mice (Samson & Garber, 2013). However, analysis of SCFA levels in the APP/PS1 model would be required to prove this contention.

We observed a significant decrease in the number of goblet cells in the villi and crypts of the ileum in fifteen-month. A potential cause for the decrease in goblet cells may be due to the impact of long-term insulin resistance. Shin et al. (2014) reported that treating mice with metformin, a type 2 diabetes drug, increased the number of goblet cells in the ileum. Interestingly, the number of goblet cells was positively correlated with the abundance of the mucin degrading bacteria, *Akkermansia*, which has previously been shown to be significantly decreased in both HFD and APP/PS1 mice (Harah et al., 2017; Schneeberger et al., 2015). It is possible that a decrease in the abundance of *Akkermansia* may also have occurred in fifteen-month APP/PS1 mice, however the lack of sensitivity in DGGE and the absence of sequencing from our study could suggest a difference was not detected in our study.

Alternatively, a decrease in gene expression may contribute to the decrease in goblet cells. A HFD has been shown to be associated with several of the

pathologies seen in AD, such as: dysbiosis, insulin resistance, leaky gut, inflammation and reduction in synaptic plasticity (Agusti et al., 2018). Mice fed a HFD have demonstrated a decrease in transcription factors involved in the differentiation of goblet cells. After 11 weeks mice fed a HFD had a decrease in the expression of *Klf4* and at 22 weeks a decrease in *Spdef*, which could explain why goblet cell numbers only became statistically significant at fifteen months (Gulhane et al., 2016).

We propose that a decrease in the number of goblet cells would also cause a decrease in the amount of mucus produced, which may enable a closer proximity of the overlying microbiota to the epithelial cells. Thaiss et al. (2016) found that the gut microbiota are able to control diurnal fluctuations in not only in their movement but also their proximity to the epithelial cells through alterations in pathways of motility and also mucus degradation. Therefore, the proximity of the microbiota to the epithelial cells in the ileum of fifteen-month mice could not only be reduced due to less mucus being secreted, but be decreased further by the diurnal fluctuations dictated by the microbiota.

The microbiota in the ileum is mainly associated with the villus tip, with some located between the villi and virtually none near the crypts, partially due to the production of anti-microbial peptides by the Paneth cells at the base of the crypts (Erdmund et al., 2013). However, a reduction in the mucus production could result in anti-microbial peptides being lost by diffusion in to the lumen, allowing the microbiota to gain access to the crypts (Birchenough et al., 2015). Since the microbiota reside in the single mucus layer of the small intestine, it is plausible to suggest that decreased proximity between the microbiota and epithelial cells promotes translocation of the microbiota and its metabolites occurs across the leaky tight junctions in both the villi and the crypts and into the systemic circulation. (Ermund et al., 2013.)

Dysbiosis is often reported in elderly AD patients, however our findings in addition to other studies suggest dysbiosis is not present in a late murine model of AD (Provasi et al., 2017; Shen, Liu & Ji, 2017, Vogt et al., 2017). Although the GI

tract is highly conserved in mammals, differences do exist in both the structure and function which are evolutionary driven, and may account for the discrepancies observed (Nguyen et al., 2015). Furthermore, environmental factors are tightly controlled in the laboratory environment, unlike in real life. The dysbiosis in AD patients may be due to several environmental factors, for example diet, hospital stay, prescribed drug use, which may not be normalised in studies. However, weaknesses of the APP/PS1 animal model such as the absence of tau pathology may also account for the differences (Radde et al., 2006).

7.4 Sex specific differences

Several of the 16S rDNA DGGE profiles indicated clustering based on sex and not genotype. Animals were housed in same sex mixed genotype cages and therefore it is plausible that the observation was due to cage effects. Org et al. (2016) has noted a hormonal induced difference between the microbiota compositions between male and female mice on a variety of genetic backgrounds, and therefore our observations may not be due to cage effects. Unfortunately males and female cannot be cohoused due to mating, and no such controls such as mixing the bedding were taken in our study.

In addition, sex specific differences may also account for differences observed in previous studies of dysbiosis in APP/PS1 mice. Harach et al., (2017) studied male and female mice, whereas Zhang et al., (2017), Shen, Liu & Ji (2017) and Brandscheid et al., (2017) used only male mice. This could explain differences observed between the studies, and suggest caution must be taken when making direct comparisons.

7.5 Early life microbiota is crucial in the development of disease

Our study suggests that dysbiosis is associated with the early pathology in AD and is mostly normalised by late AD, supporting the hypothesis that the early life microbiota is crucial in development of disease. The microbiota of infants has a crucial role in influencing brain development and immune system development and therefore microbiota perturbations at this time point increases the risk of developing diseases associated with altered immune and/or brain function (Martin et al., 2010; Ximenez & Torres, 2017).

Increasing amounts of evidence in the literature highlight the importance of dysbiosis occurring in infants and adolescence and the potential for disruption of the GBA and a variety of diseases. For example, antibiotic use before six-months of age is correlated with the development of asthma by six years of age (Risnes et al., 2011). Low microbiota diversity from one month to twelve months of age is associated with the increased of developing allergies (Bisgaard et al, 2011). Furthermore, perturbations in the gut microbiota of infants in the first year of life has also shown to increase the risk of developing IBD (Kronman et al, 2012).

One suggestion for altered immune system function as a result of microbiota perturbation is the hygiene hypothesis. Life-style behaviours such as sanitation, antibiotic use and clean drinking water decreases our exposure to microbial organisms. This leads to inadequate stimulation of the immune response, resulting in an underdeveloped and deregulated immune system that makes an individual more susceptible to disease (Okada et al, 2010). The hygiene hypothesis has been implicated in the cause of AD as Fox et al., (2013) identified that countries with high levels of pathogen exposure is associated with lower prevalence of AD. However, it must also be considered that cleaner environments are often associated with a population that has a longer lifespan, and therefore has a higher prevalence of AD.

7.6 Utilising the microbiota in the diagnosis and treatment of AD

Although a few studies have identified dysbiosis in elderly AD patients (Provasi et al, 2017; Vogt et al., 2017), there has been no study looking at the development of dysbiosis before or during AD. In our study we found evidence that dysbiosis occurs four months before cognitive impairment in spatial learning and memory in the APP/PS1 mouse model is apparent. (Serneels et al., 2009). This highlights that studies need to focus on individuals who have a high risk of developing AD, and those in the early stages of AD.

The importance of our findings lie with its ability to act as a predictor of AD, which at present is diagnosed following cognitive decline at which severe neuronal loss has occurred. Only 50% of people in high-income countries receive a diagnosis which goes down to only 10% in middle-to-low income. Improving the diagnosing AD is a crucial target, not just finding a cure (Prince et al., 2016). Identifying a microbiota profile at different life stages that are typical of an individual who develops AD would be beneficial to high-risk individuals.

Our results suggest that it is the mucosal associated microbiota that is significant in the development of AD, and therefore investigating the microbiota in faecal samples would not suffice. A mucosal swab during a colonoscopy of individuals who have a family history of AD would enable a more accurate indication of whether an individual would be at risk. Furthermore, the most appropriate and crucial time-point at which testing should be undertaken will also need be determined.

In addition to diagnostics, characterising the gut microbiota could open up doors to a new treatment of AD. Dysbiosis associated with the risk of developing AD could be altered through the use of probiotics and prebiotics by suppressing or enhancing microbiota populations to a desirable composition. However, it would be important to identify the nature of the dysbiosis in each individual case, since giving a high dose of one probiotic when a lower concentration is required may provide no benefit or even be detrimental by exacerbating the dysbiosis more.

Very few studies have looked at the benefits of probiotics in humans. Of note, Akbari et al., (2016) found giving probiotics to AD patients containing the genera *Lactobacillus* and *Bifidobacterium* for 12 weeks improved cognitive functioning and metabolic defects such as insulin resistance, however there was no difference in inflammation or oxidative stress. Furthermore, this is not based on an individual's degree of dysbiosis or natural variations due to age, geography and diet. In contrast, probiotic studies have been carried out more numerously in diseases such as IBS, where severity of symptoms was shown to be reduced (Ducrotté et al., 2012; Guglielmetti et al., 2011; Roberts et al., 2013).

7.7 Altering life style behaviours may prevent AD

Whilst decreasing the risk of AD through the use of probiotics would have clear benefits, the most efficient method would be to change and adopt lifestyle behaviours that promote a 'healthy microbiota profile' that is low risk of the individual developing AD.

The easiest and possibly most effective adjustment would be a change in diet. As discussed previously the Mediterranean diet has been shown to have beneficial effects of cognitive functioning and decrease the risk of several diseases including AD (Scarmeas et al., 2006). The benefits of a Mediterranean diet has been shown in other GBA diseases as greater adherence has shown to decrease the age of onset in PD and decrease the risk of cardiovascular disease (Alcalay et al., 2012; Estruch et al., 2013). Furthermore, poor adherence to a Mediterranean diet was seen in individuals with IBS, particularly females, compared to healthy controls. Interestingly, this appeared to be most prevalent in the younger age group of 17-34, which further supports the hypothesis that the early microbiota in early life is important in disease development (Zito et al., 2016).

Since it has been reported that environmental factors influencing the gut microbiota in neonates can influence disease it may be required to take precautions *in utero*. In humans a HFD during pregnancy has been shown to cause a decrease in Bacteroidetes in, which was still apparent at six weeks of age. (Chu et al.,2016). A maternal HFD in the non-human primate *Macaca fuscata* was shown to induce dysbiosis in the offspring, which at one year of age, the equivalent to three years old in humans, could only be partially corrected post weaning using a low fat diet (Ma et al, 2014). This highlights the potential long-term consequences of maternal diet on the infant gut microbiome, and suggests that diet alterations may have to be made during pregnancy.

As previously discussed antibiotic use can cause dysbiosis, and the problem is likely to be exacerbated by inappropriate prescribing and use of antibiotics. In 2016 the UK government pledged in 2016 to half the number of inappropriate prescriptions by 2020 highlighting the need for education on the detrimental consequences to health (WWW, health media.blog.gov). In addition, AD will become even more of a global problem in the future, with the life expectancy of low economically developed countries increasing. One study in a community of Ethiopia found over a third (35.9%) of antibiotic users did not use them appropriately with the majority terminating their course early. In addition, over a third (36.8%) acquired their antibiotics without prescription (Erku, Mekuria & Belachew, 2017). This highlights the need for education in both high and low economically developed countries to reduce antibiotic use.

7.8 Future work

Although we found significant differences in the microbial profiles of APP/PS1 mice using qRT-PCR and DGGE techniques, these methods provide only a brief insight in to the dysbiosis in the gut. For qRT-PCR we utilised phylum specific primers, which only provided information on the higher taxonomic levels and

DGGEs are only indicative of dysbiosis and lack specificity as more than one species can be represented by a single band on the gradient gel (Tabit, 2016).

Future work will require using pyrosequencing to gain a more in depth understanding of dysbiosis at the lower taxonomic levels. This may help to elucidate the cause of the downstream effects we observed, such as changes in the colonic crypt depth, EEC and goblet cell numbers. Using pyrosequencing on region specific mucosal-associated microbiota will also enable better comparisons to be made with previous literature that have used pyrosequencing from faecal pellet samples (Shen, Liu & Ji, 2017). This may determine the most appropriate method to analyse microbiota and may influence future research by making studies more accurate and comparable.

In addition to pyrosequencing other techniques should also be employed, such as flow cytometry and transmission electron microscopy. This may enable a more accurate representation of AD associated microbiota profiles, as individual techniques used on the same sample have been shown to produce conflicting results (Hugon et al., 2013).

It would also be interesting to investigate changes in the number of Paneth cells in the ileum of fifteen-month APP/PS1 mice using fluorescent IHC. We have reported a decrease in the number of goblet cells in the ileum and suggest this may result in less mucus secreted, which could allow increased translocation of the microbiota and metabolites across the leaky gut barrier. Since the mucus layer normally serves as a barrier between the epithelial cells and microbiota, it would be interesting to see how the population of Paneth cells is affected, and whether it contributes or tries to reduce the pathology.

Metabolic profiling using gas chromatography coupled to mass spectrometry of microbial metabolites in the dysbiotic regions would also be required in future studies as described by González-Domínguez, García-Barrera & Gómez-Ariza (2015). Since the use of mucosal samples is unique to previous studies it would be necessary to assess the effects that mucosal dysbiosis has on metabolite

production in the regions where differences have been reported in the APP/PS1 mice. This would provide a better understanding of the consequences of dysbiosis and how this would impact the functioning of the GBA. Comparing results to previous metabolomic studies that utilised faecal pellets would also provide a better understanding in to the functionality of the samples with regards to the most appropriate sample (Sanguinetti et al., 2018).

In our study we reported a decrease in the number of goblet cells in the villi and crypts of the ileum in fifteen-month APP/PS1 mice. Future work would benefit from determining if this results in less mucus secreted in the ileum, by measuring the thickness. Quantification of mucus thickness has previously been carried out using different methods including a modified version of the PAS/AB stain, as described by Jordan et al. (1998) and using an *ex vivo* model utilising a horizontal perfusion chamber and measuring mucus thickness using a micropipette as described by Gustafsson et al. (2012). If a decrease in mucus production were observed, it would be interesting to see if translocation of the microbiota across the leaky gut is increased in the ileum. Fluorescent *in situ* hybridisation (FISH) could be used to quantify the penetrance of bacteria across the mucus and translocation across the leaky gut barrier in APP/PS1 mice using 16S rRNA probes (Johansson et al., 2014).

Future research outside of this project requires longitudinal studies characterising the human gut microbiota through life in individuals who go on to develop AD. The findings needs to confirm at roughly what age that the gut microbiota is pivotal in determining whether an individual has an increased risk of developing AD. This could be accomplished by determining what age divergence between non-AD and AD microbiota profiles occurs. From this it may be necessary to identify a criteria and time point at which looking at an individual's microbiota profile would be appropriate in order to identify the risk of developing AD.

8. Conclusion

In this study we utilised the APP/PS1 mouse model at three, seven and fifteen-months old to characterise changes in the mucosal and luminal-associated microbiota in specific regions of the GI tract using qRT-PCR and 16 rDNA DGGE. Changes in gut architecture and differences in goblet cell and EEC numbers were also investigated using PAS/AB stain and fluorescent IHC in APP/PS1 mice compared to WT littermates.

To our knowledge this is the first study to investigate dysbiosis within the mucosal and luminal-associated microbiota and at specific regions in the GI tract in a model of AD. The main finding of this project was that dysbiosis in the mucosal-associated microbiota occurs in three-month APP/PS1 mice and is normalised by the time the mice are fifteen-months old. The dysbiosis was associated with an increase in diversity in the mucosal associated microbiota of three-month mice, and a reduction in the phylum Firmicutes in seven-month APP/PS1 mice.

An increase in diversity at three-months may have resulted in the increased production of SCFAs, which increased the number of EEC's in the colon. Although we did not differentiate the type of EEC affected, we propose mechanisms of both L cells and EC cells. An increase in L cells would increase the secretion of GLP-1 and PYY resulting in decreased GI transit, promoting the growth of the microbiota resulting in dysbiosis. An increase in EC cells could result in increased secretion of 5-HT which in contrast to GLP-1 and PYY, may cause an increase in intestinal. Furthermore, an increase in colonic crypt depth was also observed in the three-month APP/PS1 mice, which we suggested could be due to a dysbiosis induced increase in SCFA which inhibits proliferation of stem cells at the base of the crypts.

Seven-month APP/PS1 mice displayed no difference in diversity of the microbiota however exhibited a decrease in the phylum Firmicutes. Since several of the important butyrate producers are within the Firmicutes phylum we

suggest this may have resulted in the decrease in EEC numbers observed in the colon.

At fifteen-months there was no observed gut dysbiosis, however there was a decrease in goblet cell numbers in the villi and crypts of the ileum. We propose this is due to the downstream consequences enhanced by dysbiosis, such as insulin resistance. We predict the decrease in goblet cells is able to exacerbate the pathology by decreasing the distance between the microbiota and the leaky epithelial barrier, allowing enhanced translocation of the microbiota and metabolites across the barrier.

Furthermore, we propose that dysbiosis occurs in the large intestine drives changes in the architecture, EEC and goblet cell numbers, which exacerbate the dysfunction of the GBA further. GBA dysfunction in addition to a genetic predisposition through the possession of the ApoE4 allele is the trigger in initiating AD pathology. As the AD progresses the dysbiosis begins to recover, however the long-term impact of GBA dysfunction including: leaky tight junctions, inflammation and insulin resistance continues to exacerbate the pathology. Furthermore, we propose that altering life style factors such as: Western diet, antibiotic use and prolonged hospital stays may perpetuate the gut microbiota further.

The implications for this research lie with the possibility of identifying a mucosal-associated microbiota profile that predicts the likelihood of an individual developing AD. Individuals who are at risk and those who are in the early stages of AD could have their microbiota altered to one that is associated with a lower risk through the administration of probiotics and adopting life style changes such as a Mediterranean diet. At present, with the absence of an effective treatment and no cure, this seems like a highly plausible diagnostic and therapeutic tool that could drastically decrease the prevalence of AD and improve the lives of millions of people worldwide.

9. References

- Abot, A., Cani, P.D., Knauf, C. 2018, Impact of Intestinal Peptides on the Enteric Nervous System: Novel Approaches to Control Glucose Metabolism and Food Intake. *Front Endocrinol*, 9: 328.
- Adebakin, A., Bradley, J., Gümüşgöz, S., Waters, E.J., Lawrence, C.B. 2012. Impaired Satiety and Increased Feeding Behaviour in the Triple-Transgenic Alzheimer's Disease Mouse Model. *PLoS One*, 7(10): e45179.
- Agusti, A., García-Pardo, M., López-Almela, I., Campillo, I., Maes, M., Román-Pérez, M., Sanz, Y. 2018. Interplay Between the Gut-Brain Axis, Obesity and Cognitive Function. *Front Neurosci*, 12: 155.
- Ahern, G.P. 2011. 5-HT and the immune System. *Curr Opin Pharmacol*, 11(1): 29-33.
- Akbari, E., Asemi, Z., Kakhaki, D.R., Bahmani, F., Kouchaki, E., Tamtaji, O.R., Hamidi, G.A., Salami, M. 2016. Effect of Probiotic Supplementation on Cognitive Function and Metabolic Status in Alzheimer's Disease: A Randomized, Double-Blind and Controlled Trial. *Front Aging Neurosci*, 8: 256.
- Alcalay, R.N., Gu, Y., Mejia-Santana, H., Cote, L., Marder, K.S., Scarmeas, N. 2012. The association between Mediterranean diet adherence and Parkinson's disease. *Mov Disord*, 27(6): 771-774.
- Amato, A., Baldassano, S., Liotta, R., Serio, R., Mulè, F. 2014, Exogenous glucagon-like peptide 1 reduces contractions in human colon circular muscle. *J Endocrinol*, 221(1): 29-37.
- Amon, P., Sanderson, I. 2017. What is the microbiome? *Arch Dis Child Educ Pract Ed* 102(2): 258-261.
- Ardisson, A.N., de la Cruz, D.M., Davis-Richardson, A.G., Rechcigl, K.T., Li, N., Drew, J.C., Murgas-Torrazza, R., Sharma, R., Hudak, M.L., Triplett, E.W., Neu, J., 2014. Meconium Microbiome Analysis Identifies Bacteria Correlated with Premature Birth. *PLoS One*, 9(3): e90784.
- Bauer, P.V., Hamr, S.C., Duca, F.A. 2016. Regulation of energy balance by a gut-brain axis and involvement of the gut microbiota. *Cell Mol Life Sci*, 73(4): 737-755.
- Bedse, G., Di Domenico, F., Serviddio, G., Cassano, T. 2015. Aberrant insulin signalling in Alzheimer's disease: current knowledge. *Front Neurosci*, 9(204): doi: 10.3389/fnins.2015.00204.

- Biagi, E., Nylund, L., Candela, M., Ostan, R., Bucci, L., Pini, E., Nikkila, J., Monti, D., Satokari, R., Franceschi, C., Brigidi, P., De Vos, W. 2010. Through Ageing, and Beyond: Gut Microbiota and Inflammatory Status in Seniors and Centenarians. *PLoS One*, 5(5): e10667.
- Birchenough, G.M.H., Johansson, M.E.V., Gustafsson, J.K., Bergström, J.H., Hansson, G.C. 2015. New developments in goblet cell mucus secretion and function. *Mucosal Immunol*, 8(4): 712-719.
- Bisgaard, H., Li, N., Bonnelykke, K., Chawes, B.L.K., Skov, T., Paludan-Müller, G., Stokholm, J., Smith, B., Krogfelt, K.A. 2011. Reduced diversity of the intestinal microbiota during infancy is associated with increased risk of allergic disease at school age. *J Allergy and Clin Immunol*, 128(3): 646-652.
- Blennow, K., Hampel, H., Weiner, M., Zetterberg, H. 2010. Cerebrospinal fluid and plasma biomarkers in Alzheimer's disease. *Nat Rev Neurol*, 6(3): 131-144.
- Bonfilli, L., Cecarini, V., Berardi, S., Scarpona, S., Suchodolski, J.S., Nasuti, C., Fiorini, D., Boarelli, M.C., Rossi, G., Eleuteri, A.M. 2017. Microbiota modulation counteracts Alzheimer's disease progression influencing neuronal proteolysis and gut hormones plasma levels. *Sci Rep*, 7(1): 2426.
- Brandscheid, C., Schuck, F., Reinhardt, S., Schäfer, K.H., Pietrzik, C.U., Grimm, M., Hartmann, T., Schwiertz, A., Endres, K. 2017. Altered Gut Microbiome Composition and Tryptic Activity of the 5xFAD Alzheimer's Mouse Model. *J Alzheimers Dis*, 56(2): 775-788.
- Braniste, V., Al-Asmakh, M., Kowal, C., Anuar, F., Abbaspour, A., Tóth, M., Korecka, A., Bakocevic, N., Ng, L.G., Kundu, P., Gulyás, B., Halldin, C., Hultenby, K., Nilsson, H., Hebert, H., Volpe, B.T., Diamond, B., Pettersson, S. 2014. The gut microbiota influences blood-brain barrier permeability in mice. *Sci Transl Med*, 6(263): 263ra158.
- Breit, S., Kupferberg, A., Rogler, G., Hasler, G. 2018. Vagus Nerve as Modulator of the Brain-Gut Axis in Psychiatric and Inflammatory Disorders. *Front Psychiatry*, 9: 44.
- Butzlaff, M., Ponimaskin, E. 2016. The role of Serotonin Receptors in Alzheimer's disease. *Opera Medica Et Physiologica*, 2(1): 77-86.
- Cai, Z., Hussain, M.D., Yan, L.J. 2014. Microglia, neuroinflammation, and beta-amyloid protein in Alzheimer's disease. *Int J Neurosci*, 124(5): 307-321.
- Carding, S., Verbeke, K., Vipond, D.T., Corfe, B.M., Owen, L.J. 2015. Dysbiosis of the gut microbiota in disease. *Microb Ecol Health Dis*, 26(1).

- Chételat, G., La Joie, R., Villain, N., Perrotin, A., de La Sayette, V., Eustache, F., Vandenberghe, R. 2013. Amyloid imaging in cognitively normal individuals, at-risk populations and preclinical Alzheimer's disease. *NeuroImage: Clin*, 2: 356-365.
- Cho, I., Blaser, M.J. 2012. The human microbiome: at the interface of health and disease. *Nat Rev Genet*, 13(4): 260-270.
- Chow, V.W., Mattson, M.P., Wong, P.C., Gleichmann, M. 2010. An Overview of APP Processing Enzymes and Products. *Neuromolecular Med*, 12(1): 1-12.
- Christiansen, C.B., Gabe, M.B.N., Svendsen, B., Dragsted, L.O., Rosenkilde, M.M., Holst, J.J. 2018. The impact of short-chain fatty acids on GLP-1 and PYY secretion from the isolated perfused rat colon. *Am J Physiol Gastrointest Liver Physiol*, 315(1): G53-G65.
- Chu, D.M., Antony, K.M., Ma, J., Prince, A.L., Showalter, L., Moller, M., Aagaard, K.M. 2016. The early infant gut microbiome varies in association with a maternal high-fat diet. *Genome Med*, 8: 77.
- Claesson, M.J., Cusack, S., O'Sullivan, O., Greene-Diniz, R., de Weerd, H., Flannery, E., Marchesi, J.R., Falush, D., Dinan, T., Fitzgerald, G., Stanton, C., van Sinderen, D., O'Connor, M., Harnedy, N., O'Connor, K., Henry, C., O'Mahony, D., Fitzgerald, A.P., Shanahan, F., Twomey, C., Hill, C., Ross P.R, O'Toole, P.W. 2011. Composition, variability, and temporal stability of the intestinal microbiota of the elderly. *Proc Natl Acad Sci USA*, 108(Supplement 1): 4586-4591.
- Clapp, M., Aurora, N., Herrera, L., Bhatia, M., Wilen, E., Wakefield, S. 2017. Gut microbiota's effect on mental health: The gut-brain axis. *Clin Pract*, 7(4): 987.
- Collado, M.C., Rautava, S., Aakko, J., Isolauri, E., Salminen, S. 2016. Human gut colonisation may be initiated *in utero* by distinct microbial communities in the placenta and amniotic fluid. *Sci Rep*, 6: 23129.
- Cooper, J.A. 2014. Factors affecting circulating levels of peptide YY in humans: a comprehensive review. *Nutr Res Rev*, 27(1): 186-197.
- Corder, E.H., Saunders, A.M., Strittmatter, W.J., Schmechel, D.E., Gaskell, P.C., Small, G.W., Roses, A.D., Haines, J.L., Pericak-Vance, M.A. 1993. Gene dose of apolipoprotein E type 4 allele and the risk of Alzheimer's disease in late onset families. *Science*, 261(5123): 921-923.
- Cremer, J., Arnoldini, M., Hwa, T. 2017. Effect of water flow and chemical environment on microbiota growth and composition in the human colon. *Proc Natl Acad Sci USA*, 114(25): 6438-6443.

D'Argenio, V., Salvatore, F. 2015. The role of the gut microbiome in the healthy adult status. *Clin Chim Acta*, 451(Part A): 97-102.

David, L.A., Materna, A.C., Friedman, J., Campos-Baptista, M.I., Blackburn, M.C., Perrotta, A., Erdman, S.E., Alm, E.J. 2014. Host lifestyle affects human microbiota on daily timescales. *Genome Biol*, 15(7): r89.

David, L.A., Maurice, C.F., Carmody, R.N., Gootenberg, D.B., Button, J.E., Wolfe, B.E., Ling, A.V., Delvin, A.S., Varma, Y., Fischbach, M.A., Biddinger, S.B., Dutton, R.J., Turnbaugh, P.J. 2014. Diet rapidly and reproducibly alters the human gut microbiome. *Nature*, 505(7484): 559-563.

Den Besten, G., van Eunen, K., Groen, A.K., Venema, K., Reijngoud, D.J., Bakker, B.M. 2013. The role of short-chain fatty acids in the interplay between diet, gut microbiota, and host energy metabolism. *J Lipid Res*, 54(9): 2325-2340.

Dethlefsen, L., Relman, D.A. 2011. Incomplete recovery and individualized responses of the human distal gut microbiota to repeated antibiotic perturbation. *Proc Natl Acad Sci USA*, 108(Supplement 1): 4554-4561.

Dineley, K.T., Jahrling, J.B., Denner, L. 2014. Insulin resistance in Alzheimer's disease. *Neurobiol Dis*, 72: 92-103.

Dominguez-Bello, M.G., Costello, E.K., Contreras, M., Magris, M., Hidalgo, G., Fierer, N., Knight, R. 2010. Delivery mode shapes the acquisition and structure of the initial microbiota across multiple body habitats in newborns. *Proc Natl Acad Sci USA*, 107(26): 11971-11975.

Donohoe, D.R., Garge, N., Zhang, X., Sun, W., O'Connell, T.M., Bunger, M.K., Bultman, S.J. 2011. The Microbiome and Butyrate Regulate Energy Metabolism and Autophagy in the Mammalian Colon. *Cell Metab*, 13(5): 517-526.

Eckburg, P.B., Bik, E.M., Bernstein, C.N., Purdom, E., Dethlefsen, L., Sargent, M., Gill, S.R., Nelson, K.E., Relman, D.A. 2005. Diversity of the Human Intestinal Microbial Flora. *Science*, 308(5728): 1635-1638.

Erickson, M.A., Hartvigson, P.E., Morofuji, Y., Owen, J.B., Butterfield, D.A., Banks, W.A. 2012. Lipopolysaccharide impairs amyloid beta efflux from brain: altered vascular sequestration, cerebrospinal fluid reabsorption, peripheral clearance and transporter function at the blood-brain barrier. *J Neuroinflammation*, 9: 150.

Ericsson, A.C., Gagliardi, J., Bouhan, D., Spollen, W.G., Givan, S.A., Franklin, C.L. 2018. The influence of caging, bedding and diet on the composition of the microbiota in different regions of the mouse gut. *Sci Rep*, 8(1): 4065.

- Erku, D.A., Mekuria, A.B., Belachew, S.A. 2017. Inappropriate use of antibiotics among communities of Gondar town: Ethiopia: a threat to the development of antimicrobial resistance. *Antimicrob Resist Infect Control*, 6(1): 112.
- Ermund, A., Schütte, A., Johansson, M.E., Gustafsson, J.K., Hansson, G.C. 2013. Studies of mucus in mouse stomach, small intestine and colon. I. Gastrointestinal mucus layers have different properties depending on location as well as over Peyer's patches. *Am J Physiol Gastrointest Liver Physiol*, 305(5): G341-347.
- Erny, D., de Angelis, A.L.H., Jaitin, D., Wieghofer, P., Staszewski, O., David, E., Keren-Shaul, H., Mhlahoi, T., Jakobshagen, K., Buch, T., Schwierzeck, V., Utermöhlen, O., Chun, E., Garrett, W.S., McCoy, K.D., Diefenbach, A., Staeheli, P., Stecher, B., Amit, I., Prinz, M. 2015. Host microbiota constantly control maturation and function of microglia in the CNS. *Nat Neurosci*, 18(7): 965-977.
- Estruch, R., Ros, E., Salas-Salvadó, J., Covas, M.I., Corella, D., Arós, F., Gómez-Gracia, E., Ruiz-Gutiérrez, V., Fiol, M., Lapetra, J., Lamuela-Raventós, R.M., Serra-Majem, L., Pintó, X., Basora, J., Muñoz, M.A., Sorlí, J.V., Martínez, J.A., Martínez-González, M.A. 2013. Primary Prevention of Cardiovascular Disease with Mediterranean Diet. *N Engl J Med*, 368(14): 1279-1290.
- Fischer, S.G., & Lerman, L.S. 1983. DNA fragments differing by single base-pair substitutions are separated in denaturing gradient gels: correspondence with melting theory. *Proc Natl Acad Sci USA*, 80(6): 1579-1583.
- Fox, M., Knapp, L.A., Andrews, P.W., Fincher, C.L. 2013. Hygiene and the world distribution of Alzheimer's disease: Epidemiological evidence for a relationship between microbial environment and age-adjusted disease burden. *Evol Med Public Health*, 2013(1): 173-186.
- Furness, J.B. 2012. The enteric nervous system and neurogastroenterology. *Nat Rev Gastroenterol Hepatol*, 9: 286-294.
- Furness, J.B., Rivera, L.R., Cho, H.J., Bravo, D.M., Callaghan, B. 2013. The gut as a sensory organ. *Nat Rev Gastroenterol Hepatol*, 10(12): 729-740.
- Geldenhuys, W.J. & Darvesh, A.S., 2015. Pharmacotherapy of Alzheimer's disease: current and future trends. *Expert Rev Neurother*, 15(1): 3-5.
- Gill, S., Chater, P.I., Wilcox, M.D., Pearson, J.P., Brownlee, I.A. 2018. The impact of dietary fibres on the physiological processes of the large intestine. *Bioact Carbohydr Dietary Fibre*, <https://doi.org/10.1016/j.bcdf.2018.06.001>.
- González-Domínguez, R., García-Barrera, T., Gómez-Ariza, J.L. 2015. Metabolite profiling for the identification of altered metabolic pathways in Alzheimer's disease.

Goodall, E.F., Wang, C., Simpson, J.E., Baker, D.J., Drew, D.R., Heath, P.R., Saffrey, M.J., Romero, I.A., Wharton, S.B. 2018. Age-associated changes in the blood-brain barrier: comparative studies in human and mouse. *Neuropathol Appl Neurobiol*, 44(3): 328-340.

Goodrich, J.K., Di Rienzi, S.C., Poole, A.C., Koren, O., Walters, W.A., Caporaso, G.J., Knight, R., Ley, R.E. 2014. Conducting a Microbiome Study. *Cell*, 158(2): 250-262.

Grant, W.B. 2014. Trends in diet and Alzheimer's disease during the nutrition transition in Japan and developing countries. *J Alzheimers Dis*, 38(3): 611-620.

Grasset, E., Puel, A., Charpentier, J., Collet, X., Christensen, J.E., Tercé, F., Burcelin, R. 2017. A Specific Gut Microbiota Dysbiosis of Type 2 Diabetic Mice Induces GLP-1 Resistance through an Enteric NO-Dependent and Gut-Brain Axis Mechanism. *Cell Metab*, 25(5): 1075-1090.

Gratuze, M., Julien, J., Petry, F.R., Morin, F., Planel, E. 2017. Insulin deprivation induces PP2A inhibition and tau hyperphosphorylation in hTau mice, a model of Alzheimer's disease-like tau pathology. *Sci Rep*, 7(1): 46359.

Gregory, R.E., Ettinger, D.S. 1998. 5-HT₃ Receptor Antagonists for the Prevention of Chemotherapy-Induced Nausea and Vomiting. A comparison of their pharmacology and clinical efficacy. *Drugs*, 55(2): 173-189.

Greiner, T.U., Bäckhed, F. 2016. Microbial regulation of GLP-1 and L-cell biology. *Mol Metab*, 5(9): 753-758.

Guglielmetti, S., Mora, D., Gschwender, M., Popp, K. 2011. Randomised clinical trial: *Bifidobacterium bifidum* MIMBb75 significantly alleviates irritable bowel syndrome and improves quality of life—a double-blind, placebo-controlled study. *Aliment Pharmacol Ther*, 33(10): 1123-1132.

Gulhane, M., Murray, L., Lourie, R., Tong, H., Yong, H., Sheng, Y.H., Wang, R., Kang, A., Schreiber, V., Wong, K.Y., Magor, G., Denman, S., Begun, J., Florin, T.H., Perkins, A., Cuív, P.Ó., McGuckin, M.A., Hasnain, S.Z. 2016. High Fat Diet Induce Colonic Epithelial Cell Stress and Inflammation that is Reversed by IL-22. *Sci Rep*, 6(1): 28990.

Gunawardene, A.R., Corfe, B.M., Staton, C.A. 2011. Classification and functions of enteroendocrine cells of the lower gastrointestinal tract. *Intl J Exp Pathol*, 92(4): 219-231.

Guo, S., Al-Sadi, R., Said, H.M., Ma, T.Y. 2013. Lipopolysaccharide Causes and Increase in Intestinal Tight Junction Permeability *in Vitro* and *in Vivo* by Inducing Enterocyte Membrane Expression and Localisation of TLR-4 and CD14. *Am J Pathol*, 182(2): 375-387.

Gustafsson, J.K., Ermund, A., Johansson, M.E., Schütte, A., Hansson, G.C., Sjövall, H. 2012. An ex vivo method for studying mucus formation, properties, and thickness in human colonic biopsies and mouse small and large intestinal explants. *Am J Physiol Gastrointest Liver Physiol*, 302(4): G430-G438.

Hakansson, A., Molin, G. 2011. Gut Microbiota and Inflammation. *Nutrients*, 3(6): 637-682.

Harach, T., Marungruang, N., Duthilleul, N., Cheatham, V., Mc Coy, K.D., Frisoni, G., Neher, J.J., Fåk, F., Jucker, M., Lasser, T., Bolmont, T. 2017. Reduction of A β amyloid pathology in APPPS1 transgenic mice in the absence of gut microbiota. *Sci Rep*, 7(1): 41802.

Hardy, J.A., Higgins, G.A. 1992. Alzheimer's disease: the amyloid cascade hypothesis. *Science*, 256(5054): 184-185.

Hartz, A.M.S., Bauer, B., Soldner, E.L.B., Wolf, A., Boy, S., Backhaus, R., Mihaljevic, I., Bogdahn, U., Klünemann, H.H., Schuierer, G., Schlachetzki, F. 2012. Amyloid- β Contributes to Blood-Brain Barrier Leakage in Transgenic Human Amyloid Precursor Protein Mice and in Humans With Cerebral Amyloid Angiopathy. *Stroke*, 43(2): 514-523.

Hata, T., Asano, Y., Yoshihara, K., Kimura-Todani, T., Miyata, N., Zhang, X.T., Takakura, S., Aiba, Y., Koga, Y., Sudo, N. 2017. Regulation of gut luminal serotonin by commensal microbiota in mice. *PLoS One*, 12(7): e0180745.

He, C., Cheng, D., Peng, C., Li, Y., Zhu, Y., Lu, N. 2018. High-Fat Diet Induces Dysbiosis of Gastric Microbiota Prior to Gut Microbiota in Association with Metabolic Disorders in Mice. *Front Microbiol*, 9: 639.

He, Y., Zheng, M.M., Ma, Y., Han, X.J., Ma, X.Q., Qu, C.Q., Du, Y.F. 2012. Soluble oligomers and fibrillar species of amyloid β -peptide differentially affect cognitive functions and hippocampal inflammatory response. *Biochem Biophys Res Commun*, 429(3-4): 125-130.

Hendricksen, M., Thomas, A.J., Ferrier, I.N., Ince, P., O'Brien, J.T. 2004. Neuropathological Study of the Dorsal Raphe Nuclei in Late-Life Depression and Alzheimer's Disease With and Without Depression. *Am J Psychiatry*, 161(6): 1096-1102.

Heneka, M.T., Golenbock, D.T., Latz, E. 2015. Innate immunity in Alzheimer's disease. *Nat Immunol*, 16(3): 229-236.

Heppner, F.L., Ransohoff, R.M., Becher, B. 2015. Immune attack: the role of inflammation in Alzheimer disease. *Nat Rev Neurosci*, 16(6): 358-372.

Hill, J.M., Clement, C., Pogue, A.I., Bhattacharjee, S., Zhao, Y., Lukiw, W.J. 2014. Pathogenic microbes, the microbiome, and Alzheimer's disease (AD), *Front Aging Neurosci*, 6: 127.

Ho, L., Ono, K., Tsuji, M., Mazzola, P., Singh, R., Pasinetti, G.M. 2018. Protective Roles of Intestinal Microbiota Derived Short Chain Fatty Acids in Alzheimer's Disease-type Beta-Amyloid Neuropathological Mechanisms. *Expert Rev Neurother*, 18(1): 83-90.

Holzer, P. & Farzi, A. 2014. Neuropeptides and the Microbiota-Gut-Brain Axis. *Adv Exp Med Biol*, 817: 195-219.

Hosoyamada, Y., Sakai, T. 2005. Structural and mechanical architecture of the intestinal villi and crypts in the rat intestine: integrative reevaluation from ultrastructural analysis. *Anat Embryol*, 210(1): 1-12.

Hugon, P., Lagier, J.C., Robert, C., Lepolard, C., Papazian, L., Musso, D., Vialettes, B., Raoult, D. 2013. Molecular Studies Neglect Apparently Gram-Negative Populations in the Human Gut Microbiota. *J Clin Microbiol*, 51(10): 3286-3293.

Humphries, A., Wright, N.A. 2008. Colonic crypt organization and tumourigenesis. *Nat Rev Cancer*, 8(6): 415-424.

Hung, T.V., Suzuki, T. 2018. Short-Chain Fatty Acids Suppress Inflammatory Reactions in Caco-2 Cells and Mouse Colons. *J Agric Food Chem*, 66(1): 108-117.

Hviid, A., Svanström, H., Frisch, M., 2010. Antibiotic use and inflammatory bowel diseases in childhood. *Gut*, 60: 49-54.

Jakobsson, H.E., Jernberg, C., Andersson, A.F., Sjölund-Karlsson, M., Jansson, J.K., Engstrand, L. 2010. Short-Term Antibiotic Treatment Has Differing Long-Term Impacts on the Human Throat and Gut Microbiome. *PLoS One*, 5(3): e9836.

Jenkins, T.A., Nguyen, J.C.D., Polglaze, K.E., Bertrand, P.P. 2016. Influence of Tryptophan and Serotonin on Mood and Cognition with a Possible Role of the Gut-Brain Axis. *Nutrients*, 8(1): 56.

Jiang, H., Ling, Z., Zhang, Y., Mao, H., Ma, Z., Yin, Y., Wang, W., Tang, W., Tan, Z., Shi, J., Li, L., Ruan, B. 2015. Altered fecal microbiota composition in patients with major depressive disorder. *Brain Behav Immun*, 48: 186-194.

Johansson, M.E., Gustafsson, J.K., Holmén-Larsson, J., Jabbar, K.S., Xia, L., Xu, H., Ghishan, F.K., Carvalho, F.A., Gewirtz, A.T., Sjövall, H., Hansson, G.C. 2014. Bacteria penetrate the normally impenetrable inner colon mucus layer in both murine colitis models and patients with ulcerative colitis. *Gut*, 63(2): 281-291.

- Johansson, M.E., Sjövall, H., Hansson, G.C. 2013. The gastrointestinal mucus system in health and disease. *Nat Rev Gastroenterol Hepatol*, 10(6): 352-361.
- Jordan, N., Newton, J., Pearson, J., Allen, A. 1998. A novel method for the visualization of the in situ mucus layer in rat and man. *Clin Sci*, 95(1): 97-106.
- Kai, K., Hashimoto, M., Amano, K., Tanaka, H., Fukuhara, R., Ikeda, M. 2015. Relationship between Eating Disturbances and Dementia Severity in Patients with Alzheimer's Disease. *PLoS One*, 10(8): e0133666.
- Kaiko, G.E., Ryu, S.H., Koues, O.I., Collins, P.L., Solnica-Krezel, L., Pearce, E.J., Pearce, E.L., Oltz, E.M., Stappenbeck, T.S. 2016. The colonic crypt protect stem cells from microbiota-derived metabolites. *Cell*, 165(7): 1708-1720.
- Kaji, I., Karaki, S., Tanaka, R., Kuwahara, A. 2011. Density distribution of free fatty acid receptor 2 (FFA2)- expressing and GLP-1 producing enteroendocrine L cells in human and rat lower intestine, and increased cell numbers after ingestion of fructo-oligosaccharide. *J Mol Histol*, 42(1): 27-38.
- Ke, Y.D., Delerue, F., Gladbach, A., Götz, J., Ittner, L.M. 2009. Experimental diabetes mellitus exacerbates tau pathology in a transgenic mouse model of Alzheimer's disease. *PLoS One*, 4(11): e7917.
- Kelly, J.R., Allen, A.P., Temko, A., Hutch, W., Kennedy, P.J., Farid, N., Murphy, E., Boylan, G., Bienenstock, J., Cryan, J.F., Clarke, G., Dinan, T.G. 2017. Lost in translation? The potential psychobiotic *Lactobacillus rhamnosus* (JB-1) fails to modulate stress or cognitive performance in healthy male subjects. *Brain Behav Immun*, 61: 50-59.
- Kelly, J.R., Kennedy, P.J., Cryan, J.F., Dinan, T.G., Clarke, G., Hyland, N.P. 2015. Breaking down the barriers: the gut microbiome, intestinal permeability and stress-related psychiatric disorders. *Front Cell Neurosci*, 9: 392.
- Kennedy, P.J., Cryan, J.F., Dinan, T.G., Clarke, G. 2014. Irritable bowel syndrome: A microbiome-gut-brain axis disorder? *World J Gastroenterol*, 20(39): 14105-14125.
- Kleinridders, A., Ferris, H.A., Cai, W., Kahn, R.C. 2014. Insulin Action in Brain Regulates Systemic Metabolism and Brain Function. *Diabetes*, 63(7): 2232-2243.
- Kostic, A.D., Howitt, M.R., Garrett, W.S. 2013. Exploring host-microbiota interactions in animal models and humans. *Genes Dev*, 27(7): 701-718.
- Kronman, M.P., Zaoutis, T.E., Haynes, K., Feng, R., Coffin, S.E. 2012. Antibiotic Exposure and IBD Development Among Children: A Cohort Study. *Pediatrics*, 130(4): e794-803.

Kuan, Y.C., Huang, K.W., Lin, C.L., Hu, C.J., Kao, C.H. 2017. Effect of metformin exposure on neurodegenerative diseases in elderly patients with type 2 diabetes mellitus. *Prog Neuropsychopharmacol Biol Psychiatry*, 79: 77-83.

Kumar, S. & Walter, J. 2011. Phosphorylation of amyloid beta (A β) peptides – A trigger for formation of toxic aggregates in Alzheimer’s disease. *Aging*, 3(8): 803-812.

Lai, M.K., Tsang, S.W., Alder, J.T., Keene, J., Hope, T., Esiri, M.M., Francis, P.T., Chen, C.P. 2005. Loss of serotonin 5-HT_{2A} receptors in the postmortem cortex correlates with decrease in Alzheimer’s disease. *Psychopharmacology*, 179(3): 673-677.

Lankelma, J.M., van Vught, L.A., Belzer, C., Schultz, M.J., ver der Poll, T., de Vos, W.M., Wiersinga, W.J. 2017. Critically ill patients demonstrate large interpersonal variation in intestinal microbiota dysregulation: a pilot study. *Intensive Care Med*, 43(1): 59-68.

Larraufie, P., Martin-Gallausiaux, C., Lapaque, N., Dore, J., Gribble, F.M., Reimann, F., Blottiere, H.M. 2018. SCFAs strongly stimulate PYY production in human enteroendocrine cells. *Sci Rep*, 8: 74.

Latorre, R., Sternini, C., De Giorgio, R., Greenwood-van Meerveld, B. 2016. Enteroendocrine Cells: A Review of Their Role In Brain-Gut Communication. *Neurogastroenterol Motil*, 28(5): 620-630.

LeBlanc, J.G., Milani, C., de Giori, G.S., Sesma, F., van Sinderen, D., Ventura, M. 2013. Bacteria as vitamin suppliers to their hosts: a gut microbiota perspective. *Curr Opin Biotechnol*, 24(2): 160-168.

Lee, S., Tong, M., Hang, S., Deochand, C., de la Monte, S. 2014. CSF and Brain Indices of Insulin Resistance, Oxidative Stress and Neuro-Inflammation in Early versus Late Alzheimer’s Disease. *J Alzheimers Dise Parkinsonism*, 3: 128.

Lin, R., Lui, W., Piao, M., Zhu, H. 2017. A review of the relationship between the gut microbiota and amino acid metabolism. *Amino Acids*, 49(12): 2083-2090.

Linak, K.J., Schmittgen, T.D. 2001. Analysis of Relative Gene Expression Data Using Real-Time Quantitative PCR and the 2^{-Delta Delta C(T)} Method. *Methods*, 25(4): 402-408.

Louis, P., Young, P., Holtrop, G., Flint, H.J. 2010. Diversity of human colonic butyrate-producing bacteria revealed by analysis of the butyryl-CoA: acetate CoA-transferase gene. *Environ Microbiol*, 12(2): 304-314.

Lu, J., Lu, L., Yu, Y., Cluette-Brown, J., Martin, C.R., Claud, E.C. 2018. Effects of Intestinal Microbiota on Brain Development in Humanised Gnotobiotic Mice. *Sci Rep*, 8: 5443.

Lukiw, W.J. 2016. *Bacteroides fragilis* Lipopolysaccharide and Inflammatory Signalling in Alzheimer's Disease. *Front Microbiol*, 7: 1544.

Lund, M.L., Egerod, K.L., Engelstoft, M.S., Dmytriyeva, O., Theodorsson, E., Patel, B.A., Schwartz, T.W. 2018. Enterochromaffin 5-HT cells – A major target for GLP-1 and gut microbial metabolites. *Mol Metab*, 11: 70-83.

Lurie, I., Yang, Y.X., Haynes, K., Mamtani, R., Boursi, B., 2015. Antibiotic Exposure and the Risk for Depression, Anxiety, or Psychosis: A Nested Case-Control Study. *J Clin Psychiatry*, 76(11): 1522-1528.

Ma, J., Prince, A.L., Bader, D., Hu, M., Ganu, R., Baquero, K., Blundell, P., Harris, A.R., Frias, A.E., Grove, J.L., Aagaard, K.M. 2014. High-fat maternal diet during pregnancy persistently alters the offspring microbiome in a primate model. *Nat Commun*, 5: 3889.

MacIntosh, C.G., Andrews, J.M., Jones, K.L., Wishart, J.M., Morris, H.A., Jansen, J.B., Morley, J.E., Horowitz, M., Chapman, I.M. 1999. Effects of age on concentrations of plasma cholecystikinin, glucagon-like peptide 1, and peptide YY and their relation to appetite and pyloric motility. *Am J Clin Nutr*, 69(5): 999-1006.

Maier, L., Pruteanu, M., Kuhn, M., Zeller, G., Telzerow, A., Anderson, E.E., Brochado, A.R., Fernandez, K.C., Dose, H., Mori, H., Patil, K.R., Bork, P., Typas, A. 2018. Extensive impact of non-antibiotic drugs on human gut microbiota. *Nature*, 555: 623-628.

Man, A.L., Bertelli, E., Rentini, S., Regoli, M., Briars, G., Marini, M., Watson, A.J.M., Nicoletti, C. 2015. Age-associated modifications of intestinal permeability and innate immunity in the human small intestine. *Clin Sci*, 129(7): 515-527.

Marcobal, A., Sonnenburg, J.L. 2012. Human milk oligosaccharide consumption by intestinal microbiota. *Clin Microbiol Infect*, 18(Suppl 4): 12-15.

Martin, R., Nauta, A.J., Ben Amor, K., Knippels, L.M., Knol, J., Garssen, J. 2010. Early life: gut microbiota and immune development in infancy. *Benef Microbes*, 1(4): 367-382.

Mayer, E.A., Savidge, T., Shulman, R.J. 2014. Brain-Gut Microbiome Interactions and Functional Bowel Disorders. *Gastroenterology*, 146(6): 1500-1512.

Mazurek, M.F., Beal, M.F. 1991. Cholecystikinin and somatostatin in Alzheimer's disease postmortem cerebral cortex. *Neurology*, 41(5): 716-719.

- McDonald, D., Ackermann, G., Khailova, L., Baird, C., Heyland, D., Kozar, R., Lemieux, M., Derenski, K., King, J., Vis-Kampen, C., Knight, R., Wischmeyer, P.E. 2016. Extreme Dysbiosis of the Microbiome in Critical Illness. *mSphere*, 1(4): e00199-16.
- McKhann, G.M., Knopman, D.S., Chertkow, H., Hyman, B.T., Jack, C.R., Kawas, C.H., Klunk, W.E., Koroshetz, W.J., Manly, J.J., Mayeux, R., Mohs, R.C., Morris, J.C., Rossor, M.N., Scheltens, P., Carrillo, M.C., Thies, B., Weintraub, S., Phelps, C.H. 2011. The diagnosis of dementia due to Alzheimer's disease: recommendations from the National Institute on Aging-Alzheimer's Association workgroups on diagnostic guidelines for Alzheimer's disease. *Alzheimer's Dement*, 7(3): 263-269.
- Medema, J.P., Vermeulen, L. 2011. Microenvironmental regulation of stem cells in intestinal homeostasis and cancer. *Nature*, 474(7351): 318-326.
- Medina, M., Hernández, F., Avila, J. 2016. New Features about Tau Function and Dysfunction. *Biomolecules*, 6(2): 21.
- Michel, L., Prat, A. 2016. One more role for the gut: microbiota and blood brain barrier. *Ann Transl Med*, 4(1): 15.
- Montagne, A., Barnes, S.R., Sweeney, M.D., Halliday, M.R., Sagare, A.P., Zhao, Z., Toga, A.W., Jacobs, R.E., Liu, C.Y., Amezcua, L., Harrington, M.G., Chui, H.C., Law, M., Zlokovic, B.V. 2015. Blood-Brain Barrier Breakdown in the Aging Human Hippocampus. *Neuron*, 85(2): 296-302.
- Morrison, D.J., Preston, T. 2016. Formation of short chain fatty acids by the gut microbiota and their impact on human metabolism. *Gut Microbes*, 7(3): 189-200.
- Moser, V.A. & Pike, C.j., 2017. Obesity Accelerates Alzheimer-Related Pathology in *APOE4* but not *APOE3* Mice. *eNeuro*, 4(3): 0077-17.
- Muniz, L.R., Knosp, C., Yeretssian, G. 2012. Intestinal antimicrobial peptides during homeostasis, infection and disease. *Front Immunol*, 3: 310.
- Murphy, P.M., LeVine, H. 2010. Alzheimer's Disease and the β -Amyloid Peptide. *J Alzheimers Dis*, 19(1): 311.
- Muyzer, G., de Waal, E.C., Uitterlinden, A.G. 1993. Profiling of Complex Microbial Populations by Denaturing Gradient Gel Electrophoresis Analysis of Polymerase Chain Reaction-Amplified Genes Coding for 16S rRNA. *Appl Environ Microbiol*, 59(3): 695-700.
- Nadkarni, P., Chepurny, O.G., Holz, G.G. 2014. Regulation of Glucose Homeostasis by GLP-1. *Prog Mol Biol Transl Sci*, 121: 23-65.

- Nazem, A., Sankowski, R., Bacher, M., Al-Abed, Y. 2015. Rodent models of neuroinflammation for Alzheimer's disease. *J Neuroinflammation*, 12: 74.
- Nguyen, T.L.A., Vieira-Silva, S., Liston, A., Raes, J. 2015. How informative is the mouse for human gut microbiota research? *Dis Model Mech*, 8(1): 1-16.
- Nowacki, M.R. 1993. Cell proliferation in colonic crypts of germ-free and conventional mice – preliminary report. *Folia Histochem Cytobiol*, 31(2): 77-81.
- O'Mahony, S.M., Clarke, G., Borre, Y.E., Dinan, T.G., Cryan, J.F. 2015. Serotonin, tryptophan metabolism and the brain-gut microbiome axis. *Behav Brain Res*, 277: 32-48.
- Oakley, H., Cole, S.L., Logan, S., Maus, E., Shao, P., Craft, J., Guillozet-Bongaarts, A., Ohno, M., Disterhoft, J., Van Eldik, L., Berry, R., Vassar, R. 2006. Intraneuronal β -Amyloid Aggregates, Neurodegeneration, and Neuron Loss in Transgenic Mice with Five Familial Alzheimer's Disease Mutations: Potential Factors in Amyloid Plaque Formation. *J Neurosci*, 26(40): 10129-10140.
- Odamaki, T., Kato, K., Sugahara, H., Hashikura, N., Takahashi, S., Xiao, J., Abe, F., Osawa, R. 2016. Age-related changes in gut microbiota composition from newborn to centenarian: a cross-sectional study. *BMC Microbiol*, 16: 90.
- Okada, H., Kuhn, C., Feillet, H., Bach, J.F. 2010. The 'hygiene hypothesis for autoimmune and allergic diseases: an update. *Clin Exp Immunol*, 160(1): 1-9.
- Olson, M.I., Shaw, C.M. 1969. Presenile dementia and Alzheimer's disease in monogolism. *Brain*, 92(1): 147-156.
- Pandharipande, P.P., Girard, J.C., Morandi, A., Thompson, J.L., Pun, B.T., Brummel, N.E., Hughes, C.G., Vasilevskis, E.E., Shintani, A.K., Moons, K.G., Geevarghese, S.K., Canonico, A., Hopkins, R.O., Bernard, G.R., Dittus, R.S., Ely, E.W. 2013. Long-term Cognitive Impairment after Critical Illness. *N Engl J Med*, 369: 1306-1316.
- Park, J.Y., Choi, J., Lee, Y., Lee, J.E., Lee, E.H., Kwon, H.J., Yang, J., Jeong, B.R., Kim, Y.K., Han, P.L. 2017. Metagenome Analysis of Bodily Microbiota in a Mouse Model of Alzheimer Disease Using Bacteria-Derived Membrane Vesicles in Blood. *Exp Neurobiol*, 26(6): 369-379.
- Perez-Muñoz, M.E., Arrieta, M.C., Ramer-Tait, A.E., Walter, J. 2017. A critical assessment of the "sterile womb" and "in utero colonization" hypothesis: implications for research on the pioneer infant microbiome. *Microbiome*, 5:48.
- Perez-Pardo, P., Hartog, M., Garssen, J., Kraneveld, A.D. 2017. Microbes Tickling Your Tummy: the Importance of the Gut-Brain Axis in Parkinson's Disease. *Curr Behav Neurosci Rep*, 4(4): 361-368.

- Petersen, R.C. 2009. Early Diagnosis of Alzheimer's Disease: is MCI Too Late? *Curr Alzheimer Res*, 6(4): 324-330.
- Pistollato, F., Cano, S.S., Elio, I., Vergara, M.M., Giampieri, F., Battino, M. 2016. Role of gut microbiota and nutrients in amyloid formation and pathology of Alzheimer's disease. *Nutr Rev*, 74(10): 624-634.
- Prince, M., Comas-Herrera, A., Knapp, M., Guerchet, M., Karagiannidou, M. 2016. World Alzheimer Report 2016: Improving healthcare for people living with dementia. Alzheimer's Disease International, London.
- Provasi, S., Ferrari, C., Festari, C., Boccardi, M., Frisoni, G., Cattaneo, A. 2017. Gut bacteria and Alzheimer's disease: from dysbiosis to beta-amyloid plaques. *Eur Neuropsychopharmacol*, 27(Supplement 4): S1027.
- Psichas, A., Sleeth, M.L., Murphy, K.G., Brooks, L., Bewick, G.A., Hanyaloglu, A.C., Ghatei, M.A., Bloom, S.R., Frost, G. 2015. The short chain fatty acid propionate stimulates GLP-1 and PYY secretion *via* free fatty acid receptor in rodents. *Int J Obes*, 39(3): 424-429.
- Rabot, S., Jaglin, M., Daugé, V., Naudon, L. 2016. Impact of the gut microbiota on the neuroendocrine and behavioural responses to stress in rodents. *OCL*, 23(1): D116.
- Radde, R., Bolmont, T., Kaeser, S.A., Coomaraswamy, J., Lindau, D., Stoltze, L., Calhoun, M.E., Jäggi, F., Wolburg, H., Gengler, S., Haass, C., Ghetti, B., Czech, C., Hölscher, C., Matthews, P.M., Jucker, M. 2006. A β 42-driven cerebral amyloidosis in transgenic mice reveals early and robust pathology. *EMBO Rep*, 7(9): 940-946.
- Reigstad, C.S., Salmonson, C.E., Rainey, J.F., Szurszewski, J.H., Linden, D.R., Sonnenburg, J.L., Farrugia, G., Kashyap, P.C. 2015. Gut microbes promote colonic serotonin production through an effect of short-chain fatty acids on enterochromaffin cells. *FASEB J*, 29(4): 1395-1403.
- Reisi, P., Ghaedamini, A.R., Golbidi, M., Shabrang, M., Arabpoor, Z., Rashidi, B. 2015. Effect of cholecystokinin on learning and memory, neuronal proliferation and apoptosis in the rat hippocampus. *Adv Biomed Res*, 4: 227.
- Richardson, K., Fox, C., Maidment, I., Steel, N., Loke, Y.K., Arthur, A., Myint, P.K., Grossi, C.M., Mattishent, K., Bennett, K., Campbell, N.L., Boustani, M., Robinson, L., Brayne, C., Matthews, F.E., Savva, G.M. 2018. Anticholinergic drugs and risk of dementia: case-control study. *BMJ*, 361: k1315.
- Risnes, K.R., Belanger, K., Murk, W., Bracken, M.B. 2011. Antibiotic Exposure by 6 Months and Asthma and Allergy at 6 Years: Findings in a Cohort of 1,401 US Children. *Am J Epidemiol*, 173(3): 310-318.

Roberts, L.M., McCahon, D., Holder, R., Wilson, S., Hobbs, R. 2013. A randomised controlled trial of a probiotic 'functional food' in the management of irritable bowel syndrome. *GMC Gastroenterol*, 13: 45.

Rogers, M.A.M., Aronoff, D.M. 2016. The Influence of Nonsteroidal Anti-Inflammatory Drugs on the Gut Microbiome. *Clin Microbiol Infect*, 22(2): 178.e1-178.e9.

Saito, T., Suemoto, T., Brouwers, N., Slegers, K., Funamoto, S., Mihira, N., Matsuba, Y., Yamada, K., Nilsson, P., Takano, J., Nishimura, M., Iwata, N., Van Broeckhoven, C., Ihara, Y., Saido, T.C. 2011. Potent amyloidogenicity and pathogenicity of A β 43. *Nat Neurosci*, 14(8): 1023-1032.

Samson, S.L., Garber, A. 2013. GLP-1R agonist therapy for diabetes: benefits and potential risks. *Curr Opin Endocrinol Diabetes Obes*, 20(2): 87-97.

Sanguinetti, E., Collado, M.C., Marrachelli, V.G., Monleon, D., Selma-Royo, M., Pardo-Tendero, M.M., Burchielli, S., Iozzo, P. 2018, Microbiome-metabolome signatures in mice genetically prone to develop dementia, fed a normal or fatty diet. *Sci Rep*, 8: 4907.

Sasaguri, H., Nilsson, P., Hashimoto, S., Nagata, K., Saito, T., De Strooper, B., Hardy, J., Vassar, R., Winblad, B., Saido, T.C. 2017. APP mouse models for Alzheimer's disease preclinical studies. *EMBO J*, 36(17): 2473-2487.

Savage, A.P., Adrian, T.E., Carolan, G., Chatterjee, V.K., Bloom, S.R. 1987. Effects of peptide YY (PYY) on mouth to caecum intestinal transit time and on the rate of gastric emptying in healthy volunteers. *Gut*, 28(2): 166-170.

Scarmeas, N., Stern, Y., Tang, M.X., Mayeux, R., Luchsinger, J.A. 2006. Mediterranean Diet and Risk for Alzheimer's Disease. *Ann Neurol*, 59(6): 912-921.

Schemmert, S., Schartmann, E., Zafiu, C., Kass, B., Hartwig, S., Lehr, S., Bannach, O., Langen, K.J., Shah, N.J., Kutzsche, J., Willuweit, A., Willbold, D. 2018. A β Oligomer Elimination Restores Cognition in Transgenic Alzheimer's Mice with Full-Blown Pathology. *Mol Neurobiol*, <https://doi.org/10.1007/s12035-018-1209-3>.

Schneeberger, M., Everard, A., Gómez-Valadés, A.G., Matamoros, S., Ramírez, S., Delzenne, N.M., Gomis, R., Claret, M., Cani, P.D. 2015. *Akkermansia muciniphila* inversely correlates with the onset of inflammation, altered adipose tissue metabolism and metabolic disorders during obesity in mice. *Sci Rep*, 5(1): 16643.

Sekirov, I., Russell, S.L., Antunes, L.C., Finlay, B.B. 2010. Gut Microbiota in Health and Disease. *Physiol Rev*, 90(3): 859-904.

Serneels, L., Van Biervliet, J., Craessaerts, K., Dejaegere, T., Horr , K., Van Houtvin, T., Esselmann, H., Paul, S., Sch fer, M.K., Berezovska, O., Hyman, B.T., Sprangers, B., Sciot, R., Moons, L., Jucker, M., Yang, Z., May, P.C., Karren, E., Wiltfang, J., D'Hooge, R., De Strooper, B. 2009. γ -Secretase Heterogeneity in the Aph1 Subunit: Relevance for Alzheimer's Disease. *Science*, 324(5927): 639-642.

Shajib, M.S., Khan, W.I. 2014. The role of serotonin and its receptors in activation of immune responses and inflammation. *Acta Physiol*, 213(3): 561-574.

Shen, L., Liu, L., Ji, H.F. 2017. Alzheimer's Disease Histological and Behavioural in Transgenic Mice Correlate with Specific Gut Microbiome State. *J Alzheimers Dis*, 56(1): 385-390.

Sherwin, E., Sandhu, K.V., Dinan, T.G., Cryan, J.F. 2016. May the Force Be With You: The Light and Dark Sides of the Microbiota-Gut-Brain Axis in Neuropsychiatry. *CNS Drugs*, 30(11): 1019-1041.

Shin, N.R., Lee, J.C., Lee, H.Y., Kim, M.S., Whon, T.W., Lee, M.S., Bae, J.W. 2014. An increase in the *Akkermansia* spp. population induced by metformin treatment improves glucose homeostasis in diet-induced obese mice. *Gut*, 63(5): 727-735.

Simr n, M., Barbara, G., Flint, H.J., Spiegel, B.M., Spiller, R.C., Vanner, S., Verdu, E.F., Whorwell, P.J., Zoetendal, E.G. 2013. Intestinal microbiota in functional bowel disorders: a Rome foundation report. *Gut*, 62(1): 159-176.

Steimle, A., Autenrieth, I.B., Frick, J.S. 2016. Structure and function: Lipid A modifications in commensals and pathogens. *Int J Med Microbiol*, 306(5): 290-301.

Steinert, R.E., Feinle-Bisset, C., Asarian, L., Horowitz, M., Beglinger, C., Geary, N. 2016. Ghrelin, CCK, GLP-1 and PYY (3-36): Secretory Controls and Physiological Roles in Eating and Glycemia in Health, Obesity and After RYGB. *Physiol Rev*, 97(1): 411-463.

Tabit, F.T. 2016. Advantage and limitations of potential methods for the analysis of bacteria in milk: a review. *J Food Sci Technol*, 53(1): 42-49.

Tamburini, S., Shen, N., Wu, H.C., Clemente, J.C. 2016. The microbiome in early life: implications for health outcomes, *Nat Med*, 22(7): 713-722.

Tang, M.S., Poles, J., Leung, J.M., Wolff, M.J., Davenport, M., Lee, S.C., Lim, Y.A., Chua, K.H., Loke, P., Cho, I. 2015. Inferred metagenomic comparison of mucosal and fecal microbiota from individuals undergoing routine screening colonoscopy reveals similar differences observed during active inflammation. *Gut Microbes*, 6(1): 48-56.

Tanzi, R.E., Bertram, L. 2005. Twenty Years of the Alzheimer's Disease Amyloid Hypothesis: A Genetic Perspective. *Cell*, 120(4): 545-555.

Thaiss, C.A., Levy, M., Korem, T., Dohnalová, L., Shapiro, H., Jaitin, D.A., David, E., Winter, D.R., Gury-Benari, M., Tatirovsky, E., Tuganbaev, T., Federici, S., Zmora, N., Zeevi, D., Dori-Bachash, M., Pevsner-Fischer, M., Kartvelishvily, E., Brandis, A., Harmelin, A., Shibolet, O., Halpern, Z., Honda, K., Amit, I., Segal, E., Elinav, E. 2016. Microbiota Diurnal Rhythmicity Programs Host Transcriptome Oscillations. *Cell*, 167(6): 1495-1510.

Tillisch, K., Labus, J., Kilpatrick, L., Jiang, Z., Stains, J., Ebrat, B., Guyonnet, D., Legrain-Raspaud, S., Trotin, B., Nailboff, B., Mayer, E.A. 2013. Consumption of Fermented Milk Product with Probiotic Modulates Brain Activity. *Gastroenterol*, 144(7): 1394-1401.

Timmerman, H.M., Rutten, N.B., Boekhorst, J., Saulnier, D.M., Kortman, G.A.M., Contractor, N., Kullen, M., Floris, E., Harmsen, H.J.M., Vlieger, A.M., Kleerebezem, M., Rijkers, G.T. 2017. Intestinal colonisation patterns in breastfed and formula-fed infants during the first 12 weeks of life reveal sequential microbiota signatures. *Sci Rep*, 7(1): 8327.

Tottey, W., Feria-Gervasio, D., Gaci, N., Laillet, B., Pujos, E., Martin, J.F., Sebedio, J.L., Sion, B., Jarrige, J.F., Alric, M., Brugère, J.F. 2017. Colonic Transit Time Is a Driven Force of the Gut Microbiota Composition and Metabolism: In Vitro Evidence. *J Neurogastroenterol Motil*, 23(1): 124-134.

Tran, L., Greenwood-Van Meerveld, B. 2013. Age-Associated Remodelling of the Intestinal Epithelial Barrier. *J Gerontol A Biol Sci Med Sci*, 68(9): 1045-1056.

Tsabouri, S., Priftis, K.N., Chaliasos, N., Siamopoulou, A. 2014. Modulation of gut microbiota downregulates the development of food allergy in infancy. *Allergol Immunopathol*, 42(1): 69-77.

Tse, J.K.Y. 2017. Gut Microbiota, Nitric oxide, and Microglia as Prerequisites for Neurodegenerative Disorders. *ACS Chem Neurosci*, 8(7): 1438-1447.

Van den Abbeele, P., Van de Wiele, T., Verstraete, W., Possemiers, S. 2011. The host selects mucosal and luminal associations of coevolved gut microorganisms: a novel concept, *FEMS Microbiol Rev*, 35(4): 681-704.

Van der Kant, R., Goldstein, L.S.B. 2015. Cellular Functions of the Amyloid Precursor Protein from Development to Dementia. *Dev Cell*, 32(4): 502-515.

Vogt, N.M., Kerby, R.L., Dill-McFarland, K.A., Harding, S.J., Merluzzi, A.P., Johnson, S.C., Carlsson, C.M., Asthana, S., Zetterberg, H., Blennow, K., Bendlin, B.B., Rey, F.E. 2017. Gut microbiome alterations in Alzheimer's disease. *Sci Rep*, 7: 13537.

Wang, M., Li, M., Wu, S., Lebrilla, C.B., Chapkin, R.S., Ivanov, I., Donovan, S.M. 2015. Fecal Microbiota Composition of Breast-fed Infants is Correlated with Human Milk Oligosaccharides Consumed. *J Pediatr Gastroenterol Nutr*, 60(6): 825-833.

Westfall, S., Lomis, N., Kahouli, I., Dia, S.Y., Singh, S.P., Prakash, S. 2017. Microbiome, probiotics and neurodegenerative diseases: deciphering the gut brain axis. *Cell Mol Life Sci*, 74(20): 3769-3787.

Wichmann, A., Allahyar, A., Greiner, T.U., Plovier, H., Lundén, G.Ö., Larsson, T., Drucker, D.J., Delzenne, N.M., Cani, P.D., Bäckhed, F. 2013. Microbial Modulation of Energy Availability in the Colon Regulates Intestinal Transit. *Cell Host Microbe*, 14(5): 582-590.

Wikkelsö, C., Ekman, R., Westergren, I., Johansson, B. 1991. Neuropeptides in Cerebrospinal Fluid in Normal-Pressure Hydrocephalus and Dementia. *Eur Neurol*, 31(2): 88-93.

Winblad, B., Amouyel, P., Andrieu, S., Ballard, C., Brayne, C., Brodaty, H., Cedazo-Minguez, A., Dubois, B., Edvardsson, D., Feldman, H., Fratiglioni, L., Frisoni, G.B., Gauthier, S., Georges, J., Graff, C., Iqbal, K., Jessen, F., Johansson, G., Jönsson, L., Kivipelto, M., Knapp, M., Mangialasche, F., Melis, R., Nordberg, A., Rikkert, M.O., Qiu, C., Sakmar, T.P., Scheltens, P., Schneider, L.S., Sperling, R., Tjernberg, L.O., Waldemar, G., Wimo, A., Zetterberg, H. 2016. Defeating Alzheimer's disease and other dementias: a priority for European science and society. *Lancet Neurol*, 15(5): 455-532.

Wiseman, F.K., Al-Janabi, T., Hardy, J., Karmiloff-Smith, A., Nizetic, D., Tybulewicz, V.L.J., Fisher, E.M.C., Strydom, A. 2015. A genetic cause of Alzheimer disease: mechanistic insights from Down syndrome. *Nat Rev Neurosci*, 16(9): 564-574.

Ximenez, C., Torres, J. 2017. Development of Microbiota in Infants and its Role in Maturation of Gut Mucosa and Immune System. *Arch Med Res*, 48(8): 666-680.

Yan, H., Ajuwon, K.M. 2017. Butyrate modifies intestinal barrier function in IPEC-J2 cells through a selective upregulation of tight junction proteins and activation of the Akt signalling pathway. *PLoS One*, 12(6): e0179586.

Yang, I., Corwin, E.J., Brennan, P.A., Jordan, S., Murphy, J.R., Dunlop, A. 2016. The Infant Microbiome: Implications for Infant Health and Neurocognitive Development. *Nurs Res*, 65(1): 76-88.

Yano, J.M., Yu, K., Donaldson, G.P., Shastri, G.G., Ann, P., Ma, L., Nagler, C.R., Ismagilov, R.F., Mazmanian, S.K., Hsiao, E.Y. 2015. Indigenous bacteria from the gut microbiota regulate host serotonin biosynthesis. *Cell*, 161(2): 264-276.

Zhang, C., Zhang, M., Wang, S., Han, R., Cao, Y., Hua, W., Mao, Y., Zhang, X., Pang, X., Wei, C., Zhao, G., Chen, Y., Zhao, L. 2010. Interactions between gut microbiota,

host genetics and diet relevant to development of metabolic syndromes in mice. *The ISME J*, 4(2): 232-241.

Zhang, L., Wang, Y., Xiayu, X., Shi, C., Chen, W., Song, N., Fu, X., Zhou, R., Xu, Y.F., Huang, L., Zhu, H., Han, Y., Qin, C. 2017. Altered Gut Microbiota in a Mouse Model of Alzheimer's Disease. *J Alzheimers Dis*, 60(4): 1241-1257.

Zhang, R., Miller, R.G., Gascon, R., Champion, S., Katz, J., Lancero, M., Narvaez, A., Honrada, R., Ruvalcaba, D., McGrath, M.S. 2009. Circulating endotoxin and systemic immune activation in sporadic amyotrophic lateral sclerosis (sALS). *J Neuroimmunol*, 206(1-2): 121-124.

Zhang, X., Zhao, Y., Xu, J., Xue, Z., Zhang, M., Pang, X., Zhang, X., Zhao, L. 2015. Modulation of the gut microbiota by berberine and metformin during the treatment of high-fat-diet-induced obesity in rats. *Sci Rep*, 5: 14405.

Zhao, Y., Cong, L., Jaber, V., Lukiw, W.J. 2017. Microbiome-Derived Lipopolysaccharide Enriched in the Perinuclear Region of Alzheimer's Disease Brain. *Front Immunol*, 8: 1064.

Zhao, Y., Cong, L., Lukiw, W.J. 2017. Lipopolysaccharide (LPS) Accumulates in Neocortical Neurons of Alzheimer's Disease (AD) Brain and Impairs Transcription in Human Neuronal-Glial Primary Co-cultures. *Front Aging Neurosci*, 9: 407.

Zheng, C., Zhou, X.W., Wang, J.Z. 2016. The dual roles of cytokines in Alzheimer's disease: update on interleukins, TNF- α and IFN- γ . *Transl Neurodeger*, 5: 7.

Zhernakova, A., Kurilshikov, A., Bonder, M.J., Tigchelaar, E.F., Schirmer, M., Vatanen, T., Mujagic, Z., Vila, A.V., Falony, G., Vieira-Silva, S., Wang, J., Imhann, F., Brandsma, E., Jankipersadsing, S.A., Joossens, M., Cenit, M.C., Deelen, P., Swertz, M.A., Weersma, R.K., Feskens, E.J., Netea, M.G., Gevers, D., Jonkers, D., Franke, L., Aulchenko, Y.S., Huttenhower, C., Raes, J., Hofker, M.H., Xavier, R.J., Wijmenga, C., Fu, J. 2016. Population-based metagenomics analysis reveals markers for gut microbiome composition and diversity. *Science*, 352(6285): 565-569.

Zito, F.P., Polese, B., Vozzella, L., Gala, A., Genovese, D., Verlezza, V., Medugno, F., Santini, A., Barrea, L., Cargioli, M., Andreozzi, P., Sarnelli, G., Cuomo, R. 2016. Good adherence to Mediterranean diet can prevent gastrointestinal symptoms: A survey from Southern Italy. *World J Gastrointest Pharmacol Ther*, 7(4): 564-571.

Websites

Health Media (Accessed 20/8/2018)

<https://healthmedia.blog.gov.uk/2016/05/27/amr/>

NIH Microbiome Project (Accessed 22/08/2018)

<https://www.hmpdacc.org/hmp/>